THE REPLACEMENT OF REFLECTORS BY

ALBEDO - TYPE BOUNDARY CONDITIONS

by

PANAGIOTIS CONSTANTINOS KALAMBOKAS

DIPLOMA, Electrical Engineering,National Technical University of

Athens, GREECE (July 1971)

M.S., Nuclear Engineering,Massachusetts Institute of Technology

May (1974)

SUBMITTED IN PARTIAL FULFILLMENT OF THE

REQUIREMENTS FOR THE DEGREE OF

DOCTOR OF SCIENCE

at the

MASSACHUSETTS INSTITUTE OF TECHNOLOGY

November 1975
(i.e. February 1976)

Signature of Author_____

Department of Nuclear Engineering, 11/8/75

Certified by_____

Thesis Supervisor

Accepted by_____

Chairman, Departmental Committee on Graduate Studies

THE REPLACEMENT OF REFLECTORS BY
ALBEDO - TYPE BOUNDARY CONDITIONS

by

PANAGIOTIS CONSTANTINOS KALAMBOKAS

Submitted to the Department of Nuclear Engineering on November 12,
1975 in partial fulfillment of the requirements for the degree of
Doctor of Science.

ABSTRACT

The idea of the representation of reflectors by boundary conditions
in static and dynamic reactor calculations is investigated. Ana-
lytical, group-diffusion theory boundary conditions relating
neutron flux to normal current at core-reflector interfaces in
terms of the reflector parameters are derived and applied for the
implicit treatment of reflectors. Kirchhoff's formula of optics,
translated into the neutron-diffusion language, is the general
relation from which boundary conditions for various reflector con-
figurations (slab, wedge, elbow), geometrically separable or not,
are obtained. The integral form of these boundary conditions in
space and/or time generally being unswited for computer implemen-
tation, a reduction to simle, approximate algebraic forms is car-
ried out. The finite diffusion length and/or the finite neutron
lifetime in various reflector materials are exploited in the above
reduction.

The bulk of the applications of the reflector-replacement method
are for two-dimensional, light water-reflected reactor models with
typical, step-like core-reflector interfaces, in steady state. With
these models it is found that, if the reflector is viewed as con-
sisting of many, narrow channels perpendicular to the interface
and the transchannel leakage is neglected, (so that the one-di-
mensional-slab boundary conditions can be used to represent the
reflector), the accuracy of the method, is extremely good for
large, shrouded cores, decreases with core-size and is poor when
the surface of a small, unshrouded core contains reentrant corners.
In the latter case the accuracy is improved by either the explicit
treatment of a light water buffer zone, about 2 cm thick, adjacent
to the core and the representation of the rest of the reflector by
one-dimensional-slab boundary conditions, or the employment of

2

numerical corrections generated internally during the computation or the employment of simple, analytical corrections derived from the infinite-wedge-shaped reflector configuration.

The replacement of light water reflectors in transients and the replacement of heavy water or graphite reflectors in steady state or transients are studied in a preliminary way. Excellent results are obtained from the implicit treatment of light water reflectors of one-dimensional-slab geometry in fast transients. Heavy water or graphite reflectors are found to be more difficult to replace by boundary conditions because of their longer diffusion lengths and neutron lifetimes.

In all cases, the computational cost is reduced by about 40% when the reflector is treated implicitly.

Thesis Supervisor: Allan F. Henry

Title: Professor of Nuclear Engineering

3

In Memory of Dr. Neophytos Papanastasiou, my Teacher.

III. THE WEDGE - SHAPED REFLECTOR

IV. TIME - DEPENDENT ANALYSIS

V. NUMERICAL TESTS AND RESULTS

6

7

8

LIST OF FIGURES

9

11

LIST OF TABLES

12

ACKNOWLEDGEMENTS

It was Professor A.F. Henry who first suggested to me the idea of replacement of reflectors by boundary conditions. For this, and for the help which he gave me in its evolution, I am deeply grateful and appreciative.

Also, I wish to thank Professor K.F. Hansen for serving as thesis reader, Dr. J.W. Stewart, R.A. Shober, J.H. Mason and V.A. Miethe for their advice at various stages of the research, O.K. Kadiroglu for attending to my unfinished business during my absence, and Myra Sbarounis for typing the thesis.

P.C. Kalambokas

I. I N T R O D U C T I O N

1.1 THEME AND OBJECTIVE OF THE THESIS.

The theme of the present thesis is analogous to that of the
well-known Thévenin's theorem of electrical engineering.

The theorem, a useful tool in the analysis of electric networks
and circuits, permits the determination of the currents and voltages
in a certain, arbitrary, part of a network without necessitating a
calculation of the currents and voltages in the entire network. The
means for this determination consists in:

i)   a "bissection"of the network into two parts:

   (a) the part of immediate interest (i.e. the part mentioned
       above) and

   (b) the rest of the network

and

ii)   a representation of part (b) by a simple, a priori obtainable,
equivalent. (The equivalent is, of course, meant with regard to the
electrical effect of part (b) on part (a)).

The present dissertation concerns the determination of the neutron distribution in a nuclear reactor core without a full, core-reflector calculation.

The "bissection", from a computational point of view, of the reactor into

    (a) the core, as the region of immediate interest and

    (b) the reflector, as the rest of the reactor, is natural, because information about the neutron distribution in the reflector is rarely needed[*]. It is the neutron distribution in the core that is of interest to the reactor designer. This is due to the fact that the core is the hot and depletable part of the reactor. Knowledge of the neutron flux in the core allows for the evaluation of the temperature - and depletion - patterns in the core, both very important pieces of information, pertaining to the safety of the reactor and to the management of the nucle-

_____

[*]In fact, after the flux-distribution in the core is found, the flux-distribution in the reflector can be evaluated by means of Kirchhoff's formula (presented in Chapter 2). The formula, which involves a line-integral and not a differential equation, must then be applied once for each reflector-point of interest.

16

ar fuel.

The derivation and testing of a simple, a priori obtainable, equivalent to represent the reflector (or, more accurately, to represent the effect of the reflector on the core) is the objective of this thesis. We shall carry out the development with a diffusion-theory reactor model, two energy groups, one and two spatial dimensions, steady and transient states.

1.2 MOTIVATION.

The anticipation of a significant savings in calculational effort provides the motivation for the present work.

The source of this savings is obvious. Typically, about 1/3 of the total number of spatial mesh-points, employed in a finite-difference, PWR computation, are located in the reflector region.[*]

---

[*] This fraction may seem too large. However it is a common practice, for programming convenience, to augment the number of the reflector mesh-points by additional mesh-points, which "fill" the space between the actual, cylindrical outer-boundary of the reflector and its circumscribed rectangular parallelopiped. The addition of these points does not disturb the flux-distribution in the reactor, because the computed values of the flux at the additional points are very small.

Replacement of the reflector by a mathematical equivalent,
therefore, means the elimination of all the reflector mesh points
and the consequent proportional reduction of the number of un-
knowns in the problem. Thus we anticipate significant savings
especially in multi-dimensional, static and -more important-
time-dependent calculations.

1.3 MATHEMATICAL FORM OF THE REFLECTOR - EQUIVALENT.

The reflector is coupled to the core at the core-reflector
interface, and on this interface we shall apply a boundary con-
dition to represent the reflector.

The mathematical form which we choose for this boundary con-
dition is:

$$
\begin{bmatrix} \Phi_1 \\ \Phi_2 \end{bmatrix} = \begin{bmatrix} \alpha_{11} & 0 \\ \alpha_{21} & \alpha_{22} \end{bmatrix} \begin{bmatrix} J_{1n} \\ J_{2n} \end{bmatrix} \tag{1.1}
$$

(where the Φ's and J_n's are two - group fluxes and normal currents
at the interface) or, inversely.

18

$$
\begin{bmatrix} J_{1n} \\ \\ J_{2n} \end{bmatrix} = \begin{bmatrix} \beta_{11} & 0 \\ \\ \beta_{21} & \beta_{22} \end{bmatrix} \begin{bmatrix} \Phi_1 \\ \\ \Phi_2 \end{bmatrix} \tag{1.2}
$$

where the β - parameters are related to the α's by the equations:

$$
\beta_{11} \equiv \frac{1}{\alpha_{11}} \ , \ \beta_{22} \equiv \frac{1}{\alpha_{22}} \ , \ \beta_{21} \equiv - \frac{\alpha_{21}}{\alpha_{11} \cdot \alpha_{22}} \tag{1.3}
$$

Eqs. (1.1), (1.2) with the α's and β's constant depending only on the reflector properties are exact for one-dimensional-slab geometry and steady state conditions.[*] For the same geometry but for a transient state, Eq. (1.1) can be replaced by an exact integral relation,[**] which, reduces approximately to the form (1.1). For two-dimensional geometry and for steady-state, Eq. (1.1) can

---

[*] The formulation (1.1), (1.2) is an extension of that employed by Prof. A.F. Henry in his work for control rod blades. Specifically, Henry's formulation is for purely absorbing blades (see material leading to the definition of blackness coefficients in Ref. [H-2]). The extension, due to Dr. Y.Lukic and Prof. Henry, is for scatter-ing media (see Ref. [L-3]).

[**] See Chapter 4 of the present dissertation.

again be replaced by an exact integral relation,[*] which, too,

reduces approximately to the form (1.1).

The boundary conditions (1.1),(1.2) are of the homogenous type.

1.4 COMPUTATIONAL FEATURES OF OUR REFLECTOR - EQUIVALENT.

The replacement of the reflector leaves the core-reflector

interface as the "outer boundary" for reactor calculations.

The interface having a step-like form, some extra programming

will be required for the implementation of boundary conditions on

such a jagged outer boundary, and extra programming means, of

course, increased computational cost. However, estimates of this

extra cost can be obtained by means of runs of the same, full,

core-reflector problem, once with the code CITATION[F-1], which is

programmed to accept group-dependend boundary conditions for

regions with jagged boundaries[**], and once with another diffusion -

theory code which does not have such a provision. Such comparisons

have been made and show that the extra-cost in question is small and

should not be a problem.

As was already mentioned, the boundary conditions (1.1), (1.2)

are exact only for a one-dimensional slab in steady-state and ap-

---

[*] See Chapters 2 and 3 of the present dissertation.
[**] Meant to be control rod regions.

proximate for all other cases. There will be, therefore, errors

associated with the representation of reflectors by these boundary

conditions in all cases but the steady-state, one-dimensional

slab. We shall see however that, for the general class of light

water moderated power reactors, these errors are small. Moreover,

even though approximate, the boundary conditions (1.1), (1.2),

being derived analytically, are free of the truncation error which

accompanies explicit representations of reflectors. This is another

reason that the number of spatial mesh points saved when (1.1),

(1.2) can legitimately be used is as much as 33%.

1.5   BACKGROUND AND ITS RELATION TO THE PRESENT WORK.

For static cases, the idea of replacing the explicit represen-

tation of reflector regions by boundary conditions at the core -

reflector interface is not new.

The one-group, nodal code FLARE[D-1] and the also-one-group,

coarse-mesh scheme by Robinson and Eckard[R-1] employ simple expres-

sions of the form:

$$J_n = \beta \cdot \Phi \qquad\qquad\qquad (1.4)$$

to relate normal current to flux at the interface, where the

constant-along-the-interface value of β is determined empirically

(i.e. by means of fitting to experimental data or to the results of

more accurate calculations).

The multigroup code CITATION[F-1] accepts group-dependent boundary conditions of the form:

$$J_{g_n} = \beta_g \cdot \Phi_g \qquad (1.5)$$

where the β_g's are constant along the interface.

For two energy groups, the boundary conditions (1.5) may be written in the form:

$$\begin{bmatrix} J_{1_n} \\ J_{2_n} \end{bmatrix} = \begin{bmatrix} \beta_1 & 0 \\ 0 & \beta_2 \end{bmatrix} \begin{bmatrix} \Phi_1 \\ \Phi_2 \end{bmatrix} \qquad (1.5)'$$

Let us compare the form of Eqs. (1.5)' with that of the static, two-group balance equations in the reflector:

$$\begin{bmatrix} \nabla \cdot J_1 \\ \nabla \cdot J_2 \end{bmatrix} = \begin{bmatrix} -\Sigma_1 & 0 \\ \Sigma_{1 \to 2} & -\Sigma_2 \end{bmatrix} \begin{bmatrix} \Phi_1 \\ \Phi_2 \end{bmatrix} \qquad (1.6)$$

22

We see that Eqs. (1.5)' treat the two energy groups symmetrically while Eqs. (1.6) do not. The asymmetry associated with the thermal group is absorbed by β_2 in Eqs. (1.5)'.

Galanin [G-1] employs a boundary condition to replace not only the reflector but also ribbons of the core adjacent to the core - reflector interface and describes the thermal flux in the remaining (interior) part of the core by a one-group-type equation:

$$\nabla^2 \Phi_2 + B_2^2 \cdot \Phi_2 = 0 \tag{1.7}$$

His boundary condition is of the type:

$$J_{2_n} = \beta_2 \cdot \Phi_2 \tag{1.8}$$

For β_2 he uses values calculated from one-dimensional, two-group, reflected reactor models. The thus-determined values for β_2 contain built into them the contribution of the thermal-group asymmetry mentioned above.

Galanin applies this method to obtain quick estimates for the critical dimensions of reflected cores of simple geometrical shapes: slab, cylinder and sphere. For cylindrical cores of finite height he introduces a transverse-buckling-correction to β_2.

23

In the present work we employ boundary conditions of the type (1.1), (1.2). These boundary conditions provide, via β_{21}, an extra degree of freedom over conditions (1.5)'.

The conditions (1.1), (1.2) are found from consideration of the physical and geometrical characteristics of the reflector alone. On the contrary, the values of β_2 in (1.5)' and in (1.8) depend on characteristics of both the reflector and the core.

To see this latter dependence, let us rearrange the second of Eqs. (1.2),

$$J_{2_n} = \beta_{21} \cdot \Phi_1 + \beta_{22} \cdot \Phi_2,$$

into the form:

$$J_{2_n} = \left(\beta_{21} \cdot \frac{\Phi_1}{\Phi_2} + \beta_{22} \right) \cdot \Phi_2 \qquad (1.9)$$

If we denote the quantity in parentheses in (1.9) by β_{22}^*, Eqs. (1.2) take the form:

24

$$\begin{bmatrix} J_{1_n} \\ \\ J_{2_n} \end{bmatrix} = \begin{bmatrix} \beta_{11} & 0 \\ \\ 0 & \beta_{22}^* \end{bmatrix} \begin{bmatrix} \Phi_1 \\ \\ \Phi_2 \end{bmatrix} \qquad\qquad (1.2)'$$

Eqs. (1.2)' are group-wise symmetrical: the thermal-group asymmetry has been lumped into β_{22}^*. However we see that β_{22}^* depends on the group-flux ratio. Hence, this ratio must somehow be estimated, before the value of β_{22}^* is found. Since the group-flux ratio under discussion depends on both the core and reflector characteristics, it follows that the parameter β_{22}^* does too.

The a priori estimation of the group-flux ratio is a source of uncertainty for the value of β_{22}^*, with possibly undesirable consequences. By making use of Eqs. (1.1), (1.2) in the present work we eliminate this uncertainty. The non-zero value for β_{21}, which makes the elimination possible, requires no extra program-ming for its computer implementation.

To determine the values of the coefficients in our boundary conditions, we make use, like Galanin, of algebraic formulas - as

opposed to the empirical values* used in [D-1] and [R-1]. However

we develop an alternative to Galanin's transverse-buckling cor-

rection to account for transverse leakage effects for two

dimensional cases.

Finally for time-dependent cases, the author is not aware of

any previous work in the area of replacement of reflectors by

boundary conditions.

1.6 ORGANIZATION OF THE THESIS.

This thesis is organized as follows:

Chapter II contains the derivation of the general, steady-

state, flux-to-normal-current relation along the boundary of a

reflector of an arbitrary configuration. We call this relation

Kirchhoff's formula. In the same chapter we give the specialized

versions of Kirchhoff's formula for four reflector configurations

of practical interest: the one-dimensional slab, the 90^0 wedge,

---

*
 Empirical methods are, from a practical standpoint, themselves

valuable. However, when systematic, theoretically founded ap-

proaches are available, they are preferable, for the insight and

security they offer.

the 270^0 wedge and the right-angled elbow.

Chapter III contains an alternative derivation of the steady-state, flux-to-normal current relation along the boundary of a wedge-shaped reflector.

Chapter IV is the unsteady-state counterpart of Chapter II, except that we only examine the one-dimensional slab as a special case.

In Chapter V we describe various numerical tests, performed to determine the accuracy of the "reflector replacement" method and present the results.

The conclusions and recommendations for further work on the implicit representation of reflectors are given in Chapter VI.

II. KIRCHHOFF'S FORMULA

2.1 KIRCHHOFF'S FORMULA FOR ONE ENERGY GROUP.

To begin, we consider the diffusion of one-energy-group neutrons in a homogeneous, non-multiplying medium which occupies a two-dimensional region A bounded by the closed curve Γ:
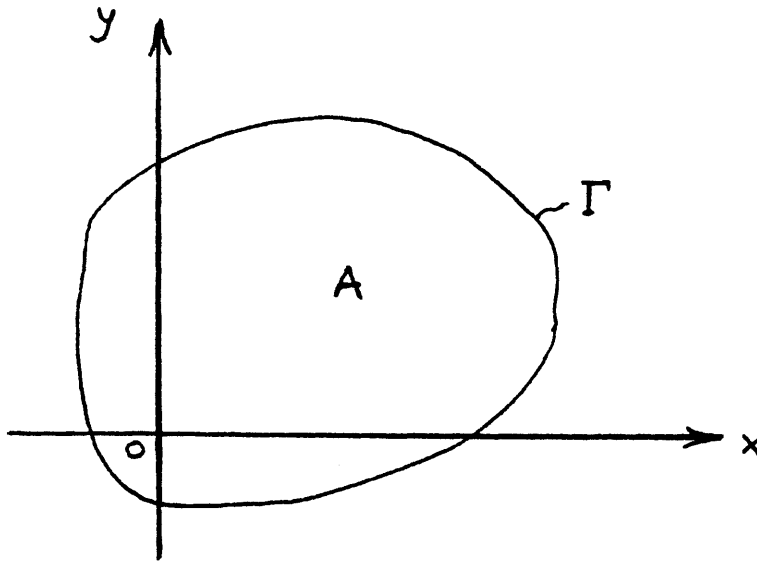
Figure 2.1

Two-dimensional region, A, bounded by curve Γ.

In the steady state, the balance between the local neutron - leakage and reaction rates is expressed by the following equation:

$$\frac{\partial^2 \phi}{\partial x^2} + \frac{\partial^2 \phi}{\partial y^2} - \frac{1}{L^2} \cdot \phi = 0 \qquad (2.1)$$

where $\Phi = \Phi(x,y)$ is the neutron flux, and L is the neutron diffusion length.

It can be shown[*] that Eq. (2.1) implies the following expression for the flux at any point in the interior of region A in terms of the distributions of flux and normal current along the boundary Γ:

$$\phi(x,y) = \frac{1}{2\pi} \cdot \int_{\Gamma} \left[\phi(x',y') \cdot \frac{\partial K_0(\rho/L)}{\partial n} + \frac{1}{D} \cdot J_n(x',y') \cdot K_0(\rho/L) \right] \cdot d\ell$$

(2.2)

where:

(x,y) is a point in the interior of region A,

"(x', y') is a point on the boundary curve Γ,"

$_\Gamma\int [...]$dl denotes integration along Γ,

$\partial/\partial n$ denotes differentiation along a line normal to the curve Γ, toward its interior,

$J_n(x',y')$ is defined by:

_____

[*] See discussion below (in this section) and also part (b) of Section (2.6).

29

$$J_n(x', y') \equiv -D \cdot \frac{\partial \phi}{\partial n}\bigg|_{x', y'} \qquad (2.3)$$

D is the neutron diffusion coefficient, K_0 is the modified Bessel function of order zero (second kind) and ρ is defined by:

$$\rho \equiv \sqrt{(x'-x)^2 + (y'-y)^2} \qquad (2.4)$$

Eq. (2.2) is the analogue of the so-called Kirchhoff's formula of wave theory[*]. For convenience, in the remaining of the present dissertation we shall refer to Eq. (2.2) specifically as Kirchhoff's formula.

---

[*] The wave equation,

$$\nabla^2 \psi = b \cdot \frac{\partial^2 \psi}{\partial t^2} \; ; \qquad b = \text{real and constant,}$$

and Kirchhoff's formula reduce, respectively, to Eqs. (2.1) and (2.2) in the special case of an exponential time-dependence and of two spatial dimensions.

A derivation of Kirchhof's formula from the wave equation is given in Ref . [P-1].

It can be verified by substitution that Eq. (2.2) satisfies

Eq. (2.1). A direct proof, starting from Eq. (2.1), is outlined

in Section 2.7, part b).

If we take the point (x,y) at a distance ε from the boundary

Γ and let $\varepsilon \to 0$, Kirchhoff's formula (Eq. (2.2)) becomes an

integral relation between the boundary flux and normal current.

This relation is a formal boundary condition which contains all

the information, physical and geometrical, relevant to the dif-

fusion of one-energy-group neutrons in region A. The effect of

the diffusing medium in region A on the neutron distribution in

any surrounding regions is reproduced mathematically by the above

boundary condition. In this sense, the boundary condition formally

represents region A.

2.2 THE ONE-DIMENSIONAL SLAB.

Suppose the region A is a one-dimensional slab of thickness

Δ, oriented with respect to the x-y coordinate system as shown in

Figure 2.2:
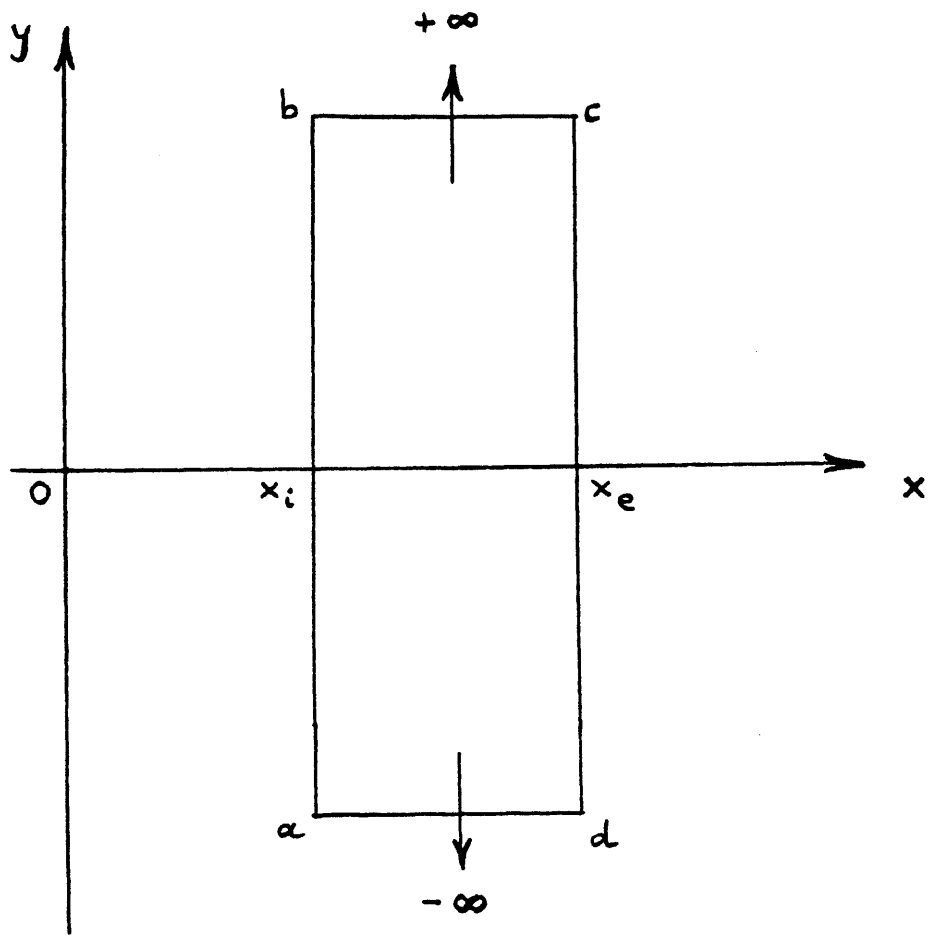
Figure 2.2

One dimensional slab, A, of thickness $\Delta \equiv x_e - x_i$.

In the above configuration, the steady-state flux distribution is independent of y. Therefore,

$$\phi(x,y) = \phi(x) \qquad (2.6)$$

and $\quad J_y(x,y) = 0$ (2.7)

Furthermore, the value of

$$\frac{\partial}{\partial n} K_0(\rho/L) \equiv \frac{\partial}{\partial n} K_0 \left(\sqrt{\left(\frac{x'-x}{L}\right)^2 + \left(\frac{y'}{L}\right)^2} \right)$$

on the horizontal segments bc and da of the boundary curve Γ

tends to zero as $|ab| = |cd| \to \infty$.

This latter fact and Eq. (2.7) imply that the segments bc and

da do not contribute to the line integral of Eq. (2.2). Therefore,

for the configuration of Fig. (2.2), Eq. (2.2) becomes:

$$\phi(x) = I^{ab} - I^{dc}$$ (2.8)

where :

$$I^{ab} \equiv \frac{1}{2\pi} \cdot \left[\phi(x') \cdot \frac{\partial}{\partial n} + \frac{1}{D} \cdot J_n(x') \right] \cdot \int_{-\infty}^{+\infty} K_0 \left(\frac{\rho}{L}\right) dy' \Bigg|_{x'=x_i}$$

(2.9)

33

$$I^{dc} \equiv \frac{1}{2\pi} \cdot \left[\phi(x') \cdot \frac{\partial}{\partial n} + \frac{1}{D} \cdot J_n(x') \right] \cdot \int_{-\infty}^{+\infty} K_0 \left(\frac{\rho}{L} \right) dy' \Bigg|_{x'=x_e} \tag{2.10}$$

and $\quad \rho \equiv \sqrt{(x'-x)^2 + y'^2} \tag{2.11}$

Next we evaluate the integral which appears in (2.9) and (2.10):

$$\int_{-\infty}^{+\infty} K_0 \left(\frac{\rho}{L} \right) dy' = L \cdot \pi \cdot \exp \left(-\frac{|x'-x|}{L} \right) \tag{2.12}$$

substitute (2.12) into (2.9) and (2.10) and obtain:

$$I^{ab} = \frac{L}{2} \cdot \left[\phi(x') \cdot \frac{\partial}{\partial n} + \frac{1}{D} \cdot J_n(x') \right] \cdot \exp \left(-\frac{x-x'}{L} \right) \Bigg|_{x'=x_i} \tag{2.13}$$

$$I^{dc} = \frac{L}{2} \cdot \left[\phi(x') \cdot \frac{\partial}{\partial n} + \frac{1}{D} \cdot J_n(x') \right] \cdot \exp \left(-\frac{x'-x}{L} \right) \Bigg|_{x'=x_e} \tag{2.14}$$

34

We carry out the differentiations indicated in (2.13) and (2.14) and substitute the resulting expressions into the right hand side of Eq. (2.8) to get:

$$\phi(x) =$$

$$= \frac{1}{2} \cdot \left[\phi(x_i) \cdot \exp\left(-\frac{x-x_i}{L}\right) + \phi(x_e) \cdot \exp\left(-\frac{x_e-x}{L}\right) \right] +$$

$$+ \frac{1}{2} \cdot \frac{L}{D} \cdot \left[J_x(x_i) \cdot \exp\left(-\frac{x-x_i}{L}\right) - J_x(x_e) \cdot \exp\left(-\frac{x_e-x}{L}\right) \right]$$

$$(2.15)$$

We evaluate Eq. (2.15) at $x = x_i$ and at $x = x_e$ and use the quantity Δ to denote the difference $x_e - x_i$. We find:

$$\phi(x_i) = \phi(x_e) \cdot \exp\left(-\frac{\Delta}{L}\right) +$$
$$+ \frac{L}{D} \cdot \left[J_x(x_i) - J_x(x_e) \cdot \exp\left(-\frac{\Delta}{L}\right) \right]$$

$$\phi(x_e) = \phi(x_i) \cdot \exp\left(-\frac{\Delta}{L}\right) +$$
$$+ \frac{L}{D} \cdot \left[J_x(x_i) \cdot \exp\left(-\frac{\Delta}{L}\right) - J_x(x_e) \right]$$

$$(2.16)$$

After some rearrangement, we get from Eqs.(2.16).

35

$$
\begin{bmatrix} \phi(x_e) \\ \\ J_x(x_e) \end{bmatrix} = \begin{bmatrix} \cosh\left(\frac{\Delta}{L}\right), & -\frac{L}{D}\cdot\sinh\left(\frac{\Delta}{L}\right) \\ \\ -\frac{D}{L}\sinh\left(\frac{\Delta}{L}\right), & \cosh\left(\frac{\Delta}{L}\right) \end{bmatrix} \begin{bmatrix} \phi(x_i) \\ \\ J_x(x_i) \end{bmatrix}
$$

$$(2.17)$$

The 2×2 matrix in Eq. (2.17) expresses the transfer proper-
ties of the slab, in the sense that it allows for the determi-
nation of flux and normal current on the right face of the slab,
given the flux and normal current on the left face. For con-
venience, we shall denote this matrix by $[M_{i \to e}]$.

At this point we consider two special subcases:
(a) Suppose the right face of the slab is an outer boundary. Then,

$$\phi(x_e) = 0 \qquad\qquad (2.18)$$

and the first of Eqs. (2.17) implies:

$$\phi(x_i) = \frac{L}{D}\cdot\tanh\left(\frac{\Delta}{L}\right)\cdot J_x(x_i) \qquad (2.19)$$

If $\Delta = \infty$ (semi-infinite slab), Eq. (2.19) reduces to:

$$\phi(x_i) = \frac{L}{D} \cdot J_x(x_i) \qquad (2.20)$$

(b) Suppose we have a two-zone slab, as shown in Figure 2.3
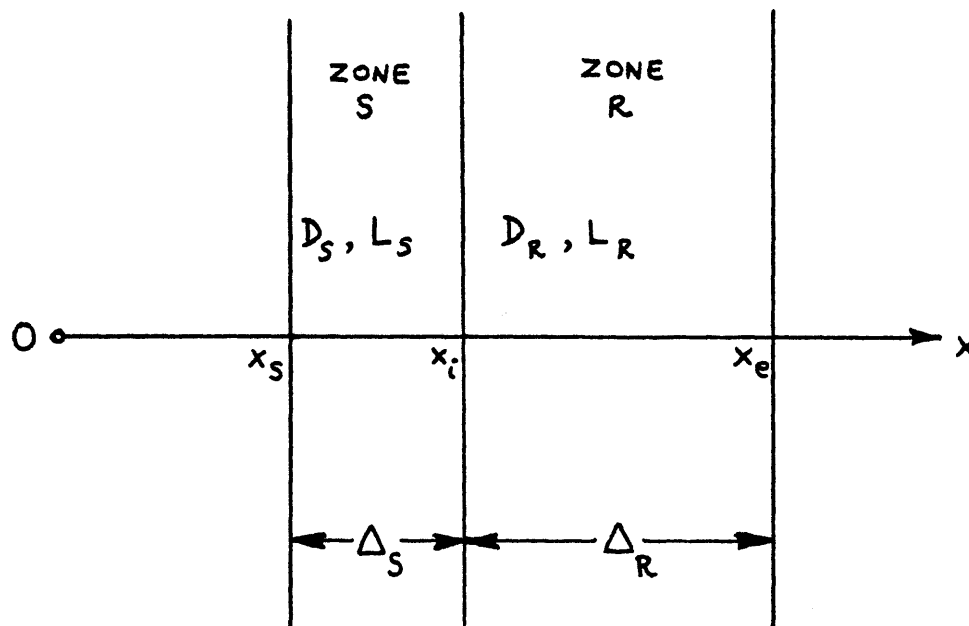
Figure 2-3

Two - Zone Slab

The letters S and R denote the two zones. The physical and geometrical parameters of slab S (D_S, L_S, and Δ_S) are not necessarily equal to the respective parameters of slab R (D_R, L_R and Δ_R).

We write Eq. (2.17) for zones S and R and take into account

the continuity of flux and normal current at the interface

between the two zones:

$$Col\left[\phi(x_i), J_x(x_i)\right] =$$
$$= \left[M_{s \to i}\right] \cdot Col\left[\phi(x_s), J_x(x_s)\right] \qquad (2.21)$$

$$Col\left[\phi(x_e), J_x(x_e)\right] =$$
$$= \left[M_{i \to e}\right] \cdot Col\left[\phi(x_i), J_x(x_i)\right] \qquad (2.21)'$$

We substitute (2.21) into (2.21)' and obtain:

$$Col\left[\phi(x_e), J_x(x_e)\right] =$$
$$= \left[M_{i \to e}\right]\left[M_{s \to i}\right] \cdot Col\left[\phi(x_s), J_x(x_s)\right] \qquad (2.22)$$

The product matrix, $[M_{i \to e}][M_{s \to i}]$, in Eq. (2.22) expresses

the transfer properties of the composite (two-zone) slab. We shall

denote the product matrix by $[M_{s \to e}]$. The expressions of the

elements of $[M_{s \to e}]$ in terms of the zone-parameters, D_s, L_s,

Δ_s, D_R, L_R and Δ_R, are:

38

$$M_{S \to e}\big|_{11} = \cosh\left(\frac{\Delta_R}{L_R}\right) \cdot \cosh\left(\frac{\Delta_S}{L_S}\right) +$$

$$+ \frac{L_R}{D_R} \cdot \frac{D_S}{L_S} \cdot \sinh\left(\frac{\Delta_R}{L_R}\right) \cdot \sinh\left(\frac{\Delta_S}{L_S}\right),$$

$$M_{S \to e}\big|_{12} = -\frac{L_S}{D_S} \cdot \cosh\left(\frac{\Delta_R}{L_R}\right) \cdot \sinh\left(\frac{\Delta_S}{L_S}\right) -$$

$$- \frac{L_R}{D_R} \cdot \sinh\left(\frac{\Delta_R}{L_R}\right) \cdot \cosh\left(\frac{\Delta_S}{L_S}\right),$$

$$M_{S \to e}\big|_{21} = -\frac{D_R}{L_R} \cdot \sinh\left(\frac{\Delta_R}{L_R}\right) \cdot \cosh\left(\frac{\Delta_S}{L_S}\right) -$$

$$- \frac{D_S}{L_S} \cdot \cosh\left(\frac{\Delta_R}{L_R}\right) \cdot \sinh\left(\frac{\Delta_S}{L_S}\right),$$

$$M_{S \to e}\big|_{22} = \frac{D_R}{L_R} \cdot \frac{L_S}{D_S} \cdot \sinh\left(\frac{\Delta_R}{L_R}\right) \cdot \sinh\left(\frac{\Delta_S}{L_S}\right) +$$

$$+ \cosh\left(\frac{\Delta_R}{L_R}\right) \cdot \cosh\left(\frac{\Delta_S}{L_S}\right)$$

(2.23)

2.3 THE 90°- AND THE 270° - WEDGE.

(a) Suppose the region A is a 90° - wedge, occupying the first quadrangle of the x-y plane.
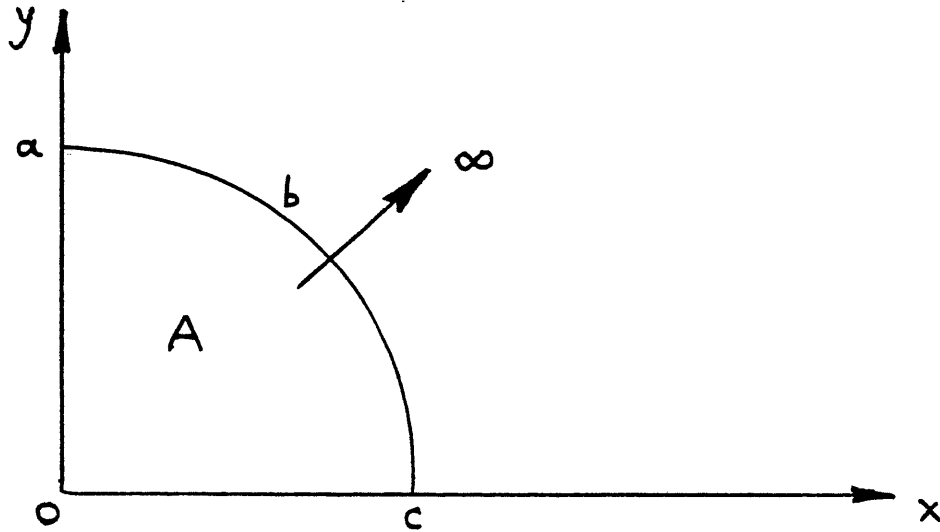
Figure 2.4

90° - Wedge

Eq. (2.2) becomes:

$$\phi(x,y) = I^{o\alpha} - I^{oc} \qquad (2.24)$$

where

$$I^{o\alpha} \equiv \frac{1}{2\pi} \cdot \int_0^\infty \left[\phi(x',y') \cdot \frac{\partial}{\partial x'} + \frac{1}{D} \cdot J_x(x',y') \right] \cdot$$

$$\cdot K_0 \left(\sqrt{\left(\frac{x'-x}{L}\right)^2 + \left(\frac{y'-y}{L}\right)^2} \right) \Bigg|_{x'=0} \cdot dy' \qquad (2.25)$$

40

and

$$I^{oc} \equiv \frac{1}{2\pi} \cdot \int_0^\infty \left[\phi(x',y') \cdot \frac{\partial}{\partial y'} + \frac{1}{D} \cdot J_y(x',y') \right] \cdot$$

$$\cdot K_0 \left(\sqrt{\left(\frac{x'-x}{L}\right)^2 + \left(\frac{y'-y}{L}\right)^2} \right) \Bigg|_{y'=0} \cdot dx'$$

(2.26)

The segment abc does not contribute to the line integral in Eq. (2.2), because ϕ and J_n vanish at large distances from the origin.

We evaluate Eq. (2.24) at the points: (x, ε) and (ε, y), where ε is a small, positive quantity and we let ε approach zero. Thus we obtain two boundary conditions, c_1 and c_2, relating, in an integral form, the four quantities: $\phi(x,0)$, $J_y(x,0)$, $\phi(0,y)$ and $J_x(0,y)$.

In the special case where the neutron distribution is symmetrical with respect to the line $y = x$, we have

$$\phi(x,0) = \phi(0,y)$$

and

$$J_y(x,0) = -J_x(0,y)$$

(2.27)

41

and the boundary conditions c_1 and c_2 reduce to a single relation which reads:

$$\phi(x,0) =$$

$$= -\frac{1}{2\pi} \cdot \lim_{\epsilon \to 0} \int_0^\infty \left\langle \frac{\partial}{\partial u} \left[K_0\left(\sqrt{\left(\frac{x'-x}{L}\right)^2 + \left(\frac{u-\epsilon}{L}\right)^2}\right) + \right. \right.$$

$$\left. + K_0\left(\sqrt{\left(\frac{u-x}{L}\right)^2 + \left(\frac{x'-\epsilon}{L}\right)^2}\right)\right]_{u=0} \cdot \phi(x',0) +$$

$$+ \frac{1}{D} \cdot \left[K_0\left(\sqrt{\left(\frac{x'-x}{L}\right)^2 + \left(\frac{\epsilon}{L}\right)^2}\right) + \right.$$

$$\left. \left. + K_0\left(\sqrt{\left(\frac{x}{L}\right)^2 + \left(\frac{x'-\epsilon}{L}\right)^2}\right)\right] \cdot J_y(x',0) \right\rangle dx'$$

(2.28)

(b) Suppose the region A is a 270^0 - wedge, occurying the second, third and fourth quadrangles of the x - y plane.

Figure 2-5

270^0 - Wedge
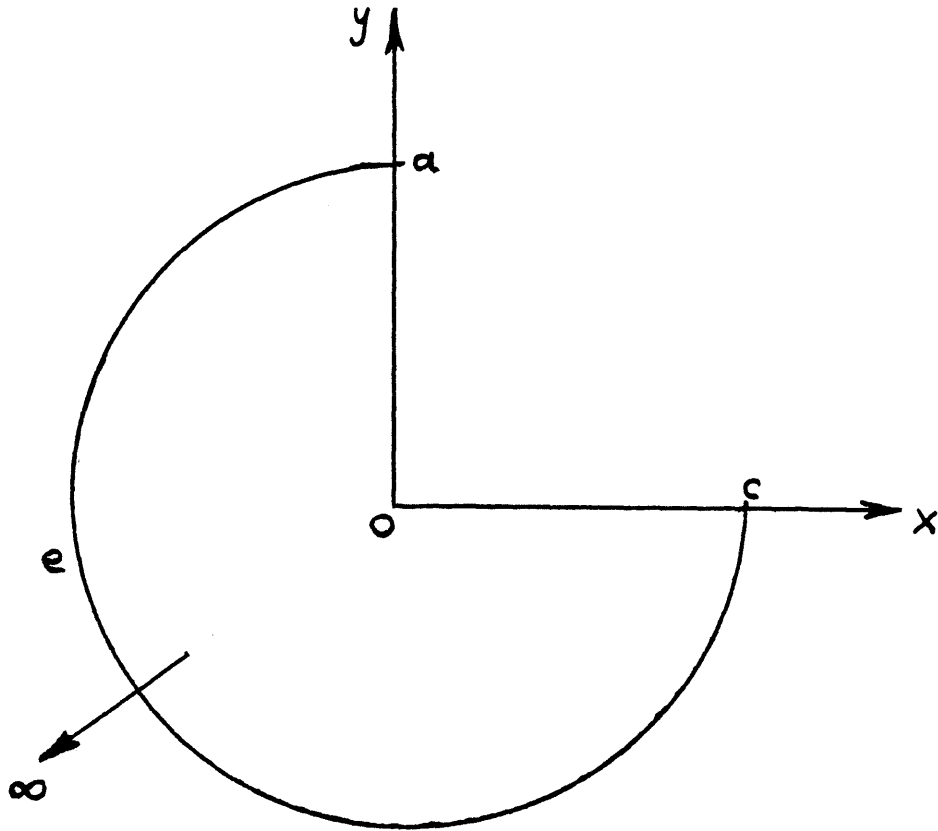
Eq. (2.2) becomes:

$$\phi(x,y) = I^{oc} - I^{oa} \tag{2.29}$$

where I^{oc} and I^{oa} are defined by (2.26) and (2.25), respectively.

2.4 THE RIGHT - ANGLED ELBOW.

Suppose the region A is a right-angled elbow, oriented with respect to the x - y coordinate system as shown in Figure 2.6
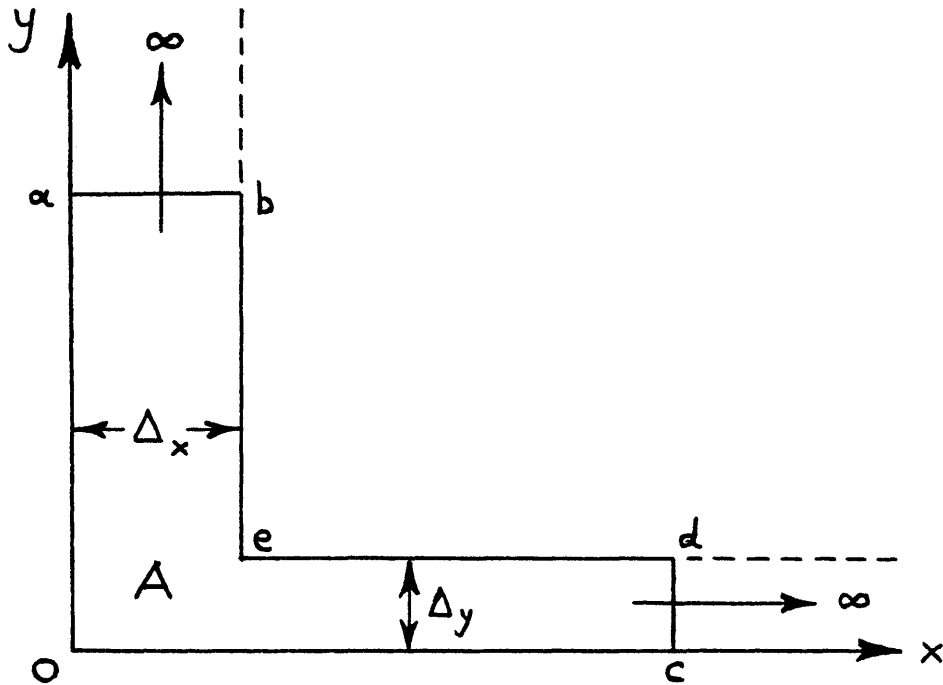
Figure 2-6

Right - Angled Elbow

Eq. (2.2) becomes:

$$\phi(x,y) = I^{oa} - I^{eb} + I^{ed} - I^{oc} \qquad (2.30)$$

where: I^{oa} and I^{oc} are defined by equations (2.25) and (2.26), respectively,

$$I^{eb} \equiv \frac{1}{2\pi} \cdot \int_{\Delta_y}^{\infty} \left[\phi(x',y') \cdot \frac{\partial}{\partial x'} + \frac{1}{D} \cdot J_x(x',y') \right] \cdot$$

$$\cdot K_0 \left(\sqrt{\left(\frac{x'-x}{L}\right)^2 + \left(\frac{y'-y}{L}\right)^2} \right) \Bigg|_{x'=\Delta_x} \cdot dy'$$

(2.31)

and

$$I^{ed} \equiv \frac{1}{2\pi} \cdot \int_{\Delta_x}^{\infty} \left[\phi(x',y') \cdot \frac{\partial}{\partial y'} + \frac{1}{D} \cdot J_y(x',y') \right] \cdot$$

$$\cdot K_0 \left(\sqrt{\left(\frac{x'-x}{L}\right)^2 + \left(\frac{y'-y}{L}\right)^2} \right) \Bigg|_{y'=\Delta_y} \cdot dx'$$

(2.32)

2.5 KIRCHHOFF'S FORMULA FOR TWO ENERGY GROUPS.

In the steady state, the balance equations for fast (group - 1) and thermal (group - 2) neutrons are

$$\frac{\partial^2 \phi_1}{\partial x^2} + \frac{\partial^2 \phi_1}{\partial y^2} - \frac{1}{L_1^2} \cdot \phi_1 = 0 \qquad (2.33)$$

45

$$\frac{\partial^2 \phi_2}{\partial x^2} + \frac{\partial^2 \phi_2}{\partial y^2} - \frac{1}{L_2^2} \cdot \phi_2 = - \frac{\Sigma_{1 \to 2}}{D_2} \cdot \phi_1 \qquad (2.34)$$

respectively, where:

Φ_1 and Φ_2 are the group fluxes,

L_1 and L_2 are the group diffusion lengths,

$\Sigma_{1 \to 2}$ is the scattering cross section from group 1 to group

2 and

D_1 and D_2 are the group diffusion coefficients.

The equation for the fast group, Eq. (2.33), is identical to the one-group equation, (2.1). Therefore, we may immediately write the one-group Kirchhoff's formula, Eq. (2.2), in terms of the fast group quantities:

$$\phi_1(x,y) = \frac{1}{2\pi} \cdot \int_\Gamma \left[\phi_1(x',y') \cdot \frac{\partial K_0(\rho/L_1)}{\partial n} + \frac{1}{D_1} \cdot J_{1n}(x',y') \cdot K_0(\rho/L_1) \right] d\ell$$

$$(2.35)$$

46

where

$$J_{1_n}(x',y') \equiv -D_1 \cdot \frac{\partial \phi_1}{\partial n}\bigg|_{x',y'} \qquad (2.36)$$

The equation for the thermal group, Eq. (2.34), is a non-homogeneous differential equation. Its solution, $\Phi_2(x,y)$ can be expressed as:

$$\phi_2(x,y) = \phi_{2h}(x,y) + \phi_{2p}(x,y) \qquad (2.37)$$

where $\Phi_{2h}(x,y)$ is the general solution of the nomogeneous equation:

$$\frac{\partial^2 \phi_{2h}}{\partial x^2} + \frac{\partial^2 \phi_{2h}}{\partial y^2} - \frac{1}{L_2^2} \cdot \phi_{2h} = 0 \qquad (2.38)$$

and $\Phi_{2p}(x,y)$ is a particular solution of the full, nonhomogeneous equation (2.34).

The homogeneous equation (2.38) is identical to the one-group equation, (2.1). Therefore, we may write:

47

$$\phi_{2h}(x,y) = \frac{1}{2\pi} \cdot \int_{\Gamma} \left[\phi_{2h}(x',y') \cdot \frac{\partial K_0(\rho/L_2)}{\partial n} + \right.$$

$$\left. + \frac{1}{D_2} \cdot J_{2h_n}(x',y') \cdot K_0(\rho/L_2) \right] d\ell$$

$$(2.39)$$

where:

$$J_{2h_n}(x',y') \equiv - D_2 \cdot \left. \frac{\partial \phi_{2h}}{\partial n} \right|_{x',y'} \qquad (2.40)$$

A particular solution of Eq. (2.34) is:

$$\phi_{2p}(x,y) = \frac{\Sigma_{1\to 2}/D_2}{\frac{1}{L_2^2} - \frac{1}{L_1^2}} \cdot \phi_1(x,y) \qquad (2.41)$$

We substitute $\Phi_1(x,y)$ from Eq. (2.35) into Eq. (2.41):

48

$$\phi_{2p}(x,y) = \frac{\Sigma_{1 \to 2}/D_2}{\frac{1}{L_2^2} - \frac{1}{L_1^2}} \cdot \frac{1}{2\pi} \cdot \int_\Gamma \left[\phi_1(x',y') \cdot \right.$$

$$\left. \cdot \frac{\partial K_o(\rho/L_1)}{\partial n} + \frac{1}{D_1} \cdot J_{1n}(x',y') \cdot K_o(\rho/L_1) \right] d\ell$$

$$(2.42)$$

We add Eqs. (2.39) and (2.42):

$$\phi_{2h}(x,y) + \phi_{2p}(x,y) =$$

$$= \frac{1}{2\pi} \cdot \int_\Gamma \left[\phi_{2h}(x',y') \cdot \frac{\partial K_o(\rho/L_2)}{\partial n} + \right.$$

$$+ \frac{1}{D_2} \cdot J_{2h_n}(x',y') \cdot K_o(\rho/L_2) \right] d\ell +$$

$$+ \frac{\Sigma_{1 \to 2}/D_2}{\frac{1}{L_2^2} - \frac{1}{L_1^2}} \cdot \frac{1}{2\pi} \cdot \int_\Gamma \left[\phi_1(x',y') \cdot \frac{\partial K_o(\rho/L_1)}{\partial n} + \right.$$

$$+ \frac{1}{D_1} \cdot J_{1n}(x',y') \cdot K_o(\rho/L_1) \right] d\ell$$

$$(2.43)$$

49

The left hand side of Eq. (2.43) is, by virtue of Eq. (2.37), equal to $\Phi_2(x,y)$.

In the right hand side of Eq. (2.43) we easily eliminate the quantities with subscript h in favor of the group-fluxes and normal currents at the boundary Γ as follows:

From Eqs. (2.37) and (2.41) we get:

$$\phi_{2h}(x,y) = \phi_2(x,y) - \frac{\Sigma_{1\to 2}/D_2}{\frac{1}{L_2^2} - \frac{1}{L_1^2}} \cdot \phi_1(x,y) \qquad (2.44)$$

We operate on Eq. (2.44) with: $-D_2 \, \partial/\partial n\big|_{x',y'}$. The resulting equation is:

$$J_{2h_n}(x,y) = J_{2_n}(x,y) - \frac{\Sigma_{1\to 2}/D_2}{\frac{1}{L_2^2} - \frac{1}{L_1^2}} \cdot \frac{D_2}{D_1} \cdot J_{1_n}(x',y') \qquad (2.45)$$

where: $J_{1n}(x',y')$ and $J_{2h_n}(x',y')$ are defined by Eqs. (2.36) and (2.40), respectively, and

$$J_{2_n}(x',y') \equiv -D_2 \cdot \frac{\partial \phi_2}{\partial n}\bigg|_{x',y'} \qquad (2.46)$$

50

We substitute Eq. (2.44) evaluated at (x',y') and Eq.
(2.45) into the right hand side of Eq. (2.43).

Kirchhoff's formula for the thermal group is, therefore:

$$\Phi_2(x,y) = \frac{1}{2\pi} \cdot \int_{\Gamma} \left[\Phi_2(x',y') \cdot \frac{\partial K_0(\rho/L_2)}{\partial n} + \right.$$

$$+ \frac{1}{D_2} \cdot J_{2_n}(x',y') \cdot K_0(\rho/L_2) +$$

$$+ \frac{\Sigma_{1\rightarrow2}/D_2}{\frac{1}{L_2^2} - \frac{1}{L_1^2}} \cdot \left\langle \Phi_1(x',y') \cdot \frac{\partial}{\partial n} \left\{ K_0(\rho/L_1) - K_0(\rho/L_2) \right\} + \right.$$

$$\left. \left. + \frac{1}{D_1} \cdot J_{1_n}(x',y') \cdot \left\{ K_0(\rho/L_1) - K_0(\rho/L_2) \right\} \right\rangle \right] d\ell$$

$$(2.47)$$

<u>The One - Dimensional Slab.</u>

i)   The two-group extension of the one-dimensional, one-zone
slab relation, Eq. (2.17), is:

$$\begin{bmatrix} \Phi_1 \\ \Phi_2 \\ J_{1x} \\ J_{2x} \end{bmatrix}_{x=x_e} = \left[M_{i\rightarrow e} \right]_{groups=2} \cdot \begin{bmatrix} \Phi_1 \\ \Phi_2 \\ J_{1x} \\ J_{2x} \end{bmatrix}_{x=x_i} \quad (2.17)'$$

where the 4×4 matrix $[M_{i \to e}]_{\text{groups}=2}$ is defined by:

$$[M_{i \to e}]_{\text{groups}=2} \equiv$$

$$\begin{bmatrix} c_1 & , & 0 & , & -L_1 \cdot \dfrac{S_1}{D_1} & , & 0 \\[2mm] (c_1 - c_2) \cdot r & , & c_2 & , & (L_2 S_2 - L_1 S_1) \cdot \dfrac{r}{D_1} & , & -L_2 \cdot \dfrac{S_2}{D_2} \\[2mm] -D_1 \cdot \dfrac{S_1}{L_1} & , & 0 & , & c_1 & , & 0 \\[2mm] \left(\dfrac{S_2}{L_2} - \dfrac{S_1}{L_1} \right) \cdot D_2 r & , & -D_2 \cdot \dfrac{S_2}{L_2} & , & \dfrac{c_1 - c_2}{D_1} \cdot r D_2 & , & c_2 \end{bmatrix}$$

$$(2.48)$$

and

$$\left. \begin{aligned} c_g &\equiv \cosh\left(\frac{\Delta}{L_g} \right) \\[3mm] S_g &\equiv \sinh\left(\frac{\Delta}{L_g} \right) \end{aligned} \right\} \quad g = 1, 2$$

$$(2.49)$$
$$(2.50)$$

$$r \equiv \frac{\Sigma_{1 \to 2} / D_2}{\dfrac{1}{L_2^2} - \dfrac{1}{L_1^2}}$$

$$(2.51)$$

If the right face of the slab is an outer boundary, then:

$$\phi_1(x_e) = \phi_2(x_e) = 0 \qquad (2.18)'$$

and the first two of Eqs. (2.17)' implie:

$$\begin{bmatrix} \phi_1 \\ \phi_2 \end{bmatrix}_{x_i} = \begin{bmatrix} \alpha_{11} & 0 \\ \alpha_{21} & \alpha_{22} \end{bmatrix} \begin{bmatrix} J_{1x} \\ J_{2x} \end{bmatrix}_{x_i} \qquad (2.19)'$$

where:

$$\left. \begin{aligned} \alpha_{11} &\equiv \frac{L_1}{D_1} \cdot \tanh\left(\frac{\Delta}{L_1}\right) \\[2ex] \alpha_{22} &\equiv \frac{L_2}{D_2} \cdot \tanh\left(\frac{\Delta}{L_2}\right) \\[2ex] \alpha_{21} &\equiv \frac{\Sigma_{1\to 2}}{D_1 \Sigma_2 - D_2 \Sigma_1} \cdot \left\langle D_1 \cdot \alpha_{11} - D_2 \cdot \alpha_{22} \right\rangle \end{aligned} \right\}$$

$$(2.52)$$

For easy reference, we shall give the parameters α a name: we shall call them <u>Static Impedances</u> of the one-dimensional, one-zone slab A, a term inspired from electric circuitry.

Values of the α's for various reflector materials and thicknesses can be infered from Figures 2.7 and 2.8 . The value of α_{12} is always zero, due to the absence of up-scattering.

53
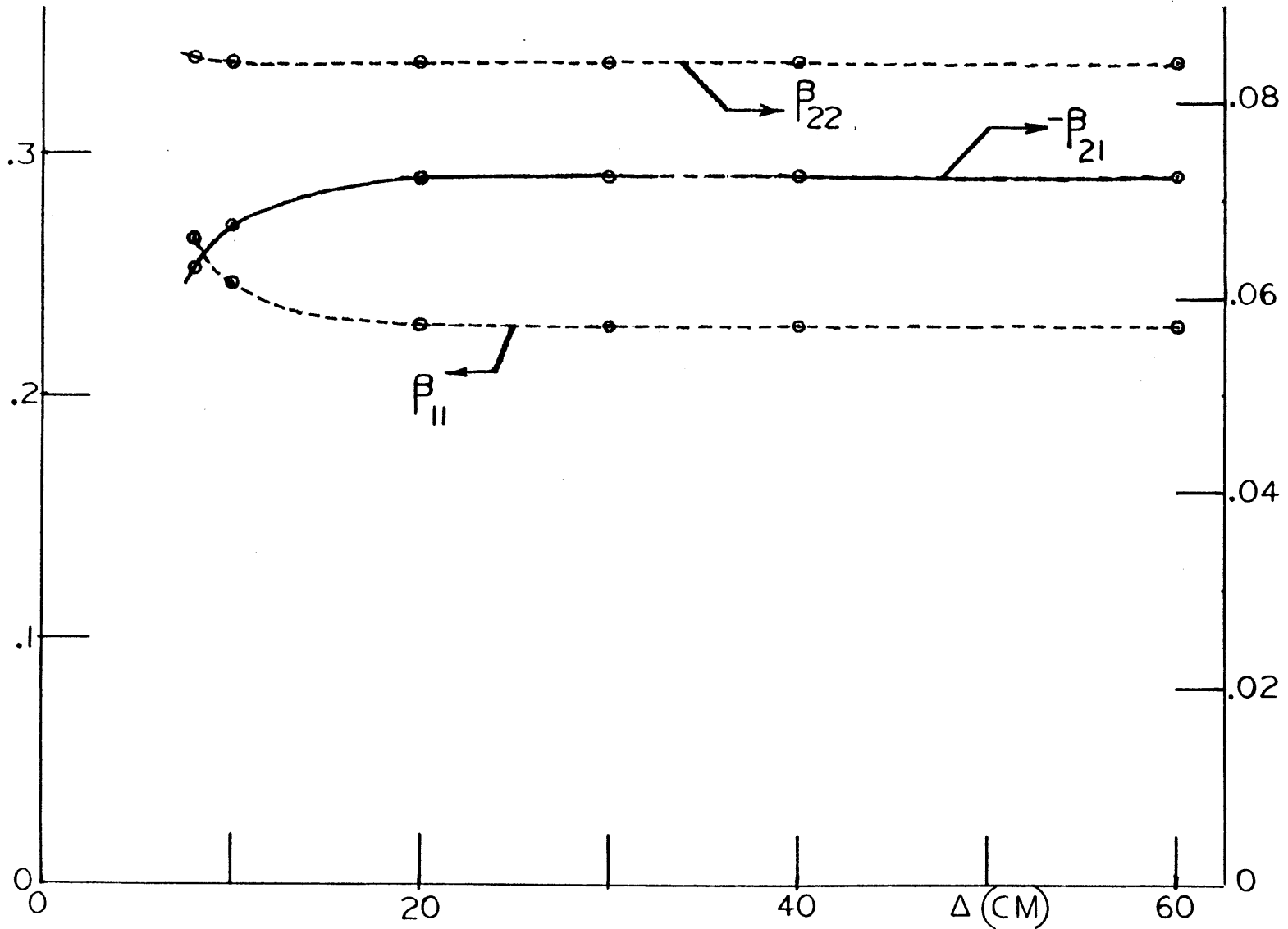
FIGURE 2.7 : INVERSE IMPEDANCES OF H_2O VS. REFLECTOR THICKNESS
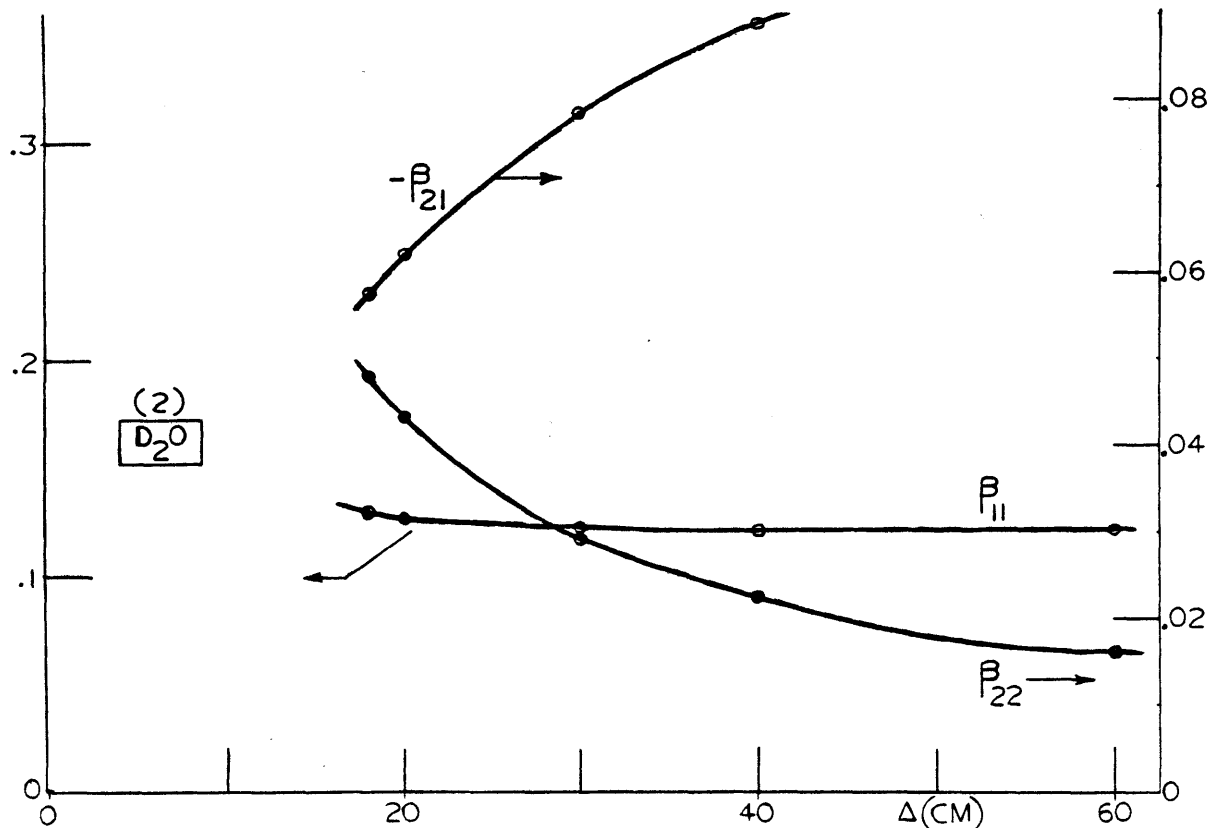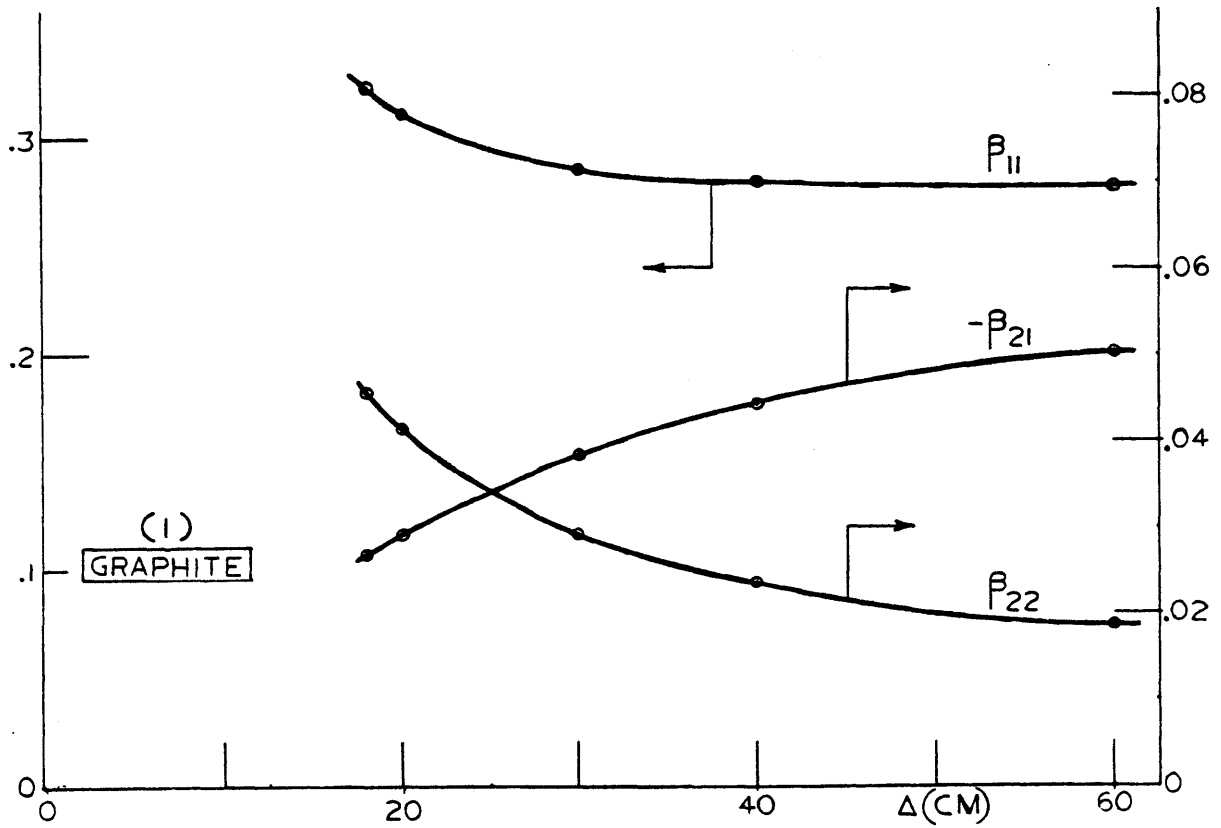
FIGURE 2.8 : INVERSE IMPEDANCES OF (1) GRAPHITE AND (2) D$_2$O VS.
REFLECTOR THICKNESS

55

ii) The two-group extension of the one-dimensional, <u>two-zone</u>

slab relation, Eq. (2.22), is:

$$
\begin{bmatrix} \phi_1 \\ \phi_2 \\ J_{1x} \\ J_{2x} \end{bmatrix}_{x=x_e} = \left[M_{i \to e} \right]_{groups=2} \cdot \left[M_{s \to i} \right]_{groups=2} \cdot \begin{bmatrix} \phi_1 \\ \phi_2 \\ J_{1x} \\ J_{2x} \end{bmatrix}_{x=x_s}
$$

(2.22)'

where the 4×4 matrix $[M_{s \to i}]_{groups} = 2$ is defined (in terms of the

physical and geometrical parameters of zone s) by the same

equation, (2.48), which defines $[M_{i \to e}]_{groups = 2}$ (in terms of the

parameters of zone R.).

If the face $x = x_e$ is an outer boundary, then:

$$
\phi_1(x_e) = \phi_2(x_e) = 0
$$

(2.18)'

and the first two of Eqs. (2.22)' can be shown to imply:

$$
\begin{bmatrix} \phi_1 \\ \phi_2 \end{bmatrix}_{x_s} = \begin{bmatrix} \alpha_{11} & 0 \\ \alpha_{21} & \alpha_{22} \end{bmatrix} \begin{bmatrix} J_{1x} \\ J_{2x} \end{bmatrix}_{x_s}
$$

(2.53)

56

where the static impedances of the composite (two-zone) slab[*] are

defined by:

$$\alpha_{gg} \equiv \frac{c_g^S \cdot S_g^R \cdot (L_g^R / D_g^R) + c_g^R \cdot S_g^S \cdot (L_g^S / D_g^S)}{(L_g^R / D_g^R) \cdot (D_g^S / L_g^S) \cdot S_g^S \cdot S_g^R + c_g^S \cdot c_g^R} \; ; \; g = 1,2$$

$$\alpha_{21} \equiv \alpha_{11} \cdot \Omega_1 - \alpha_{22} \cdot \Omega_2 \; ,$$

$$\Omega_1 \equiv \left[(c_1^S - c_2^S) \cdot r^S \cdot \frac{L_1^R}{D_1^R} \cdot S_1^R \; + \right.$$

$$+ \; c_2^S \cdot \frac{r^R}{D_1^R} \cdot (L_1^R \cdot S_1^R - L_2^R \cdot S_2^R) \; +$$

$$+ \; c_1^R \cdot \frac{r^S}{D_1^S} \cdot \left(L_1^S \cdot S_1^S - L_2^S \cdot S_2^S \right) \; +$$

$$+ \; (c_1^R - c_2^R) \cdot r^R \cdot \frac{L_2^S}{D_2^S} \cdot S_2^S \cdot \frac{D_2^R}{D_1^R} \left. \right] \Big/ \left[\begin{array}{c} \text{Numerator} \\ \text{of } \alpha_{11} \end{array} \right]$$

---

[*] For a Stainless stell-light water reflector (zone s: stainless steel,

Δ_s = 2.0 cm; zone R: light water, Δ_R = 18.0 cm), typical values

of the β_{gg}'s are:

$$\beta_{11} = \frac{1}{\alpha_{11}} = 0.1587,$$

$$\beta_{22} = \frac{1}{\alpha_{22}} = 0.1351.$$

(Two - group data of Table 5.2 used).

and

$$\Omega_2 \equiv \left[\left(\frac{S_1^S}{L_1^S} - \frac{S_2^S}{L_2^S} \right) \cdot r^S \cdot D_2^S \cdot S_1^R \cdot \frac{L_1^R}{D_1^R} + \right.$$

$$+ S_2^S \cdot \frac{r^R}{D_1^R} \cdot \frac{D_2^S}{L_2^S} \cdot \left(L_1^R \cdot S_1^R - L_2^R \cdot S_2^R \right) +$$

$$+ \left(c_1^S - c_2^S \right) \cdot r^S \cdot \frac{D_2^S}{D_1^S} \cdot c_1^R +$$

$$\left. + c_2^S \cdot \left(c_1^R - c_2^R \right) \cdot r^R \cdot \frac{D_2^R}{D_1^R} \right] \bigg/ \left[\begin{array}{c} \text{Denominator} \\ \text{of } \alpha_{11} \end{array} \right]$$

(2.54)

The quantities c_g^S, c_g^R, S_g^S, S_g^R, r^S and r^R are defined (without the superscripts) by Eqs. (2.49) - (2.51); the superscripts S and R refer to the two zones, S and R.

2.6 ON THE NATURE AND ORIGIN OF KIRCHHOFF'S FORMULA.

a)   Kirchhoff's formula expresses the flux in region A in terms of the boundary-flux and normal current. The latter two quantities are not independent of each other and cannot be both specified arbitrarily. Therefore, Kirchhoff's formula is not the solution of the diffusion equation in region A but simply a relation satisfied by the solution.

b)   The direct proof of the one-group Kirchhoff's formula rests

58

on two pillars: Green's funtion and Green's theorem.

The Green's function for the diffusion of one-group neutrons
in a homogeneous, non-multiplying medium of two dimensions is the
solution of:

$$\frac{\partial^2 \psi}{\partial x^2} + \frac{\partial^2 \psi}{\partial y^2} - \frac{1}{L^2} \cdot \psi = -2\pi \cdot \delta(\rho) \qquad (2.56)$$

where ρ is defined by Eq. (2.4).

It can be seen that if the medium occupies an infinite region,
then:

$$\psi \equiv K_0(\rho/L) \qquad (2.57)$$

Green's theorem in two dimensions reads:

$$\iint_A \left(\psi \nabla^2 \phi - \phi \nabla^2 \psi \right) dA =$$

$$= \int_\Gamma \left(-\psi \cdot \frac{\partial \phi}{\partial n} + \phi \cdot \frac{\partial \psi}{\partial n} \right) d\ell \qquad (2.58)$$

where: the two-dimensional functions ψ and ϕ must have continuous
first and second derivatives everywhere in the closed region A
and its boundary curve Γ and: $\partial/\partial n$ is taken toward the interior
of Γ.

The elimination of $\nabla^2 \phi$ and $\nabla^2 \psi$ from Eq. (2.58) with the help

of Eqs. (2.1) and (2.56) yields Kirchhoff's formula, Eq. (2.2).

c)   The proof of Kirchhoff's formula is not based on knowledge of the explicit functional form of the neutron flux in the region under consideration. The formula, therefore, provides a relation satisfied by the neutron flux regardless of the a priori availability or non-availability of analytical forms for the flux. The same argument is, of course, true for the boundary condition to which Kirchhoff's formula reduces, as the interior point (x,y) is allowed to approach and reach the boundary.

d)   In the one-dimensional slab reflector the flux can be expressed as:

$$\phi(x) = A \cdot \cosh\left(\frac{x}{L}\right) + C \cdot \sinh\left(\frac{x}{L}\right) \tag{2.59}$$

where A and C are constants. By starting from (2.59) and eliminating A and C in favor of the current at two points, x_i and x_e, one obtains (2.17) [L-3].

2.7   KIRCHHOFF'S FORMULA AS A SOURCE OF INFORMATION ABOUT THE FUNCTIONAL FORM OF THE FLUX IN REGION A.

a)   It can be easily seen that the functional form (2.59) for the flux in the one-dimensional slab reflector can be deduced from the Kirchhoff's formula for the same configuration, Eq. (2.15).

Indeed, Eq. (2.15) may be written as follows:

$$\phi(x) = A' \cdot \exp\left(-\frac{x}{L}\right) + C' \cdot \exp\left(\frac{x}{L}\right)$$

where:
<div align="right">(2.60)</div>

$$A' \equiv \frac{1}{2} \cdot \left[\phi(x_i) + \frac{L}{D} \cdot J_x(x_i)\right] \cdot \exp\left(-\frac{x_i}{L}\right)$$

and
<div align="right">(2.61)</div>

$$C' \equiv \frac{1}{2} \cdot \left[\phi(x_e) - \frac{L}{D} \cdot J_x(x_e)\right] \cdot \exp\left(-\frac{x_e}{L}\right)$$

<div align="right">(2.62)</div>

Eq. (2.60), in turn, takes the form (2.59) if the coefficients A' and C´ are expressed as:

$$A' \equiv \frac{A + C}{2}$$
<div align="right">(2.63)</div>

and

$$C' \equiv \frac{A - C}{2}$$
<div align="right">(2.64)</div>

b)   The functional form of the symmetrically distributed flux in a 90^0 - wedge-shaped reflector can be deduced from the corresponding Kirchhoff's formula.

Below we illustrate how this can be done.

The relevant Kirchhoff's formula (given by Eq. (2.28) if

the lim is omitted and ε is replaced by y) is:
$$\phi(x,y) = -\frac{1}{2\pi} \cdot \int_0^\infty \left\langle \phi(x',0) \cdot \frac{\partial}{\partial u} + \frac{1}{D} \cdot J_y(x',0) \right\rangle \cdot$$

$$\cdot \left[K_0\left(\frac{R_1}{L}\right) + K_0\left(\frac{R_2}{L}\right) \right]_{u=0} \cdot dx'$$

$$(2.65)$$

where
$$R_1^2 \equiv (x'-x)^2 + (u-y)^2 \quad (2.66)$$

and
$$R_2^2 \equiv (u-x)^2 + (x'-y)^2 \quad (2.67)$$

R_1^2 and R_2^2 may be written in the form:

$$\begin{cases} R_m^2 = (x^2+y^2) + (x'^2+u^2) - \\ \qquad - 2 \cdot \cos\beta_m \cdot \sqrt{x^2+y^2} \cdot \sqrt{x'^2+u^2} \quad ; \\ m = 1, 2 \end{cases}$$

$$(2.68)$$

where:

$$\cos\beta_1 \equiv \frac{xx' + uy}{\sqrt{x^2+y^2} \cdot \sqrt{x'^2+u^2}} \leqslant 1$$

$$(2.69$$

and

$$\cos\beta_2 \equiv \frac{yx' + ux}{\sqrt{x^2+y^2} \cdot \sqrt{x'^2+u^2}} \leq 1 \qquad (2.70)$$

Next we make use of the following integral representation for $K_0(R_1/L)$ and $K_0(R_2/L)$:

$$\begin{cases} K_0\left(\frac{R_m}{L}\right) = \frac{2}{\pi} \cdot \int_0^\infty \cosh\left[(\pi - \beta_m) \cdot p\right] \cdot K_{ip}\left(\frac{\sqrt{x^2+y^2}}{L}\right) \cdot \\ \qquad\qquad \cdot K_{ip}\left(\frac{\sqrt{x'^2+u^2}}{L}\right) \cdot dp \qquad\qquad (2.71) \\ \qquad m = 1, 2 \end{cases}$$

The substitution of (2.71) into (2.65) and the subsequent interchange of the order of the two integrations, $\int_0^\infty dx' \ldots$ and $\int_0^\infty dp \ldots$, lead to:

$$\phi(x,y) = -\frac{1}{\pi^2} \cdot \int_0^\infty K_{ip}\left(\frac{\sqrt{x^2+y^2}}{L}\right) \cdot$$

$$\cdot \left[\int_0^\infty \left\{ \left\langle \phi(x',0) \cdot \frac{\partial}{\partial u} + \frac{1}{D} \cdot J_y(x',0) \right\rangle \cdot \right.\right.$$

(Continued)

63

$$\cdot \left(\sum_{m=1}^{2} \cosh\left[(\pi - \beta_m)p\right]\right) \cdot K_{ip}\left(\frac{\sqrt{x'^2 + u^2}}{L}\right) \Bigg\}_{u=0} \cdot dx' \Bigg] dp$$

$$(2.72)$$

The quantity $\{ \ldots \}_{u=0}$, which appears in (2.72), can be reduced to the form:

$$\{ \ldots \}_{u=0} = \cosh(\theta \cdot p) \cdot F(p, x') \qquad (2.73)$$

where

$$\theta \equiv -\left(\pi - \beta_1\Big|_{u=0}\right) + \frac{3\pi}{4} = \left(\pi - \beta_2\Big|_{u=0}\right) - \frac{3\pi}{4}$$

$$(2.74)$$

and

$$F(p, x') \equiv \cosh\left(\frac{3\pi}{4} \cdot p\right) \cdot \left\langle \phi(x', 0) \cdot \frac{\partial}{\partial u} + \right.$$

$$+ \frac{1}{D} \cdot J_y(x', 0) \Bigg\rangle \cdot K_{ip}\left(\frac{\sqrt{x'^2 + u^2}}{L}\right)\Bigg|_{u=0} +$$

$$+ \sinh\left(\frac{3\pi}{4} \cdot p\right) \cdot \phi(x', 0) \cdot \frac{p}{x'} \cdot K_{ip}\left(\frac{x'}{L}\right)$$

$$(2.75)$$

64

Eq. (2.73) is substituted into (2.72) to yield the following functional form for the flux:

$$\Phi(x,y) = \int_0^\infty A(p) \cdot \cosh(\theta \cdot p) \cdot K_{ip}\left(\frac{\sqrt{x^2+y^2}}{L}\right) \cdot dp$$

(2.76)

where:
$$A(p) \equiv -\frac{1}{\pi^2} \cdot \int_0^\infty F(p, x') \, dx'$$

(2.77)

The independent variables $\sqrt{x^2+y^2}$ and Θ employed in the right hand side of (2.76) define a polar coordinate system with the origin located at (x=0, y=0) and the Θ=0-axis aligned with the axis of symmetry (x=y) of the wedge.

c)   The functional form of the symmetrically distributed flux in a 90^0- elbow-shaped reflector of thickness Δ can be deduced from the corresponding Kirchhoff's formula.

To this end, the Cartesian coordinate system, (x,y), of Section 2.4 is supplemented with a second Cartesian coordinate system, $(\hat{x},\hat{y})$ defined by:

$$\hat{x} \equiv x - \Delta \quad , \quad \hat{y} \equiv y - \Delta$$

(2.78)

65
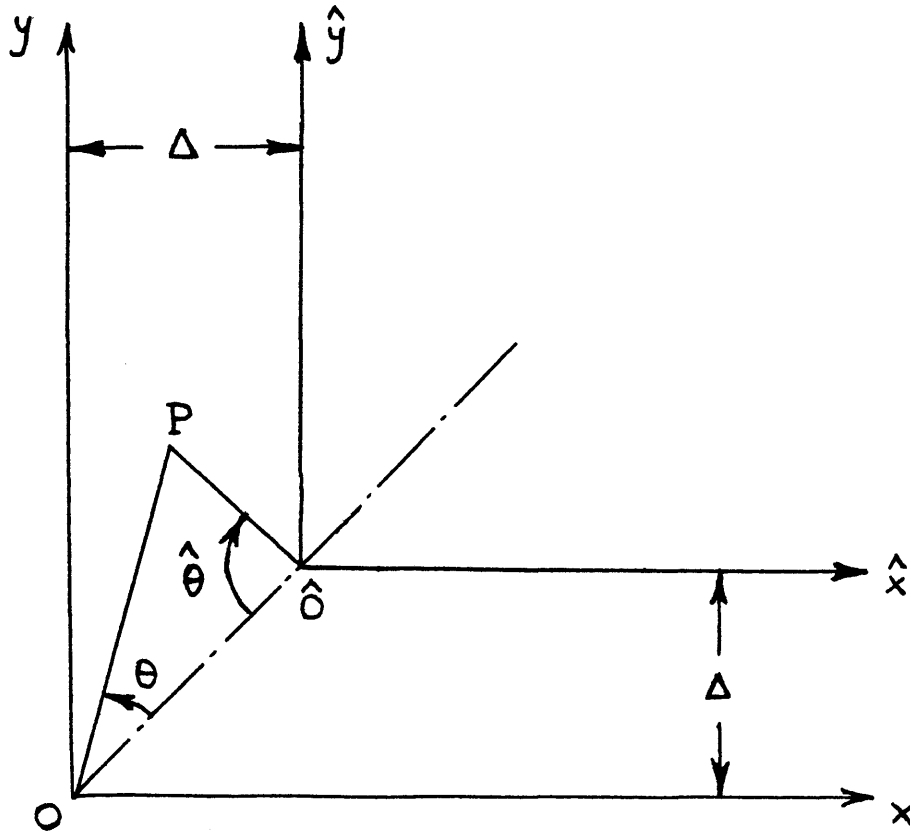
Figure 2.9

Double Coordinate System

Employed for the Analytical Expression of the Flux in a Right -

Angled Elbow.

(I.e. $(\hat{x},\hat{y})$ is the result of translation of (x,y) by the amount "(Δ,Δ). See Figure 2.9).

The relevant Kirchhoff's formula is given by Eq. (2.30).

By virtue of the formulation (2.76),

$$
I^{oa} - I^{oc} =
$$
$$
= \int_0^\infty A(p) \cdot \cosh(\theta \cdot p) \cdot K_{ip}\left(\frac{\sqrt{x^2+y^2}}{L}\right) dp
$$

(2.79)

and

$$
I^{eb} - I^{ed} =
$$
$$
= \int_0^\infty \hat{A}(p) \cdot \cosh(\hat{\theta} \cdot p) \cdot K_{ip}\left(\frac{\sqrt{\hat{x}^2+\hat{y}^2}}{L}\right) dp
$$

(2.80)

where:

67

(i) the definition of $\hat{\Theta}$ in terms of $\hat{x}$ and $\hat{y}$ is the same as that of Θ in terms of x and y; i.e.

$$\Theta \equiv \arccos\left(\frac{y}{\sqrt{x^2+y^2}}\right) - \frac{\pi}{4} \qquad (2.81)$$

$$\hat{\Theta} \equiv \arccos\left(\frac{\hat{y}}{\sqrt{\hat{x}^2+\hat{y}^2}}\right) - \frac{\pi}{4} =$$

$$= \arccos\left(\frac{y-\Delta}{\sqrt{(x-\Delta)^2+(y-\Delta)^2}}\right) - \frac{\pi}{4}$$

$$(2.82)$$

and (ii) the definition of $\hat{A}(p)$ in terms of $\hat{x}'$ is the same as that of $A(p)$ in terms x'.

Hence,

$$\phi(x,y) =$$

$$= \int_0^\infty A(p)\cdot\cosh(\Theta\cdot p)\cdot K_{ip}\left(\frac{\sqrt{x^2+y^2}}{L}\right)\cdot dp -$$

$$- \int_0^\infty \hat{A}(p)\cdot\cosh(\hat{\Theta}\cdot p)\cdot K_{ip}\left(\frac{\sqrt{(x-\Delta)^2+(y-\Delta)^2}}{L}\right)\cdot dp$$

$$(2.83)$$

68

2.8 GENERALIZED KIRCHHOFF'S FORMULA.

Let us apply Green's theorem with the following pair of functions:

$\Phi(x,y)$; solution of (2.1) in region A

and

$\Psi(x,y)$; Solution of (2.56) in a region A', which includes A.

The corresponding generalized version of Kirchhoff's formula reads:

$$\Phi(x,y) = \frac{1}{2\pi} \cdot \int_{\Gamma} \left[\Phi(x',y') \cdot \frac{\partial}{\partial n} \Psi(x,y) + \frac{1}{D} \cdot J_n(x',y') \cdot \Psi(x,y) \right] d\ell$$

(2.84)

Eq. (2.84) is mathematically equivalent to the original Kirchhoff's formula, Eq. (2.2). Furthermore, depending on the choice of the region A' and on the conditions satisfied by the function ψ on the boundary of A', Eq. (2.84) can be simpler in form than Eq. (2.2).

69

E x a m p l e s.

(a) Region A: One-dimensional slab (Fig. 2.2): $x_i \leq x \leq x_e$.

Region A': Semi-infinite, one-dimensional slab, occupying the space <u>to the left</u> of the line $x = x_e$.

Boundary condition for ψ: it vanishes at $x = x_e$.

The functional form for ψ in the above region and with the above boundary condition is found by the method of images [C-1]:

$$\psi = K_0 \left(\frac{1}{L} \cdot \sqrt{y'^2 + (x - x')^2} \right) - $$

$$- K_0 \left(\frac{1}{L} \cdot \sqrt{y'^2 + (2x_e - x - x')^2} \right),$$

where $x' = x_i , x_e$

(2.85)

Note that ψ, as defined by (2.85), vanishes for $x' = x_e$.

With the above selection for ψ, Eq. (2.84) becomes:

$$\phi(x) =$$

$$= \frac{1}{2\pi} \cdot \left[\phi(x') \cdot \frac{\partial}{\partial n} + \frac{1}{D} \cdot J_n(x') \right] \cdot \int_{-\infty}^{+\infty} \psi \, dy' \bigg|_{x' = x_i} -$$

$$- \frac{1}{2\pi} \cdot \phi(x') \cdot \frac{\partial}{\partial n} \int_{-\infty}^{+\infty} \psi \, dy' \bigg|_{x' = x_e} \qquad (2.86)$$

where

$$\int_{-\infty}^{+\infty} \psi \, dy' = L \cdot \pi \cdot \left\langle \exp\left(-\frac{|x - x'|}{L}\right) - \right.$$

$$\left. - \exp\left(-\frac{|2x_e - x - x'|}{L}\right) \right\rangle \quad (2.87)$$

After the differentiations indicated in (2.86) are carried out and the resulting equation is evaluated at $x = x_i$, the first row of Eq. (2.17) results.[*]

---

[*]Eq. (2.86) becomes an identity, when evaluated at $x = x_e$.

71

We see that by using Eq. (2.84) and selecting Ψ as given by Eq. (2.85) we _avoid the rearrangement_ which, in the treatment of Section 2.2, follows the evaluation of Eq. (2.15) at $x = x_i$. This rearrangement is easy in the present example because it consists of algebraic manipulations. It is not as easy when _integral equations_ are to be rearranged/solved (see next example).

(b)   Region A: 90^0-wedge (Fig. 2.4).

   Region A': Coincides with Region A.

   Boundary condition for ψ: $\partial \psi / \partial n$ vanishes along the boundary Γ of a region A'.

   The functional form for ψ in region A' with the above boundary condition is found by the method of images[C-1]:

$$\Psi = K_0 \left(\frac{1}{L} \sqrt{(y-y')^2 + (x-x')^2} \right) +$$

$$+ K_0 \left(\frac{1}{L} \sqrt{(-y-y')^2 + (x-x')^2} \right) +$$

$$+ K_0 \left(\frac{1}{L} \sqrt{(-y-y')^2 + (-x-x')^2} \right) +$$

$$+ K_0 \left(\frac{1}{L} \sqrt{(y-y')^2 + (-x-x')^2} \right)$$

$$(2.88)$$

With ψ defined by (2.88), the derivative $\partial \psi / \partial n$ vanishes along the positive semi-axes x' and y'.

Eq. (2.84) becomes:

$$\phi(x,y) = \frac{1}{2\pi} \cdot \int_{\Gamma} \frac{1}{D} \cdot J_n(x',y') \cdot \psi \cdot d\ell =$$

$$= \frac{1}{2\pi} \cdot \frac{1}{D} \cdot \left\langle \int_0^{\infty} J_x(0,y') \cdot \psi \bigg|_{x'=0} \cdot dy' - \int_0^{\infty} J_y(x',0) \cdot \psi \bigg|_{y'=0} \cdot dx' \right\rangle$$

$$(2.89)$$

Suppose, for simplicity, that the neutron distribution in the 90^0-wedge is symmetric with respect to the line $x = y$. Then,

$$J_y(x',0) = - J_x(0,y') \qquad (2.90)$$

and Eq. (2.89) simplifies to:

73

$$\phi(x,y) = \frac{1}{\pi D} \cdot \int_0^\infty J_x(0,y') \cdot \left\langle K_0\left(\frac{1}{L}\sqrt{(y-y')^2+x^2}\right) + \right.$$

$$+ K_0\left(\frac{1}{L}\sqrt{(-y-y')^2+x^2}\right) +$$

$$+ K_0\left(\frac{1}{L}\sqrt{y^2+(x-y')^2}\right) +$$

$$\left. + K_0\left(\frac{1}{L}\sqrt{y^2+(-x-y')^2}\right)\right\rangle dy'$$

(2.91)

If we let $x \to 0$, Eq. (2.91) becomes:

$$\phi(x,y) = \frac{1/\pi}{D/L} \cdot \int_0^\infty J_x(0,y') \cdot \left\langle K_0\left(\frac{|y-y'|}{L}\right) + \right.$$

$$\left. + K_0\left(\frac{y+y'}{L}\right) + 2\cdot K_0\left(\frac{\sqrt{y^2+y'^2}}{L}\right)\right\rangle \cdot d\left(\frac{y'}{L}\right)$$

(2.92)

<u>This last equation is equivalent to Eq. (2.28)</u>. It is also

simpler than (2.28). The mathematical operations which rearrange

(2.28) in the form (2.92) are bypassed with the use of Eqs. (2.84)

and (2.88).

74

Having given the above two applications of the generalized Kirchhoff's formula, we make a few general comments.

i) The generalized Kirchhoff's formula, Eq. (2.84), reduces to the original Kirchhoff's formula, Eq. (2.2), if the region A' is taken to extend over the entire x - y plane.

ii) By choosing the function ψ to vanish along a part Γ_i of the boundary Γ of region A, we eliminate from the generalized Kirchhoff's formula the values of the normal current, J_n, along Γ_i.

iii) By choosing $\partial \psi / \partial n$ to vanish along Γ_i, we eliminate from the generalized Kirchhoff's formula the values of the flux, Φ, along Γ_i.

iv) The function ψ, which satisfies: $\psi = 0$ or $\partial \psi / \partial n = 0$ on a certain boundary, is readily available only when the form of the boundary is sufficiently simple. Thus, the availability of an expression for ψ imposes an upper bound on the complexity of the geometrical shape of the region (A') over which we define ψ.

v) As a consequence of (iv), a continuous increase in the complexity of region A cannot be accompanied by a continuous increase in the complexity of region A'; the shape of A' must be simple. It follows that the simplification of (2.84) relative to (2.2) diminishes as region A becomes more and more complex.

75

vi) For sufficiently simple regions A, therefore, the general-
ized Kirchhoff's formula is an improvement over the original
Kirchhoff's formula, because it offers a savings in mathematical
manipulations (of integral equations, in general).

vii) For more complex regions A, however, the savings offered by
the generalized formula is relatively small, because both the
generalized and the original formula are complicated.

viii) The method of images works for point sources located inside
angles of magnitude π/m, where m is an integer, but breaks down
for angles of magnitude $n.\pi/m$, where m and n are integers, prime
to each other. The reason for the failure is that one or more
image-point sources, located inside the angle, are required by
the method for the above mentioned values of the angle in order
to create the desired zero-flux or zero-normal current condition
along the boundaries of the angle. Image-sources inside the angle
are, of course, unacceptable.

ix) An extension of the method of images devised by Sommerfeld
[S-2] and modified by Carslaw [C-1] allows for the evaluation of
Green's function, solution of Eq. (2.56), in a wedge of any angle.

III. THE WEDGE-SHAPED REFLECTOR.

3.1 BOUNDARY CONDITION FOR ONE ENERGY GROUP.

Suppose we have a two-dimensional reflector in the shape of a angle $2\Theta_0$ ($0 < \Theta_0 < \pi$). We take a polar coordinate system, (r,Θ), with the origin at the peak of the wedge and the axis for measurement of Θ on the axis of symmetry of the wedge, as shown in Figure (3.1).
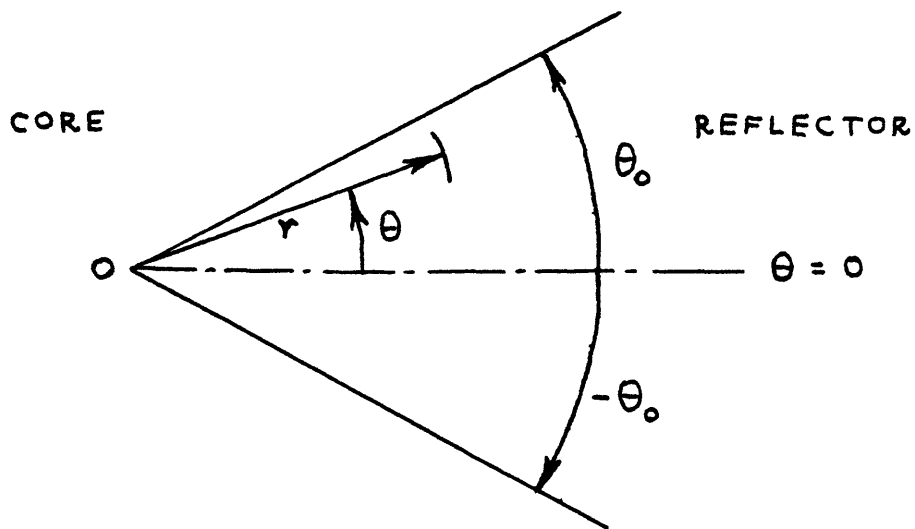
Figure 3-1

A Wedge - Shaped Reflector of Angle $2\Theta_0$

The steady-state diffusion equation for one-energy-group neutrons reads in polar coordinates as follows:

$$\frac{\partial^2 \phi}{\partial r^2} + \frac{1}{r} \cdot \frac{\partial \phi}{\partial r} + \frac{1}{r^2} \cdot \frac{\partial^2 \phi}{\partial \theta^2} - \frac{1}{L^2} \cdot \phi = 0 \qquad (3.1)$$

where

$\Phi = \Phi(r, \theta)$ is the neutron flux and

L is the neutron diffusion length.

We can easily verify that Eq. (3.1) is satisfied by the functional forms:

$$\cosh(\theta p) \cdot K_{ip}\left(\frac{r}{L}\right) \qquad \text{and} \qquad \sinh(\theta p) \cdot K_{ip}\left(\frac{r}{L}\right) \qquad (3.2)$$

where: p is a real parameter and

K_{ip} is the modified Bessel function of imaginary order.[*]

---

[*] $K_{ip}(\xi)$ satisfies the following differential equation:

$$\frac{d^2 K}{d\xi^2} + \frac{1}{\xi} \cdot \frac{dK}{d\xi} - \left(1 - \frac{p^2}{\xi^2}\right) \cdot K = 0 \qquad (3.3)$$

The integral representation:

$$K_{ip}(\xi) = \int_0^\infty e^{-\xi \cdot \cosh t} \cdot \cos(pt)\, dt \quad (3.4)$$

shows that the function $K_{ip}(\xi)$ and hence the functional forms (3.2) vanish at large distances from the origin.

Now we synthesize the general solution of Eq. (3.1) in the form [S-1]:

$$\phi(\frac{r}{L}, \theta) = \int_0^\infty \left[A(p) \cdot \cosh(\theta p) + C(p) \cdot \sinh(\theta p) \right] \cdot K_{ip}(\frac{r}{L})\, dp$$

$$(3.5)$$

where A(p) and C(p) are two functions depending on the boundary conditions imposed on the flux and current.

On physical grounds, the neutron flux must vanish at large distances from the origin. Expression (3.5) does so, because it is a superposition of components which do vanish at large distances from the origin.

We are interested to find a relation between flux and normal current at the boundary of the wedge. Since the boundary is an

79

iso - Θ line, the direction normal to the boundary is the Θ - direction.

The Θ - direction component of the neutron current is defined by:

$$J_\theta(r, \theta) \equiv -\frac{D}{r} \cdot \frac{\partial \phi(r, \theta)}{\partial \theta} \qquad (3.6)$$

where D is the diffusion coefficient of the reflector.

We operate on Eq. (3.5) with $-\frac{D}{r} \cdot \frac{\partial}{\partial \theta}$ and obtain:

$$J_\theta\left(\frac{r}{L}, \theta\right) = -\frac{D}{r} \cdot \int_0^\infty p \cdot \left[A(p) \cdot \sinh(\theta p) + C(p) \cdot \cosh(\theta p) \right] \cdot K_{ip}\left(\frac{r}{L}\right) dp \qquad (3.7)$$

Next we eliminate the functions A(p) and C(p) between Eqs. (3.5) and (3.7). To this and, we express A(p) and C(p) in terms of the distributions of the normal current along the two boundaries.

Eq. (3.7) is of the form:

$$\frac{r}{L} \cdot J_\theta\left(\frac{r}{L}, \theta\right) = \int_0^\infty M(p, \theta) \cdot K_{ip}\left(\frac{r}{L}\right) dp \qquad (3.8)$$

80

where:

$$M(p,\theta) \equiv -\frac{D}{L} \cdot p \cdot \left[A(p) \cdot \sinh(\theta p) + C(p) \cdot \cosh(\theta p) \right]$$

(3.9)

Formally, Eq. (3.8) is the integral expansion of the function $\frac{r}{L} \cdot J_\theta \left(\frac{r}{L}, \theta \right)$ with respect to r/L in terms of the function $K_{ip}(r/L)$. The amplitude function $M(p,\theta)$ for such an expansion is given by the following formula due to N.N. Lebedev[*]:

$$M(p,\theta) = \frac{2}{\pi^2} \cdot p \cdot \sinh(\pi p) \cdot \int_0^\infty J_\theta(\xi,\theta) \cdot K_{ip}(\xi) \, d\xi$$

(3.10)

We equate the right hand sides of Eqs. (3.9) and (3.10) and obtain:

$$-\frac{D}{L} \cdot \left[A(p) \cdot \sinh(\theta p) + C(p) \cdot \cosh(\theta p) \right] =$$

$$= \frac{2}{\pi^2} \cdot \sinh(\pi p) \cdot \int_0^\infty J_\theta(\xi,\theta) \cdot K_{ip}(\xi) \, d\xi$$

(3.11)

---

[*] See references [S-1], [M-1], [L-1] and [L-2].

81

By evaluating Eq. (3.11) at $\Theta = \pm \Theta_0$ we get two different linear combinations of $A(p)$ and $C(p)$. We rearrange the two relations so that they read:

$$A(p) = - \frac{1/\pi^2}{D/L} \cdot \frac{\sinh(\pi p)}{\sinh(\theta_o p)} \cdot \int_0^\infty \left[J_\theta(\xi, \theta_o) - \right.$$

$$\left. - J_\theta(\xi, -\theta_o) \right] \cdot K_{ip}(\xi) d\xi$$

$$C(p) = - \frac{1/\pi^2}{D/L} \cdot \frac{\sinh(\pi p)}{\cosh(\theta_o p)} \cdot \int_0^\infty \left[J_\theta(\xi, \theta_o) + \right.$$

$$\left. + J_\theta(\xi, -\theta_o) \right] \cdot K_{ip}(\xi) d\xi \tag{3.12}$$

We substitute Eqs. (3.12) into Eq. (3.5) and evaluate the resulting equation at $\Theta = \pm \Theta_0$. Thus we obtain:

$$\phi\left(\frac{r}{L}, \pm \theta_o\right) =$$

$$= - \frac{1/\pi^2}{D/L} \cdot \int_0^\infty \left[J_\theta(\xi, +\theta_o) \cdot R_{\pm\theta_o}\left(\xi, \frac{r}{L}\right) - \right.$$

$$\left. - J_\theta(\xi, -\theta_o) \cdot Q_{\pm\theta_o}\left(\xi, \frac{r}{L}\right) \right] d\xi$$

$$\tag{3.13}$$

where:

$$(3.14)$$

$$
\begin{bmatrix} R_{\pm\theta_0} \\ Q_{\pm\theta_0} \end{bmatrix} \equiv
$$

$$
\equiv \int_0^\infty K_{ip}(\xi) \cdot K_{ip}\left(\frac{r}{L}\right) \cdot \sinh(\pi p) \cdot \begin{bmatrix} \dfrac{1}{\tanh(\theta_0 p)} \pm \tanh(\theta_0 p) \\[2ex] \dfrac{-1}{\tanh(\theta_0 p)} \pm \tanh(\theta_0 p) \end{bmatrix} dp
$$

Equivalently, we write Eq. (3.13) in terms of the <u>asymmetry current</u>, $J_a\left(\frac{r}{L}, \theta_0\right)$, defined by:

$$
J_a\left(\frac{r}{L}, \theta_0\right) \equiv J_\theta\left(\frac{r}{L}, \theta_0\right) + J_\theta\left(\frac{r}{L}, -\theta_0\right) \quad (3.15)
$$

Eq. (3.13) becomes:

$$
\phi\left(\frac{r}{L}, \pm\theta_0\right) =
$$

$$
= -\frac{2/\pi^2}{D/L} \cdot \int_0^\infty \left\langle J_\theta(\xi, \pm\theta_0) \cdot G_{\theta_0}\left(\xi, \frac{r}{L}\right) + \right.
$$

$$
\left. + \frac{1}{2} \cdot J_a(\xi, \theta_0) \cdot Q_{+\theta_0} \right\rangle d\xi
$$

$$(3.16)$$

83

where:

$$G_{\theta_0}\left(\xi, \frac{r}{L}\right) \equiv \frac{1}{2} \cdot \left[R_{+\theta_0} - Q_{+\theta_0}\right] =$$

$$= \int_0^\infty K_{ip}(\xi) \cdot K_{ip}\left(\frac{r}{L}\right) \cdot \frac{\sinh(\pi p)}{\tanh(\theta_0 p)} \cdot dp \qquad (3.17)$$

In the special case where the neutron distribution is symmetric with respect to the axis $\theta = 0$, the asymmetry current vanishes and Eq. (3.16) reduces to:

$$\phi\left(\frac{r}{L}, \theta_0\right) = -\frac{2/\pi^2}{D/L} \cdot \int_0^\infty J_\theta(\xi, \theta_0) \cdot G_{\theta_0}\left(\xi, \frac{r}{L}\right) d\xi$$

$$(3.18)$$

3.2 EVALUATION OF THE KERNEL $G_\theta\left(\xi, \frac{r}{L}\right)$ FOR THE WEDGES OF ANGLES $2\theta_0 = 180^0$, 90^0 AND 270^0.

(a) $2\theta_0 = 180^0$.

From Eq. (3.17) we get:

84

$$G_{\frac{\pi}{2}}\left(\xi, \frac{r}{L}\right) =$$

$$= \int_0^\infty K_{ip}(\xi) \cdot K_{ip}\left(\frac{r}{L}\right) \cdot \frac{\sinh(\pi p)}{\tanh\left(\frac{\pi}{2}p\right)} \cdot dp \qquad (3.19)$$

We use the identity:

$$\frac{\sinh(\pi p)}{\tanh\left(\frac{\pi}{2}p\right)} = 1 + \cosh(\pi p) \qquad (3.20)$$

and the integral formula:

$$\int_0^\infty K_{ip}(\xi) \cdot K_{ip}\left(\frac{r}{L}\right) \cdot \cosh\left[(\pi - \phi)p\right] \cdot dp =$$

$$= \frac{\pi}{2} \cdot K_0\left(\sqrt{\xi^2 + \left(\frac{r}{L}\right)^2 - 2 \cdot \xi \cdot \frac{r}{L} \cdot \cos\phi}\right)$$

$$(3.21)$$

85

to find:

$$G_{\frac{\pi}{2}}\left(\xi, \frac{r}{L}\right) = \frac{\pi}{2} \cdot \left\{ K_0\left(\xi + \frac{r}{L}\right) + K_0\left(\left|\xi - \frac{r}{L}\right|\right) \right\}$$

(3.22)

(b) $2\Theta_0 = 90^0$.

From Eq. (3.17) we get:

$$G_{\frac{\pi}{4}}\left(\xi, \frac{r}{L}\right) =$$

$$= \int_0^\infty K_{ip}(\xi) \cdot K_{ip}\left(\frac{r}{L}\right) \cdot \frac{\sinh(\pi p)}{\tanh\left(\frac{\pi}{4}p\right)} \cdot dp$$

(3.23)

We use the identity:

$$\frac{\sinh(\pi p)}{\tanh\left(\frac{\pi}{4}p\right)} = 1 + \cosh(\pi p) + 2 \cdot \cosh\left(\frac{\pi}{2}p\right)$$

(3.24)

and the integral formula (3.21) to find:

86

$$G_{\frac{\pi}{4}}\left(\xi,\frac{r}{L}\right) = \frac{\pi}{2}\cdot\left\{K_0\left(\xi+\frac{r}{L}\right) + K_0\left(\left|\xi-\frac{r}{L}\right|\right) + \right.$$

$$\left. + 2\cdot K_0\left(\sqrt{\xi^2+\left(\frac{r}{L}\right)^2}\right)\right\} \qquad (3.25)$$

c) $2_{\theta_0} = 270.^0$

A general, series expression, Eq. (A.27), of G_{θ_0} for an arbitrary value of the angle Θ_0 is derived by means of contour integration in Appendix A. By evaluating Eq. (A.27) at $\Theta_0 = 3\pi/4$ and solving for G_{θ_0} we get:

$$G_{\frac{3\pi}{4}}\left(\xi,\frac{r}{L}\right) = \frac{2\pi}{3}\cdot I_0(\xi)\cdot K_0\left(\frac{r}{L}\right) +$$

$$+ \frac{4\pi}{3}\cdot\sum_{n=1}^{\infty} I_{\frac{4n}{3}}(\xi)\cdot K_{\frac{4n}{3}}\left(\frac{r}{L}\right) \qquad (3.26)$$

Eq. (3.26) is valid for $\xi < \frac{r}{L}$.

For values $\xi > \frac{r}{L}$, the kernel $G_{3\pi/4}$ is given by Eq. (3.26) with the roles of ξ and r/L interchanged.

87

3.3 RE-DERIVATION OF THE ONE-DIMENSIONAL BOUNDARY CONDITION FOR THE SEMI-INFINITE SLAB.

A semi-infinite slab occupying on the cartesian x-y plane the space:

$$x \geq x_i$$

may be viewed as a wedge with its peak at the origin and its edges coinciding with the semi - axes: $\{x = x_i, \quad y > 0\}$ and $\{x = x_i, \quad y < 0\}$. Furthermore, a one-dimensional - independent of y - distribution of neutrons <u>in the slab</u> may be viewed as a special-featured distribution of neutrons <u>in the wedge</u>, the special features being:

(i) symmetry with respect to the semi-axis $\{x > x_i, \quad y = 0\}$ and

(ii) constancy of flux and normal current along the edges of the wedge.

For the above reasons, we expect to be able to deduce the flux-current relation for the one-dimensional, semi-infinete slab, Eq. (2.20), from the "symmetrical" formula for the wedge, Eq. (3.18), by:

(a) taking the constant J_θ out of the integral:

88

$$\phi\left(\frac{r}{L}, \frac{\pi}{2}\right) =$$

$$= -\frac{2/\pi^2}{D/L} \cdot J_\theta\left(\frac{r}{L}, \frac{\pi}{2}\right) \cdot \int_0^\infty G_{\frac{\pi}{2}}\left(\xi, \frac{r}{L}\right) d\xi \, ,$$

(b) substituting for $G_{\frac{\pi}{2}}$ the expression (3.22):

$$\phi\left(\frac{r}{L}, \frac{\pi}{2}\right) =$$

$$= -\frac{1/\pi}{D/L} \cdot J_\theta\left(\frac{r}{L}, \frac{\pi}{2}\right) \cdot \int_0^\infty \left[K_0\left(\xi + \frac{r}{L}\right) + K_0\left(\left|\xi - \frac{r}{L}\right|\right)\right] d\xi ,$$

(c) evaluating the resulting integral:

$$\int_0^\infty \left[K_0\left(\xi + \frac{r}{L}\right) + K_0\left(\left|\xi - \frac{r}{L}\right|\right)\right] d\xi = \pi$$

so that

$$\phi\left(\frac{r}{L}, \frac{\pi}{2}\right) = -\frac{L}{D} \cdot J_\theta\left(\frac{r}{L}, \frac{\pi}{2}\right) ,$$

(d) changing coordinates from polar to cartesian:

$$\phi(x_i, y) = + \frac{L}{D} \cdot J_x(x_i, y) \quad \text{and}$$

(e) dropping the superfluous notation of a y-dependence.

We indeed obtain Eq. (2.20)

3.4 A SIMPLE, APPROXIMATE BOUNDARY CONDITION FOR THE 90^0 - WEDGE.

By inspecting the expression for the kernel $G_{\frac{\pi}{4}}(\xi, \frac{r}{L})$, Eq. (3.25), we identify a feature which motivates an approximation/ simplification of the exact, "symmetrical" boundary condition for the 90^0 - wedge, Eq. (3.18). The feature is the resonance-like behavior of $G_{\frac{\pi}{4}}$ at the value $\xi = \frac{r}{L}$ and, if r is sufficiently small, at $\xi = 0$.

(i) At $\xi = \frac{r}{L}$, $G_{\frac{\pi}{4}}$ exhibits a peak of infinite height, due to the term:

$$K_0\left(\left|\xi - \frac{r}{L}\right|\right).$$

The (two-sided) width of the peak is, roughly, 4L.

(ii) At $\xi = 0$ and r less than about 2L, $G_{\frac{\pi}{4}}$ exhibits a peak due to the sum:

$$K_o \left(\xi + \frac{r}{L} \right) + K_o \left(\sqrt{\xi^2 + \left(\frac{r}{L} \right)^2} \right) \; .$$

The height of the peak decreases as r increases; for $r = 0$ the height is infinite and for $r \gtrsim 2L$ it is practically zero. The (one-sided) width of the peak has an upper bound of about 2L for all relevant values of r; the upper bound is attained when $r = 0$.

From (i) and (ii) above we recognize that for the values of r for which the peak at $\xi = 0$ is non-negligible, the width of the peaks overlap. This fact motivates the following approximation:

If J_θ varies very slowly along the boundary of the 90^0 - wedge over an interval centered at r and about 4L wide, then we can write:

$$J_\theta \left(\xi, \theta_o \right) \cong J_\theta \left(\frac{r}{L}, \theta_o \right) \qquad\qquad (3.30)$$

91

(3.30) is a zero-order-truncated Taylor series expansion of J_Θ with respect to ξ about the value $\xi = \frac{r}{L}$.

If we substitute (3.30) into Eq. (3.18), J_Θ no more depends on ξ and we take it out of the integral. We carry out the remaining integration of the kernel $G_{\frac{\pi}{4}}(\xi, \frac{r}{L})$ with respect to ξ from 0 to ∞:

$$\int_0^\infty G_{\frac{\pi}{4}}\left(\xi, \frac{r}{L}\right) d\xi = \frac{\pi^2}{2} \cdot \left\{ 1 + \exp\left(-\frac{r}{L}\right) \right\} \quad (3.31)$$

and obtain:

$$\phi\left(\frac{r}{L}, \frac{\pi}{4}\right) \cong -\frac{L}{D} \cdot \left\{ 1 + \exp\left(-\frac{r}{L}\right) \right\} \cdot J_\Theta\left(\frac{r}{L}, \frac{\pi}{4}\right)$$

$$(3.32)$$

3.5 BOUNDARY CONDITIONS FOR TWO ENERGY GROUPS.

The extension of Eq. (3.16) for two energy groups reads:

92

$$\Phi_1\left(\frac{r}{L_1}, \pm\theta_0\right) =$$

$$= -\frac{2}{\pi^2} \cdot \frac{L_1}{D_1} \cdot \int_0^\infty \left[J_{1\theta}(\xi, \pm\theta_0) \cdot G_{\theta_0}\left(\xi, \frac{r}{L_1}\right) + \right.$$

$$\left. + \frac{1}{2} \cdot J_{1a}(\xi, \pm\theta_0) \cdot Q_{+\theta_0}\left(\xi, \frac{r}{L_1}\right) \right] d\xi$$

$$\text{(3.33)}$$

and

$$\Phi_2\left(\frac{r}{L_1}, \frac{r}{L_2}, \pm\theta_0\right) =$$

$$= -\frac{2}{\pi^2} \cdot \int_0^\infty \left[\frac{L_2}{D_2} \cdot \left\langle J_{2\theta}(\xi, \pm\theta_0) \cdot G_{\theta_0}\left(\xi, \frac{r}{L_2}\right) + \right.\right.$$

$$\left. + \frac{1}{2} \cdot J_{2a}(\xi, \pm\theta_0) \cdot Q_{+\theta_0}\left(\xi, \frac{r}{L_2}\right) \right\rangle +$$

$$+ \frac{\Sigma_{1\to2}/(D_1 D_2)}{\frac{1}{L_2^2} - \frac{1}{L_1^2}} \cdot \left\langle J_{1\theta}(\xi, \pm\theta_0) \cdot \left\{ L_1 \cdot G_{\theta_0}\left(\xi, \frac{r}{L_1}\right) - \right.\right.$$

$$\left. - L_2 \cdot G_{\theta_0}\left(\xi, \frac{r}{L_2}\right) \right\} +$$

$$\left. + \frac{1}{2} \cdot J_{1a}(\xi, \theta_0) \cdot \left\{ L_1 \cdot Q_{+\theta_0}\left(\xi, \frac{r}{L_1}\right) - L_2 \cdot Q_{+\theta_0}\left(\xi, \frac{r}{L_1}\right) \right\} \right\rangle \right] d\xi$$

$$\text{(3.34)}$$

In Eqs. (3.33) and (3.34) the subscripts 1 and 2 serve to distinguish between the two energy groups; otherwise the notation is that of Section 3.1.

The proof of Eqs. (3.33) and (3.34), given Eq. (3.16), proceeds along the same lines as the extension of Kirchhoff's formula from one to two energy groups (Section 2.6).

Consider now the 90^0 - wedge. The two-group extension of the approximate relation (3.32) results from the substitution:

$$J_{g\theta}(\xi, \theta_0) \cong J_{g\theta}\left(\frac{r}{L_g}, \theta_0\right) \; ; \quad g = 1, 2 \qquad (3.30)'$$

into Eqs. (3.33) and (3.34) and reads:

$$\phi_1\left(\frac{r}{L_1}, \frac{\pi}{4}\right) \cong -\frac{L_1}{D_1} \cdot \left\{1 + \exp\left(-\frac{r}{L_1}\right)\right\} \cdot J_{1\theta}\left(\frac{r}{L_1}, \frac{\pi}{4}\right)$$

and $(3.32)'$

$$\phi_2\left(\frac{r}{L_1}, \frac{r}{L_2}, \frac{\pi}{4}\right) \cong -\frac{L_2}{D_2} \cdot \left\{1 + \exp\left(-\frac{r}{L_2}\right)\right\} \cdot J_{2\theta}\left(\frac{r}{L_2}, \frac{\pi}{4}\right) - $$

$$ - \frac{\Sigma_{1 \to 2}/(D_1 D_2)}{\dfrac{1}{L_2^2} - \dfrac{1}{L_1^2}} \cdot \left\langle L_1 \cdot \left\{1 + \exp\left(-\frac{r}{L_1}\right)\right\} - \right. $$

$$ \left. - L_2 \cdot \left\{1 + \exp\left(-\frac{r}{L_2}\right)\right\}\right\rangle \cdot J_{1\theta}\left(\frac{r}{L_1}, \frac{\pi}{4}\right) \qquad (3.32)''$$

3.6 DISCUSSION

a)   The wedge-shaped reflector was re-considered in the present chapter. This time, the analytical expression for the flux provided the starting point for the derivation of a relation between the boundary values of the flux and normal current. Although this relation appears formally different than the boundary condition obtained from Kirchhoff's formula, the two must be equivalent, in the sense that each one must be reducible to the other by means of appropriate mathematical operations.

b)   The crucial step in the derivation of the boundary condition in the present chapter was the use of Lebedev's formula, Eq. (3.10). Eqs. (3.10) and (3.8) may be viewed as a pair of equations defining an integral transformation and the inverse transformation, respectively; i.e.:

$$\bar{f}(p) \equiv \frac{2}{\pi^2} \cdot p \cdot \sinh(\pi p) \cdot \int_0^\infty f(\xi) \cdot K_{ip}(\xi) \cdot d\xi \qquad (3.10)'$$

$$f(\xi) = \frac{1}{\xi} \cdot \int_0^\infty \bar{f}(p) \cdot K_{ip}(\xi) \cdot dp \qquad (3.8)'$$

The transform pair {(3.10)´, (3.8)´} may also be written in the form of a single identity:

$$f(\xi) \equiv \frac{2}{\pi^2} \cdot \frac{1}{\xi} \cdot \int_0^\infty \left[\int_0^\infty f(\xi') \cdot K_{ip}(\xi') \cdot d\xi' \right] \cdot p \cdot$$

$$\cdot \sinh(\pi p) \cdot K_{ip}(\xi) \cdot dp \qquad (3.35)$$

The proof of identity (3.35) (or, equivalently, the proof of the inversion formula (3.8)´) is to be found in Refs. [L-1] and [L-2] and is not simple.

The following <u>sufficient</u> conditions for the existence of the transform are given in [L-1] and [L-2]:

(i) $f(\xi)$ and $f'(\xi)$ must be bounded and continuous for $\xi \in (0, \infty)$

(ii) $\xi^2 f(\xi) \in L(0, \infty)$ and $\xi f'(\xi) \in L(0, \infty)$ (i.e. [T-3]: $\xi^2 f(\xi)$ and $\xi f'(\xi)$ must be measurable and $\int_0^\infty |\xi^2 f(\xi)| d\xi < \infty$ and $\int_0^\infty |\xi f'(\xi)| d\xi < \infty$).

c) The flux-to-normal-current relation along the boundary of a 90^0 - wedge is, for a symmetrical neutron distribution, given by Eq. (3.18) together with the expression (3.25) for the relevant kernel G. In the present chapter, this boundary relation was derived by means of Lebedev's formula. The same

96

boundary relation was derived in the previous chapter by means of the generalized Kirchhoff's formula. Perhaps, the above two independent derivations may provide -as a by-product of the present work- the basis for an alternative proof of Lebedev's formula.

ACKNOWLEDGEMENT.

IV. TIME-DEPENDENT ANALYSIS

4.1 TIME - DEPENDENT KIRCHHOFF'S FORMULA FOR ONE ENERGY GROUP

In Section 2.1 we presented Kirchhoff's formula, Eq. (2.2), for the:

(a) steady-state diffusion of

(b) one-energy-group neutrons in

(c) a non-multiplying medium occupying

(d) a two-dimensional region A with boundary Γ.

In the present Section we relax condition (a), above, and allow for a time-dependence of the neutron distribution while we keep conditions (b), (c) and (d) in effect. The relevant extension of Eq. (2.2) is:

$$\phi(x,y,t) =$$

$$= \frac{1}{2\pi} \cdot \int_{\Gamma} \left[\int_{0}^{\infty} \left\langle \phi(x',y',t-\tau) \cdot \frac{\partial}{\partial n} + \frac{1}{D} \cdot J_n(x',y',t- \right. \right.$$

<div align="right">Eq.cont.</div>

$$-\tau)\Big\rangle \cdot \Big\langle \frac{1}{2\tau} \cdot \exp\Big(-\frac{D \cdot v \cdot \tau}{L^2} - \frac{p^2}{4 \cdot D \cdot v \cdot \tau}\Big)\Big\rangle d\tau \Big] d\ell +$$

$$+ F_0(x, y, t) \qquad (4.1)$$

where the function F_0 depends on the initial flux distribution in region A.

In the remaining of this section we prove (4.1) and specify F_0.

We start with the following pair of functions:

(i) $\Phi(x, y, t)$: Solution of

$$\frac{\partial^2 \phi}{\partial x^2} + \frac{\partial^2 \phi}{\partial y^2} - \frac{1}{L^2} \cdot \phi = \frac{1}{D \cdot v} \cdot \frac{\partial \phi}{\partial t} \qquad (4.2)$$

in region A

and

(ii) $\Psi(\rho, t)$: Solution of

$$\frac{\partial^2 \Psi}{\partial x^2} + \frac{\partial^2 \Psi}{\partial y^2} - \frac{1}{L^2} \cdot \Psi = \frac{1}{D \cdot v} \cdot \frac{\partial \Psi}{\partial t} -$$

$$- 2\pi \cdot \delta(\rho) \cdot \delta(t) \qquad (4.3)$$

over the entire x-y plane

with initial distribution $\Psi(x, y, t = 0) = 0$ (4.4)

The Laplace transforms of (i) and (ii) with respect to t

are:

(i)´

$$\overline{\phi}(x, y, s) \equiv \int_0^\infty e^{-st} \cdot \phi(x, y, t) \, dt$$

$$(4.5):$$

Solution of

$$\frac{\partial^2 \overline{\phi}}{\partial x^2} + \frac{\partial^2 \overline{\phi}}{\partial y^2} - \frac{1}{\overline{L}^2} \cdot \overline{\phi} = - \frac{\phi(x, y, t = 0)}{D \cdot v}$$

$$(4.2)´$$

in region A

100

and

(ii)
$$\overline{\Psi}(\rho, s) \equiv \int_0^\infty e^{-st} \cdot \Psi(\rho, t)\, dt \qquad (4.6):$$

Solution of

$$\frac{\partial^2 \overline{\Psi}}{\partial x^2} + \frac{\partial^2 \overline{\Psi}}{\partial y^2} - \frac{1}{\overline{L}^2} \cdot \overline{\Psi} = -2\pi \cdot \delta(\rho) \quad (4.3)$$

over the entire x-y plane,

where:

$$\frac{1}{\overline{L}^2} \equiv \frac{1}{L^2} + \frac{S}{D \cdot \upsilon} \qquad (4.7)$$

$\overline{\Phi}$ may be expressed as:

$$\overline{\phi} = \overline{\phi}_h + \overline{\phi}_p \qquad (4.8)$$

101

where: $\overline{\Phi}_h$ is the solution of the homogeneous part of Eq. (4.2)´

and

   $\overline{\Phi}_p$ is a particular solution of the full equation (4.2)´.

The Kirchhoff's formula corresponding to the pair $\overline{\Phi}_h$ and $\overline{\Psi}$

is:

$$\overline{\Phi}_h(x,y,s) = \frac{1}{2\pi} \cdot \int_{\Gamma} \left[\overline{\Phi}_h(x',y',s) \cdot \frac{\partial}{\partial n} \overline{\Psi}(\rho,s) + \frac{1}{D} \cdot \overline{J}_{h_n}(x',y',s) \cdot \Psi(\rho,s) \right] d\ell$$

(4.9)

where:

$$\overline{J}_{h_n} \equiv -D \cdot \frac{\partial}{\partial n} \overline{\Phi}_h$$

(4.10)

102

In analogy with Eq. (4.10) we define:

$$\bar{J}_n \equiv -D \cdot \frac{\partial}{\partial n} \bar{\phi} \tag{4.11}$$

and

$$\bar{J}_{P_n} \equiv -D \cdot \frac{\partial}{\partial n} \bar{\phi}_P \tag{4.12}$$

In view of Eq. (4.8), Eqs. (4.10) - (4.12) imply:

$$\bar{J}_n = \bar{J}_{h_n} + \bar{J}_{P_n} \tag{4.13}$$

Next we eliminate from (4.9):

· on one hand $\bar{\phi}_h$ with the help of (4.8)

· and on the other hand $\bar{J}_{h_n}$ with the help of (4.13).

The result is:

$$\bar{\phi}(x,y,s) - \bar{\phi}_P(x,y,s) =$$

$$= \frac{1}{2\pi} \cdot \int_\Gamma \left[\left\langle \bar{\phi}(x',y',s) - \bar{\phi}_P(x',y',s) \right\rangle \cdot \frac{\partial}{\partial n} \bar{\Psi}(\rho,s) + \right.$$

Eq. cont.

103

Eq. cont.

$$+ \frac{1}{D} \cdot \left\langle \bar{J}(x',y',s) - \bar{J}_{p_m}(x',y',s) \right\rangle \cdot \psi(\rho, s) \Big] d\ell$$

(4.14)

$\bar{\Phi}_p$ depends on the initial flux distribution in region A, $\Phi(x,y,t = 0)$.

Eq. (4.14) is the dynamic Kirchhoff's formula in the frequency (s) - domain for an arbitrary initial flux distribution.

<u>If</u>:

(I) A steady-state distribution of neutrons existed in region A prior to t=0 and

(II) The transient, which occurs at $t \geq 0$, is driven by a force located <u>outside</u> region A,

<u>then</u>:

• the diffusion length, L, in region A maintains throughout the transient its steady-state value,

• $\Phi(x,y,t = 0)$ is the solution of the equation:

104

$$\frac{\partial^2 \phi}{\partial x^2} + \frac{\partial^2 \phi}{\partial y^2} - \frac{1}{L^2} \cdot \phi = 0 \qquad (4.15)$$

in region A and

· a particular solution of Eq. (4.2)´ is:

$$\overline{\phi}_p (x, y, s) = \frac{1}{s} \cdot \phi (x, y, t=0) \qquad (4.16)$$

We operate on (4.16) with $-D \cdot \partial / \partial n$ and obtain:

$$\overline{J}_{p_n} (x, y, s) = \frac{1}{s} \cdot \overline{J}_n (x, y, t=0) \qquad (4.17)$$

Since the initial neutron distribution is a steady-state one, the steady-state Kirchhoff's formula may be written for it:

$$\phi (x, y, t=0) = \frac{1}{2\pi} \cdot \int_{\Gamma} \left[\phi (x', y', t=0) \cdot \frac{\partial}{\partial n} K_0 \left(\frac{\rho}{L} \right) + \right.$$

$$\left. + \frac{1}{D} \cdot J_n (x', y', t=0) \cdot K_0 \left(\frac{\rho}{L} \right) \right] d\ell$$

$$(4.18)$$

We substitute (4.16) and (4.17) into Eq. (4.14), denote the resulting equation by (4.14)´, multiply Eq. (4.18) by 1/s, denote the resulting equation by (4.18)´ and add Eq. (4.18)´ to (4.14)´. The result is:

$$\overline{\Phi}(x,y,s) = \frac{1}{2\pi} \cdot \int_{\Gamma} \left[\overline{\Phi}(x',y',s) \cdot \frac{\partial}{\partial n} \overline{\Psi}(\rho,s) + \right.$$

$$+ \frac{1}{D} \cdot \overline{J}_n(x',y',s) \cdot \overline{\Psi}(\rho,s) +$$

$$+ \frac{1}{s} \cdot \left\langle \Phi(x',y',t=0) \cdot \frac{\partial}{\partial n} + \frac{1}{D} \cdot J_n(x',y',t=0) \right\rangle \cdot \left\langle \right.$$

$$\left. K_0\left(\frac{\rho}{L}\right) - \overline{\Psi}(\rho,s) \right\rangle \right] d\ell \qquad (4.19)$$

Eq. (4.19) is the dynamic Kirchhoff's formula in the frequency domain, when the initial flux distribution is the solution of Eq. (4.15).

The expression for $\overline{\Psi}(\rho,s)$ to be used with Eqs. (4.14) and (4.19) is:

$$\Psi(\rho,s) \equiv K_0(\rho/L) \qquad (4.20)$$

(4.20) is the solution of Eq. (4.3)´ over the entire x-y plane.

106

The time-domain counterparts of Eqs. (4.14) and (4.19) are obtained via operation on (4.14) and (4.19) with the inverse - Laplace - transform operator:

$$\mathcal{L}^{-1}\cdots \equiv \frac{1}{2\pi i}\cdot \int_{c-i\infty}^{c+i\infty}ds\cdot e^{st}\cdots \qquad (4.21)$$

The integration in (4.21) is to be carried out on the complex s-plane, along a straight line parallel to - and at a distance c from - the imaginary s - axis. The value of c must be sufficiently large so that the direct Laplace transform,

$$\mathcal{L}\cdots \equiv \int_{0}^{\infty}ds\cdot e^{-st}\cdots \qquad (4.22)$$

converges.[P-2]

The $\mathcal{L}^{-1}$ - operated, general equation (4.14) and special equation (4.19) are of the form:

$$\phi(x,y,t) = \frac{1}{2\pi}\cdot \mathcal{L}^{-1}\int_{\Gamma}\left[\langle \bar{\phi}(x',y',s)\cdot \frac{\partial}{\partial n}+\right.$$

(4.23)
Eq. cont.

107

$$+ \frac{1}{D} \cdot \bar{J}_n (x', y', s) \Big\rangle \cdot \bar{\Psi} (p, s) \Big] d\ell +$$

$$+ F_o (x, y, t) \qquad\qquad (4.23)$$

In (4.23), we take the operator $\mathscr{L}^{-1}$ inside the integral $\int_\Gamma \ldots$dl and get:

$$\Phi(x, y, t) = \frac{1}{2\pi} \cdot \int_\Gamma W(x, y, x', y', t) \, d\ell +$$

$$+ F_o (x, y, t) \qquad\qquad (4.24)$$

where

$$W \equiv \mathscr{L}^{-1} \Big\langle \bar{\Phi}(x', y', s) \cdot \frac{\partial}{\partial n} + \frac{1}{D} \cdot \bar{J}_n (x', y', s) \Big\rangle \cdot \bar{\Psi}(p, s)$$

$$(4.25)$$

By virtue of the Convolution Theorem [P-2], W may be expressed as:

$$W = \int_{-\infty}^{+\infty} \left\langle \phi(x',y',t-\tau) \cdot \frac{\partial}{\partial n} + \frac{1}{D} \cdot J_n(x',y',t-\tau) \right\rangle \cdot$$

$$\cdot \Psi(p,\tau) \, d\tau \qquad (4.26)$$

or, alternatively, as:

$$W = \int_{-\infty}^{+\infty} \left\langle \phi(x',y',\tau) \cdot \frac{\partial}{\partial n} + \frac{1}{D} \cdot J_n(x',y',\tau) \right\rangle \cdot$$

$$\cdot \Psi(p,t-\tau) \, d\tau \qquad (4.27)$$

In (4.26), the lower limit of the integration must be replaced by zero, because, otherwise, Eq. (4.24) would require anticipation of the future evolution of the boundary-flux and normal current from the part of the transient flux distribution in region A, a physically senseless requirement. For the same reason, in (4.27), the upper limit of the integration must be replaced by t.

The expression for $\Psi(p,t)$, to be used with (4.26) or (4.27), is:

109

$$\Psi(p,t) = \frac{1}{2t} \cdot \exp\left(-\frac{D \cdot v \cdot t}{L^2} - \frac{p^2}{4 \cdot D \cdot v \cdot t}\right)$$

$$(4.28)$$

The combination of (4.24), (4.26) and (4.28) yields Eq. (4.1).

We conclude this Section by specifying $F_0(x,y,t)$.

For an arbitrary initial flux distribution, F_0 is given by:

$$F_0(x,y,t) \equiv \mathcal{L}^{-1}\left\{ \bar{\Phi}_p(x,y,s) - \right.$$

$$-\frac{1}{2\pi} \cdot \int_{\Gamma} \left[\left\langle \bar{\Phi}_p(x',y',s) \cdot \frac{\partial}{\partial n} + \frac{1}{D} \cdot \bar{J}_{p_n}(x',y',s) \right\rangle \cdot \right.$$

$$\left. \left. \cdot \bar{\Psi}(p,s) \right] d\ell \right\} \qquad (4.29)$$

For an initial flux distribution satisfying Eq. (4.15), F_0 is given by:

$$F_0(x,y,t) \equiv \frac{1}{2\pi} \cdot \mathcal{L}^{-1} \frac{1}{s} \cdot \int_{\Gamma} \left\langle \phi(x',y',t=0) \cdot \frac{\partial}{\partial n} + \right.$$

110

$$+ \frac{1}{D} \cdot J_n (x', y', t = 0) \Big\rangle \cdot \Big\langle K_o \left(\frac{\rho}{L} \right) - \overline{\Psi} (\rho, s) \Big\rangle d\ell$$

$$(4.30)$$

4.2 THE ONE - DIMENSIONAL SLAB.

In Chapter II we derived, by starting from Eq. (2.2), the steady-state expressions (2.17) for the flux and normal current at the right face of the slab in terms of the flux and normal current at the left face.

If we replace in (2.2) and (2.17):

$$\phi \text{ by } \overline{\phi}_h , \quad J_x \text{ by } \overline{J}_{h_x} \quad \text{and} \quad L \text{ by } \overline{L} \Bigg\}$$

$$(4.31)$$

where $\overline{\phi}_h$, $\overline{J}_{h_x}$ and $\overline{L}$ are the frequency-domain quantities defined in Section 4.1, we get:

Eq. (4.9) with $\overline{\Psi}$ given by (4.20) and

111

$$
\begin{bmatrix} \overline{\phi}_h(x_e,s) \\ \overline{J}_{h_x}(x_e,s) \end{bmatrix} = \begin{bmatrix} \cosh\left(\frac{\Delta}{L}\right), & -\frac{L}{D}\cdot\sinh\left(\frac{\Delta}{L}\right) \\ -\frac{D}{L}\cdot\sinh\left(\frac{\Delta}{L}\right), & \cosh\left(\frac{\Delta}{L}\right) \end{bmatrix} \begin{bmatrix} \overline{\phi}_h(x_i,s) \\ \overline{J}_{h_x}(x_i,s) \end{bmatrix}
$$

$$(4.32)$$

respectively.

The derivation of (4.32) from (4.9) follows the same steps as the derivation of (2.17) from (2.2).

Suppose the initial flux distribution in the slab satisfies the one-dimensional version ($\partial^2 \phi/\partial y^2 = 0$) of Eq. (4.15), so that:

$$
\overline{\phi}_p(x,s) = \frac{1}{s}\cdot\phi(x,t=0)
$$

$$(4.33)$$

and, therefore,

$$
\overline{\phi}_h(x,s) = \overline{\phi}(x,s) - \frac{1}{s}\cdot\phi(x,t=0)
$$

$$(4.34)$$

and

$$
\overline{J}_{h_x}(x,s) = \overline{J}_x(x,s) - \frac{1}{s}\cdot J_x(x,t=0)
$$

$$(4.35)$$

112

The inverse Laplace transforms of (4.34) and (4.35) are:

$$\phi_h(x,t) = \phi(x,t) - \phi(x,t=0) \tag{4.36}$$

and

$$J_{h_x}(x,t) = J_x(x,t) - J_x(x,t=0) \tag{4.37}$$

Suppose further that the right face of the slab is an outer boundary. Then:

$$\phi(x_e,t=0) = \phi(x_e,t) = 0 \tag{4.38}$$

and, consequently,

$$\bar{\phi}_h(x_e,s) = 0 \tag{4.39}$$

Substitution of (4.39) into the first row of (4.32) yields:

$$\bar{\phi}_h(x_i,s) = \frac{L}{D} \cdot \tanh\left(\frac{\Delta}{L}\right) \cdot \bar{J}_{h_x}(x_i,s) \tag{4.40}$$

113

The inverse Laplace transform of (4.40) is:

$$\phi_h(x_i, t) = \int_0^\infty \alpha(\tau) \cdot J_{h_x}(x_i, t - \tau) \, d\tau \qquad (4.41)$$

Where:

$$\alpha(\tau) \equiv \mathcal{L}^{-1} \frac{\overline{L}}{D} \cdot \tanh\left(\frac{\Delta}{\overline{L}}\right) \qquad (4.42)$$

Substitution of (4.36) and (4.37) into (4.41) yields:

$$\phi(x_i, t) - \phi(x_i, t = 0) =$$

$$= \int_0^\infty \alpha(\tau) \cdot J_x(x_i, t - \tau) \, d\tau \; -$$

$$- \left[\int_0^\infty \alpha(\tau) \, d\tau \right] \cdot J_x(x_i, t = 0) \qquad (4.43)$$

The integral $\int_0^\infty \alpha(\tau) . d\tau$ is, by virtue of the moments

114

Theorem,[*] equal to the Laplace transform of $\alpha(\tau)$ evaluated at s=0.
I.e.:

$$\int_0^\infty \alpha(\tau)\,d\tau = \frac{L}{D} \cdot \tanh\left(\frac{\Delta}{L}\right) \qquad (4.44)$$

The right hand side of Eq. (4.44) is, in turn, equal to the ratio $\Phi\left(x_i, t=0\right)/J_x\left(x_i, t=0\right)$ (see Eq. (2.19)). Consequently,

$$\left[\int_0^\infty \alpha(\tau)\,d\tau\right] \cdot J_x\left(x_i, t=0\right) = \Phi\left(x_i, t=0\right) \qquad (4.45)$$

and Eq. (4.43) simplifies to:

$$\Phi(x_i, t) = \int_0^\infty \alpha(\tau) \cdot J_x\left(x_i, t-\tau\right)\,d\tau \qquad (4.46)$$

---

[*]Moments Theorem[P-2]:

$$\int_0^\infty f(t) \cdot t^k \cdot dt = (-1)^k \cdot \frac{\partial^k}{\partial s^k} \bar{f}(s)\bigg|_{s=0} \;;$$

$$k = 0, 1, 2, \dots \quad,$$

where $\bar{f}(s)$ is the Laplace transform of the function f(t).

It can be shown that Eq. (4.42) yields:

$$\alpha(\tau) = \sqrt{\frac{\upsilon}{D \cdot \pi}} \cdot \frac{1}{\sqrt{\tau}} \cdot e^{-\Sigma \cdot \upsilon \cdot \tau} \cdot \left\langle 1 + \right.$$

$$\left. + 2 \cdot \sum_{n=1}^{\infty} (-1)^n \cdot e^{-\frac{n^2 \Delta^2}{D \cdot \upsilon \cdot \tau}} \right\rangle \quad (4.47)$$

From (4.47) is follows that:

$$\lim_{\Delta \to \infty} \alpha(\tau) = \sqrt{\frac{\upsilon}{D \cdot \pi}} \cdot \frac{1}{\sqrt{\tau}} \cdot e^{-\Sigma \cdot \upsilon \cdot \tau} \qquad (4.48)$$

Inspection of (4.47) and (4.48) shows that $\alpha(\tau)$ and $\lim_{\Delta \to \infty} \alpha(\tau)$ tend

- to ∞ as τ tends to zero and

- to 0 as τ tends to ∞.

Furthermore, $\lim_{\Delta \to \infty} \alpha(\tau)$ varies monotonically with τ between $\tau=0$ and ∞ while $\alpha(\tau)$ does not. This non-monotonic variation of $\alpha(\tau)$ is due to the "reflected" terms:

$$2 \cdot \sum_{n=1}^{\infty} \cdots$$

116

in the expression (4.47), i.e. the terms which arise from the finite thickness Δ of the slab.[*]

In view of (4.46) and the above behavior of $\alpha(\tau)$ and $\lim\limits_{\Delta \to \infty} \alpha(\tau)$ we conclude that the present value of the local flux, $\Phi(x_i,t)$ depends on the present value and on the recent history of the local current, $J_x(x_i,t)$, and has no memory of the too-distant-in-the-past history of $J_x(x_i,t)$.

In order to have a measure of the memory strength of $\Phi(x_i,t)$ for various materials we define, arbitrarily, the <u>effective memory span</u> of Φ as the time within which the function $\alpha(\tau)$ drops from its 1 μsec-value[**] by a factor of 1000. Thus[***], in light water the effective memory span is $\sim$ 30 μsec for fast neutrons and $\sim$ 650 μsec for thermal neutrons. In (pure) heavy water the memory span is $\sim$ 80 μsec for fast neutrons and $\sim$ 70 msec (=70,000 μsec) for thermal neutrons.

---

[*] The value of these terms is zero at $\tau = 0$ and approaches a finite upper bound as $\tau \to \infty$.

[**] 1 μsec = 10^{-6} sec ; 1 msec = 10^{-3} sec.

[***] All numbers computed with $\Delta = \infty$ (Eq. 4.48). See Figures 4.1 and 4.2.
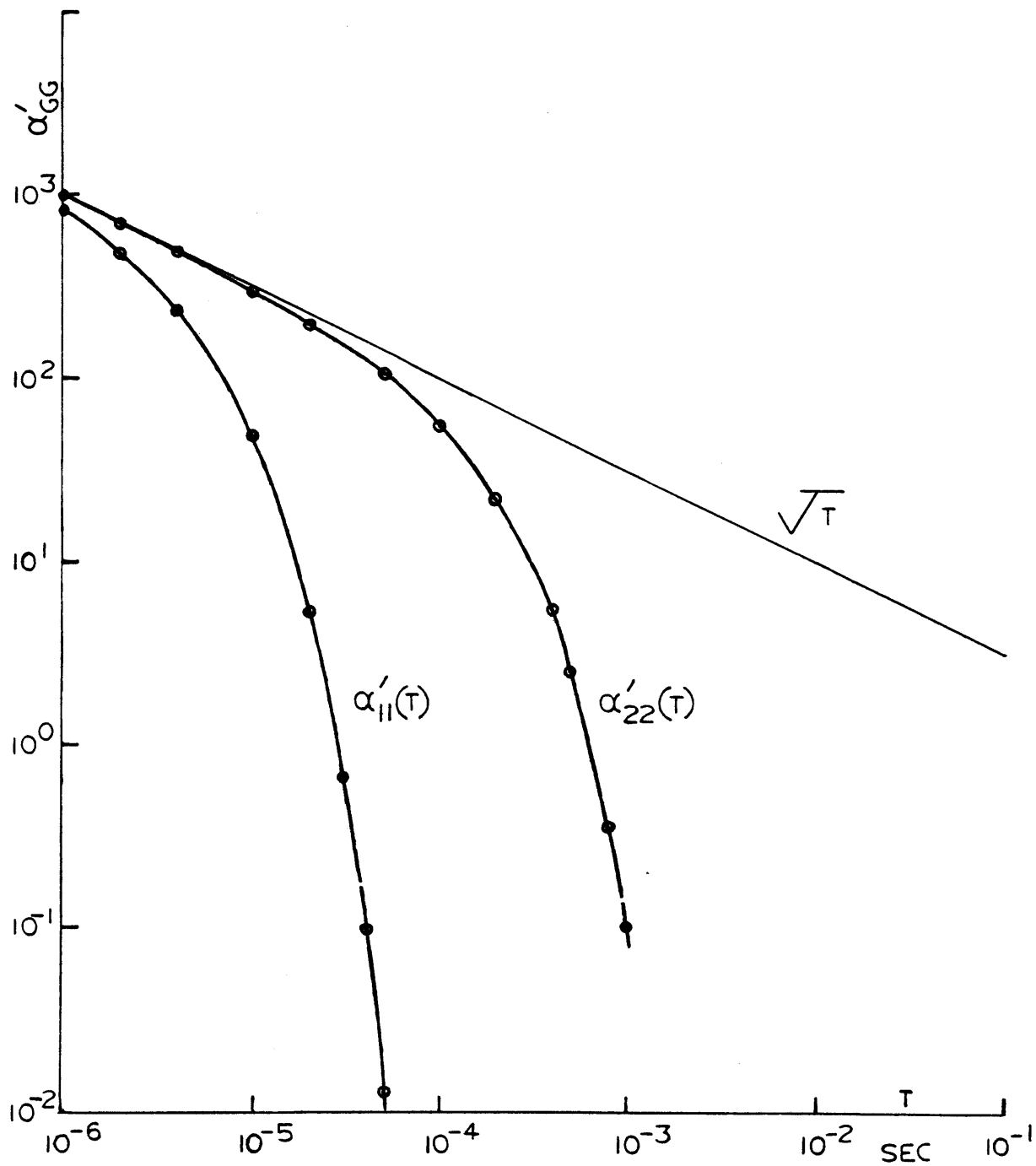
$$\alpha'_{GG}(T) = \sqrt{T} \cdot EXP(-\Sigma_G V_G T) \quad ; \quad G = 1,2$$

FIGURE 4.1 : MEMORY-FUNCTIONS $\alpha'_{11}(T)$ AND $\alpha'_{22}(T)$ FOR H_2O
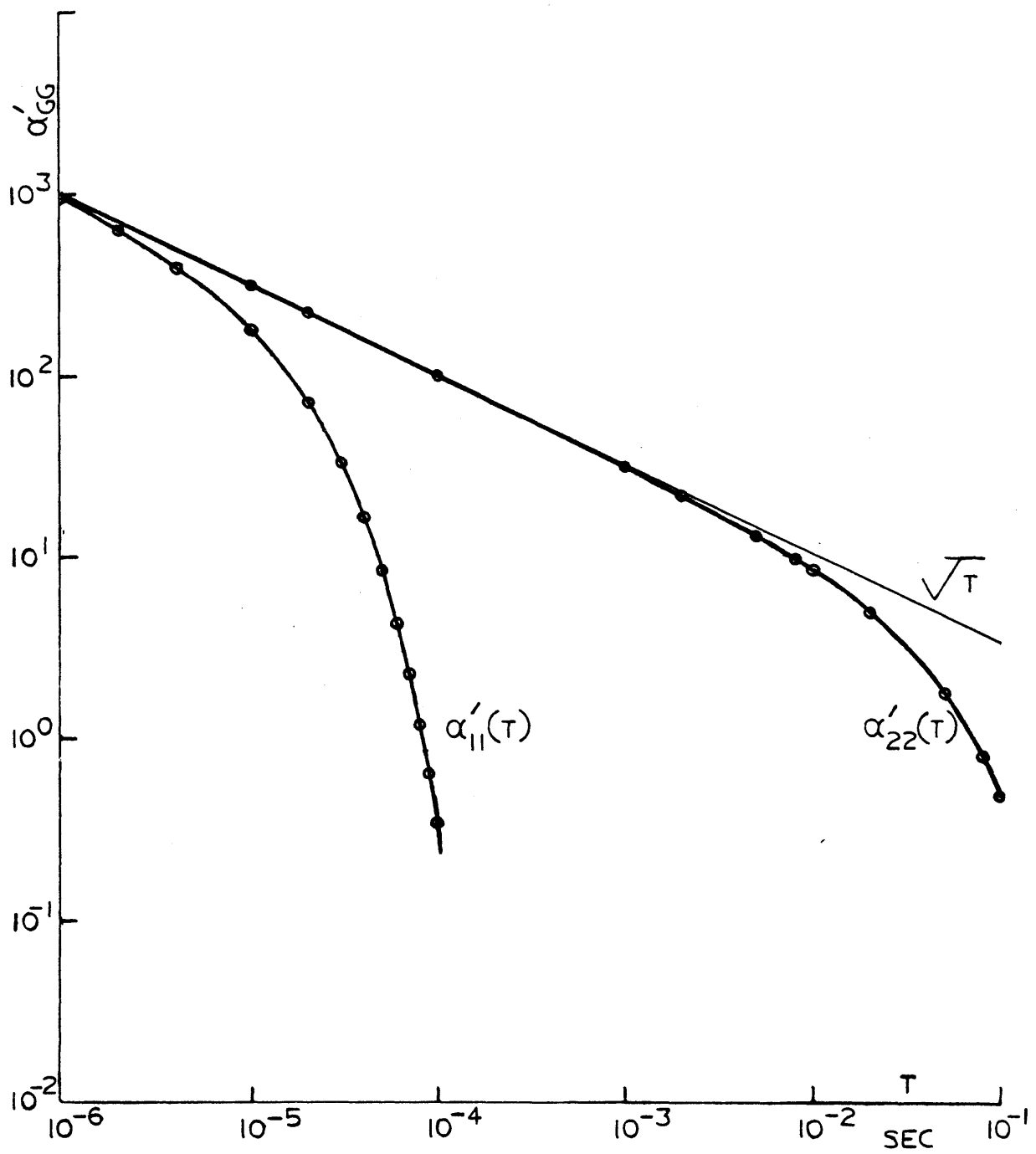
$$\alpha'_{GG}(T) = \sqrt{T} \cdot \text{EXP}(-\Sigma_G V_G T) \; ; \; G = 1, 2$$

FIGURE 4.2: MEMORY FUNCTIONS $\alpha'_{11}(T)$ AND $\alpha'_{22}(T)$ FOR D_2O

We see that:

a)   For each of the two materials, the thermal-neutron memory is much stronger than the fast-neutron one and

b)   Heavy water exhibits a much stronger memory for thermal neutrons than light water.

Feature a) is due to the strong moderating capacity of both materials* and to the group-speed differential.

Feature b) is due to the fact that heavy water is a much weaker absorber of thermal neutrons than light water.

As a consequence of a), thermal neutrons in both materials exhibit a much more sluggish transient response than fast newtrons.

As a consequence of b), thermal neutrons in light water exhibit a much more prompt transient response than in heavy water.

4.3   APPROXIMATIONS - SIMPLIFICATIONS OF EQ. (4.46)

a)   Suppose $J_x(x_i, t-\tau)$, in Eq. (4.46), is expanded in a Taylor

---

*This strong moderating capacity is responsible for the large value of the total cross section for removal of neutrons from the fast group, as compared to the value of the thermal absorption ($\equiv$ total thermal) cross section.

series with respect to τ, about the point $\tau = t$:

$$\phi(x_i,t) = \int_0^\infty \alpha(\tau) \cdot \left[J_x(x_i,t) - \dot{J}_x(x_i,t) \cdot \tau + \ddot{J}_x(x_i,t) \cdot \frac{\tau^2}{2} - \cdots \right] \cdot d\tau$$

(4.49)

If $J_x(x_i, t - \tau)$ varies sufficiently slowly with time over an interval centered at t and a few lifetimes $(\Sigma \cdot v)^{-1}$ wide, then the Taylor series can be truncated after a few terms:

$$J_x(x_i, t-\tau) \cong J_x(x_i, t)$$

(4.50)

Zero – order truncated Taylor series

$$J_x(x_i, t-\tau) \cong J_x(x_i, t) - \dot{J}_x(x_i, t) \cdot \tau$$

(4.51)

First – order truncated Taylor series

etc.

121

i)   With the approximation (4.50), Eq. (4.49) reduces to:

$$\phi(x_i, t) \cong \left[\int_0^\infty \alpha(\tau)\, d\tau \right] \cdot J_x(x_i, t) \qquad (4.52)$$

In view of Eq. (4.44), (4.52) may be written in the form:

$$\phi(x_i, t) \cong \frac{L}{D} \cdot \tanh\left(\frac{\Delta}{L}\right) \cdot J_x(x_i, t)$$

$$(4.53)$$

Eq. (4.53) is formally the same as the steady-state relation (2.19):

$$\phi(x_i) = \frac{L}{D} \cdot \tanh\left(\frac{\Delta}{L}\right) \cdot J_x(x_i) \qquad (2.19)$$

Because of this similarity we shall refer to the approximation (4.50), which leads to (4.53), as the static approximation.

ii)   With the approximation (4.51), Eq. (4.49) reduces to:

$$\phi(x_i, t) \cong \left[\int_0^\infty \alpha(\tau)\, d\tau \right] \cdot J_x(x_i, t) -$$

$$- \left[\int_0^\infty \alpha(\tau) \cdot \tau\, d\tau \right] \cdot \dot{J}_x(x_i, t) \qquad (4.54)$$

The integral $\int_0^\infty \alpha(\tau) \cdot \tau \cdot d\tau$, evaluated by means of the Moments Theorem [P-2], is found to be:

$$\int_0^\infty \alpha(\tau) \cdot \tau \, d\tau =$$

$$= \frac{L}{D} \cdot \frac{L^2}{2 \cdot D \cdot v} \cdot \left[\tanh\left(\frac{\Delta}{L}\right) - \frac{\Delta/L}{\cosh^2\left(\frac{\Delta}{L}\right)} \right]$$

$$(4.55)$$

Substitution of (4.44) and (4.55) into (4.54) yields:

$$\phi(x_i, t) \cong$$

$$\cong \frac{L}{D} \cdot \tanh\left(\frac{\Delta}{L}\right) \cdot J_x(x_i, t) -$$

$$- \frac{L}{D} \cdot \frac{L^2}{2 \cdot D \cdot v} \cdot \left[\tanh\left(\frac{\Delta}{L}\right) - \frac{\Delta/L}{\cosh^2\left(\frac{\Delta}{L}\right)} \right] \cdot \dot{J}_x(x_i, t)$$

$$(4.56)$$

123

We shall refer to the approximation (4.51), which leads to (4.56), as the _linear approximation_, the term stemming from the linearity of (4.41) with respect to τ.

The flux-normal current relation (4.53), which results from the static approximation, can be alternatively derived if the _adiabatic approximation_,

$$\text{Adiabatic approximation:} \quad \frac{\partial \phi(x,t)}{\partial t} \cong 0 \qquad (4.57)$$

is made for all points x in the reflector.

The flux-normal current relation (4.56), which results from the linear approximation, can be alternatively derived if the _constant-shape approximation_,

$$\text{Constant - shape approximation:}$$
$$\frac{\partial \phi(x,t)}{\partial t} \cong \omega(t) \cdot \phi(x) \qquad (4.58)$$

(where $\omega \equiv \dot{J}_x(x_{i,t}/J_x(x_{i,t}))$

is made for all points x in the reflector.

124

Thus, the static approximation is equivalent to the adiabatic and the linear to the constant-shape approximation.

The linear approximation boundary condition, Eq. (4.56), is not homogeneous but can be implemented on the computer as homogeneous on the basis of the following strategy:

Eq. (4.54), which is equivalent to (4.56), can be written in the form:

$$\Phi(x_i,t) \overset{\sim}{=} \left[\int_0^\infty \alpha(\tau) \cdot \left\langle 1 - \omega(x_i,t) \cdot \tau \right\rangle d\tau \right] \cdot J_x(x_i,t)$$

(4.59)

where

$$\omega(x_i,t) \equiv \frac{\dot{J}_x(x_i,t)}{J_x(x_i,t)}$$

(4.60)

The value of ω, to be used in Eq. (4.59), can be estimated, as the computation proceeds, from the values of the normal current (or flux[*]) at the two previous time-steps.

_____

[*] In view of the constant-shape approximation, Eq. (4.58), ω, by definition equal to $\dot{J}_x/J_x$, is also equal to $\dot{\Phi}/\Phi$.

Once an estimate for the instantaneous frequency ω is available, the integral in brackets in (4.59) can be evaluated. The value of the integral in terms of ω is:

$$[\cdots] = \frac{\hat{L}}{D} \cdot \tanh\left(\frac{\Delta}{\hat{L}}\right) \tag{4.61}$$

where

$$\hat{L} \equiv \sqrt{D/\left(\Sigma + \frac{\omega}{v}\right)} \tag{4.62}$$

Eq. (4.61) is obtained if the factor $\langle 1 - \omega(x_i,t) \cdot \tau \rangle$ inside the integral in (4.59) is replaced by $\exp\left(- \omega(x_i,t) \cdot \tau\right)^{**}$. This replacement is, in the context of the linear approximation, legal, because the approximation itself is valid for sufficiently slow, i.e. sufficiently low frequency-, transients.

**After this replacement is made, the resulting integral can be evaluated by means of the moments theorem. According to the theorem, the integral in (4.59) is equal to the Laplace transform of the integrand, evaluated at $s = 0$. The Laplace transform of the integrand, at $s = 0$, is $\bar{\alpha}(s=\omega)$, where $\bar{\alpha}(s)=\mathscr{L}\alpha(t)$ and $\alpha(t)$ is defined by (4.42). It can be easily seen that, provided Σ is replaced by $\Sigma + \frac{\omega}{v}$, $\bar{\alpha}(s=\omega)$ is given by the same expression as $\bar{\alpha}(s=0)$.

Substitution of (4.61) into (4.59) yields:

$$\Phi(x_i, t) \cong \frac{\hat{L}}{D} \cdot \tanh\left(\frac{\Delta}{\hat{L}}\right) \cdot J_x(x_i, t) \qquad (4.63)$$

(4.63) is the linear approximation relation in homogeneous form.

When neither the static nor the linear approximation are adequate in representing the transient behavior of a reflector, higher-order approximations can be developed. To this end, higher-order truncations of the Taylor series expansion in Eq. (4.49) can be employed.

For example, the quadratic approximation relation is:

$$\Phi(x_i, t) \cong$$

$$\cong \left[\int_0^\infty \alpha(\tau) \cdot \left\langle 1 - \omega_1(x_i, t) \cdot \tau + \omega_2^2(x_i, t) \cdot \frac{\tau^2}{2} \right\rangle d\tau \right] \cdot J_x(x_i, t)$$

$$(4.64)$$

where

$$\omega_1(x_i, t) \equiv \dot{J}_x(x_i, t) / J_x(x_i, t) \qquad (4.65)$$

127

and

$$\omega_2^2(x_i,t) \equiv \ddot{J}_x(x_i,t)/J_x(x_i,t) \tag{4.66}$$

The values of ω_1 and ω_2^2 to be used in Eq. (4.64) can be estimated, as the computation proceeds, from the values of the normal current at the two and three previous time-steps, respectively.

There is no intuitively simple equivalent (the way the adiabatic and constant-shape approximations are to the static and linear approximations, respectively) to the quadratic or to any higher-order approximation. It is the value of the Taylor series approach that it suggests a whole series of approximations while the intuitive hierarchy (adiabatic, constant-shape) ends with the constant-shape approximation.

4.4. TIME - DEPENDENT FLUX - TO - NORMAL CURRENT RELATION FOR TWO ENERGY GROUPS.

The derivation of the general, two-group, time-dependent Kirchhoff's formula and other, equivalent, flux-to-normal current

relations is straightforward: First, the time-dependent, two-group diffusion equations are Laplace-transformed with respect to time and then the procedure of Section 2.5 is followed. Thus, two-group, time-dependent flux-to-normal current relations can be obtained for the one-dimensional slab, the wedge, the elbow etc.

We shall only present, without proof, the one-dimensional slab relations here. Specifically, we shall give the time-domain relations for the semi-infinite slab and the static -and linear- approximation relations for a slab of arbitrary thickness.

The time-domain, semi-infinite slab relations are[*]:

$$\begin{cases} \Phi_1(x_i,t) = \int_0^\infty \alpha_{11}(\tau) \cdot J_{1x}(x_i,t-\tau)d\tau \\\\ \Phi_2(x_i,t) = \int_0^\infty \left\langle \alpha_{21}(\tau) \cdot J_{1x}(x_i,t-\tau) + \alpha_{22}(\tau) \cdot J_{2x}(x_i,t-\tau) \right\rangle d\tau \end{cases}$$

(4.67)

---

[*]Provided the reactor is initially in steady-state and the reflector parameters do not change with time.

where:

$$\alpha_{gg}(\tau) \equiv \sqrt{\frac{v_g}{D_g \pi}} \cdot \frac{1}{\sqrt{\tau}} \cdot \exp\left(-\Sigma_g v_g \tau\right); \quad g = 1,2 \qquad (4.68)$$

$$\alpha_{21}(\tau) \equiv \frac{\Sigma_{s 1 \to 2}/D_1 D_2}{\dfrac{1}{v_1 D_1} - \dfrac{1}{v_2 D_2}} \cdot \sqrt{m} \cdot \exp\left(-\frac{\dfrac{\Sigma_2}{D_2} - \dfrac{\Sigma_1}{D_1}}{\dfrac{1}{v_2 D_2} - \dfrac{1}{v_1 D_1}} \cdot \tau\right) \cdot$$

$$\cdot \left\{ \operatorname{erf}\sqrt{\frac{v_2 D_2 \tau}{m}} - \operatorname{erf}\sqrt{\frac{v_1 D_1 \tau}{m}} \right\} \qquad (4.69)$$

and

$$m \equiv \frac{v_1 D_1 - v_2 D_2}{v_1 \Sigma_1 - v_2 \Sigma_2} \qquad (4.70)$$

The first of Eqs. (4.67), i.e. the fast-group flux-to-normal current relation, is of the one-group form. Hence, the discussion of Section 4.2. on the effective memory span holds also for the fast-group relation.

130

The second of Eqs. (4.67), i.e. the thermal-group flux-to-normal current relation, consists of two terms: one involving J_{1x} and another involving J_{2x}. The latter term is of the one-group form and therefore the discussion on the one-group memory-span holds also for this term.

Let us now examine $\alpha_{21}(\tau)$. At $\tau = 0$ the value of α_{21} is equal to zero; as τ increases, $|\alpha_{21}|$ initially increases until it reaches a maximum value and subsequently decreases to reach the zero-value asymptotically, as $\tau \to \infty$. The maximum value, which is finite, occurs at about $\tau = 10$ μsec for H_2O and $\tau = 50$ μsec for D_2O, but the maximum is orders of magnitude broader for D_2O than for H_2O.[*]

Thus, values of J_{1x} more recent than a few microseconds have not been "noticed" yet by $\Phi_2(x_i,t)$ while long past values of J_{1x} are effectively "forgotten" by $\Phi_2(x_i,t)$, the length of this memory span being different for different reflector materials.

Expansion of the group-currents in the integrands of Eqs. (4.67) in Taylor series with respect to τ, about $\tau = 0$ and subsequent truncation of the series leads, as in the one-group case (Section 4.2), to approximate time-dependent, two-group relations. Specifically, truncation of the series after their very first term leads to the static approximation relations, truncation after the

_____

[*] See Figures (4.3) and (4.4).

131
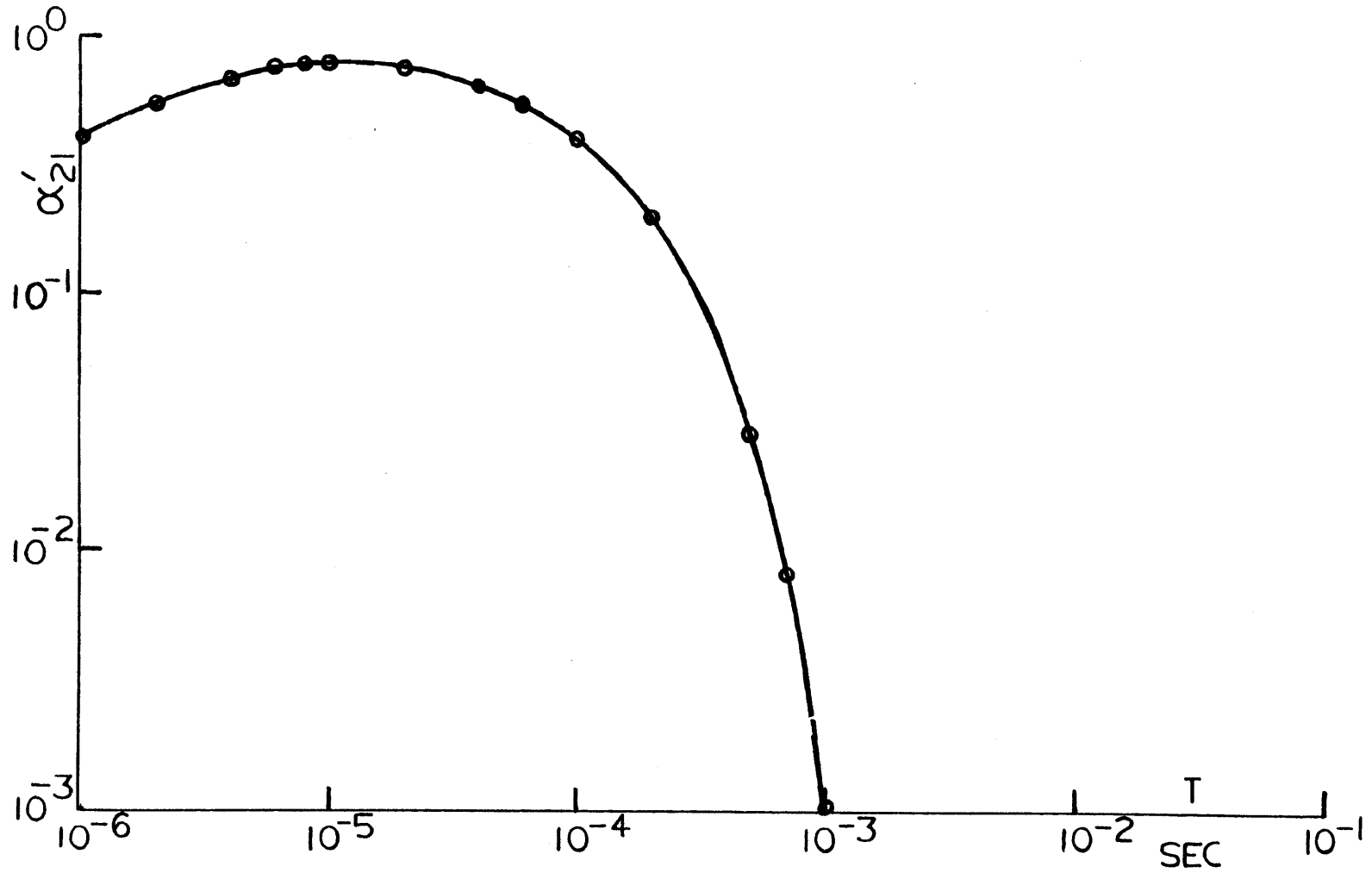
$$\alpha'_{21}(T) = EXP\left(- \frac{\Sigma_2/D_2 - \Sigma_1 D_1}{1/v_2 D_2 - 1/v_1 D_1} \cdot T\right) \cdot \left[ERF\sqrt{\frac{v_2 D_2 T}{m}} - ERF\sqrt{\frac{v_1 D_1 T}{m}}\right]$$

FIGURE 4.3: MEMORY−FUNCTION $\alpha'_{21}(T)$ FOR H_2O

133
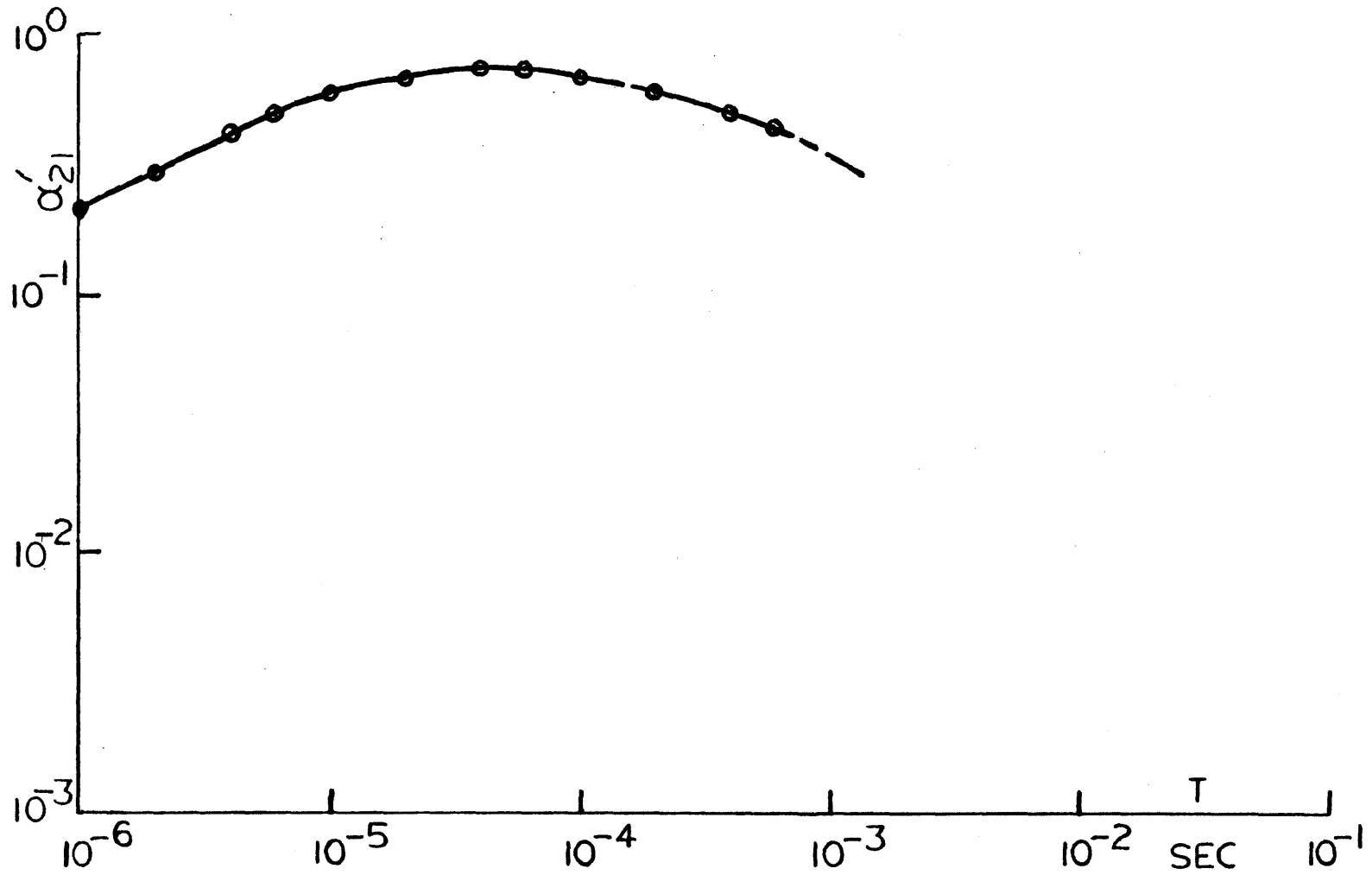
$$\alpha'_{21}(T) = EXP\left(-\frac{\Sigma_2/D_2 - \Sigma_1/D_1}{1/V_2D_2 - 1/V_1D_1}\cdot T\right)\cdot\left[ERF\sqrt{\frac{V_2D_2T}{m}} - ERF\sqrt{\frac{V_1D_1T}{m}}\right]$$

FIGURE 4.4 : MEMORY-FUNCTION $\alpha'_{21}(T)$ FOR D_2O

linear (with respect to τ) term leads to the linear approximation relations etc.

This class of approximations (static, linear, quadratic etc.) can, of course, be generalized for a slab of arbitrary thickness. The derivations are most conveniently carried out in the frequency domain[K-1]. In fact, the entire development of the present chapter can be carried out in the frequency domain, without the evaluation of the Laplace inverses of the $\bar{\alpha}(s)$'s. The time-domain analysis is presented in this dissertation because, in the opinion of the author, it is intuitively more transparent than the frequency-domain one.

For a slab of arbitrary thickness, the two-group, static-approximation relations are:

$$
\begin{bmatrix} \Phi_1(x_i,t) \\ \\ \Phi_2(x_i,t) \end{bmatrix} = \begin{bmatrix} \alpha_{11} & 0 \\ \\ \alpha_{21} & \alpha_{22} \end{bmatrix} \cdot \begin{bmatrix} J_{1x}(x_i,t) \\ \\ J_{2x}(x_i,t) \end{bmatrix} \tag{4.71}
$$

where the α's are the static impedances, defined by Eqs. (2.52)

The two-group, linear-approximation relations are also given by (4.71), where, now, in the definitions (2.52) of the α's, the

134

Σ_g's must be replaced by $\Sigma_g + \left(\dot{J}_{g_x}(x_i,t)/v_g J_{g_x}(x_i,t) \right)$. Of course, $\dot{J}_{g_x}(x_i,t)/J_{g_x}(x_i,t) = \dot{\Phi}_g(x_i,t)/\Phi_g(x_i,t)$.

ACKNOWLEDGEMENT

135

V. NUMERICAL TESTS AND RESULTS

5.1 THE "INSULATED CHANNEL" APPROXIMATION

Consider the two-dimensional diffusion equation (2.1):

$$\frac{\partial^2 \phi}{\partial x^2} + \frac{\partial^2 \phi}{\partial y^2} - \frac{1}{L^2} \cdot \phi = 0 \qquad (2.1)$$

If the partial derivative $\partial^2 \phi / \partial y^2$ is omitted from Eq. (2.1), the resulting equation is one-dimensional and the analysis of Section 2.2. is applicable.

Physically, the term $\partial^2 \phi / \partial y^2$ represents leakage of neutrons in the y-direction. Consequently, the omission of the above term means deletion of the y-direction leakage. Therefore, the neutron distribution pattern predicted by the truncated diffusion equation in region A will be one in which the neutrons diffuse in a system of parallel channels, aligned in the x-direction and insulated (neutronically) from one-another.

136

For two-group diffusion in two dimensions, the omission of both $\partial^2\phi_1/\partial y^2$ and $\partial^2\phi_2/\partial y^2$ leads to the one-dimensional, two-group diffusion equations, Eqs. (2.33) and (2.34).

Obviously, any truncations of the two-dimensional diffusion equations are approximations. Truncations as above, though, are attractive approximations because they provide sets of simple relations, (Eqs. (2.17) or (2.19) for one energy-group, Eqs. (2.17)' or (2.19)' for two groups), to represent region A, in which (2.1) is valid. Specifically, the "x-direction channel, insulated transversely" approximation provides boundary conditions to be applied along a y-direction boundary (i.e. along a boundary perpendicular to the direction of the channels) of region A. Boundary conditions along a x-direction boundary are obtained if the $\partial^2\phi/\partial x^2$-terms, instead of the $\partial^2\phi/\partial y^2$'s, are omitted from the two-dimensional diffusion equations.

To summarize, the "insulated channel" approximation permits the representation of a two-dimensional region A by means of one-dimensional, flux-to-normal current slab relations, applied on the two-dimensional boundary of region A. The one-dimensional slab relations involve the static impedances, α, defined in Chapter 2, Section 5.

5.2 NUMERICAL ACCOUNT FOR THE TRANS - CHANNEL LEAKAGE.

Consider, again, the two-dimensional diffusion equation (2.1):

$$\frac{\partial^2 \phi}{\partial x^2} + \frac{\partial^2 \phi}{\partial y^2} - \frac{1}{L^2} \cdot \phi = 0 \qquad (2.1)$$

Let us define a y-direction buckling:

$$B_y^2 \ (x,y) \equiv - \frac{1}{\phi(x,y)} \cdot \frac{\partial^2 \phi}{\partial y^2} \qquad (5.1)$$

The elimination of $\partial^2 \phi / \partial y^2$ between (2.1) and (5.1) yields:

$$\frac{\partial^2 \phi}{\partial x^2} - \left[\frac{1}{L^2} + B_y^2 \ (x,y) \right] \cdot \phi = 0 \qquad (5.2)$$

Eq. (5.2) provides no gain over (2.1), unless we know the x-and-y-dependent buvkling B_y^2 ; the latter, of course, we do not know, unless we know the solution $\phi(x,y)$ of Eq. (2.1). If however, we can find an a priori estimate of the x- and y- dependence of B_y^2

138

then Eq. (5.2) $\underline{is}$ a gain over (2.1) because (5.2) is one-dimensional. A condition which enables an a priori estimate of B_y^2 is the following:

The y-direction shape of the flux is independent of x ; i.e.:

$$B_y^2 \; (x,y) \stackrel{\sim}{=} B_y^2 \; (x_1,y) \tag{5.3}$$

where x_1 is fixed.

The above condition is expected to be satisfied $\underline{beyond}$ the immediate vicinity of interfaces between regions with different compositions, because all the severe changes in flux-shape take place near interfaces. (For more quantitative information on the range of validity of condition (5.3) see next section: "The Reflector Buffer zone").

Once condition (5.3) is valid, the problem of estimating $B_y^2 \; (x,y)$ is replaced by the problem of estimating $B_y^2 \; (x_1,y)$. In turn, once $B_y^2 \; (x_1,y)$ is known, the region $\underline{beyond \; x_1}$ can be represented by a static-impedance relation (see analysis for the one-dimensional slab). Thus, in a computation, the region $\underline{beyond \; x_1}$ can be replaced by a static-impedance boundary condition. During such a computation, the y-direction flux-shape at x_1 from each iteration

139

can be employed for an estimate of B_y^2 (x_1,y) to be used with the next iteration. In this manner, the trans-channel leakage is accounted for. The crucial point is, of course, the fulfillment of condition (5.3).

The two-group extension of the above development is straightforward. The extension starts with the definition of a y-direction buckling for each group,

$$B_{Y_g}^2 \equiv - \frac{1}{\Phi_g(x,y)} \cdot \frac{\partial^2 \Phi_g}{\partial y^2} \; ; \; g = 1,2 \qquad (5.1)'$$

and proceeds with the imposition of condition (5.3) for each group.

In the numerical tests, in order to avoid extra programming and extra iterations, we used the full core-reflector solution to determine the transverse bucklings $B_{Y_g}^2$. With the flux shapes agreeing as shown in Section 2.5, transverse bucklings inferred from the approximate shapes should be little different.

Regarding the iterative implementation of the transverse buckling it is noted that if the flux shapes $\Phi_g(x_1,y)$ at a given iteration stage are used to determine the $B_{Y_g}^2$ (x_1,y), a finite difference approximation to $\frac{\partial^2}{\partial y^2}$ will be necessary. Two-sided,

140

finite-difference approximations of the Laplacian operator will be possible at all but the end-points of a boundary segment; at the end-points one-sided approximations will be necessary. It is advisable that these one-sided approximations be of the same degree of accuracy as the two-sided ones [C-2].

5.3 THE REFLECTOR BUFFER ZONE (RBZ)

Figures 5.1 - 5.3 show thermal flux-shapes in two-dimensional reflector refions. Specifically, the flux-shapes are shown in directions parallel to -and at various distances from- core-reflector interfaces.

In Figure 5.1, the curves [1], [2], [3], [4] and [5] represent the thermal flux in a light-water reflector at distances, respectively , 0.0, 1.4, 3.8, 7.0, and 9.0 cm from the surface of the small, cross-shaped core. We note the huge difference between shapes [1] and [2]. Shapes [3], [4] and [5] are, on the contrary, very much alike.

In Figure 5.2, the curves [1], [2], [3] and [4] represent the thermal flux again in a light-ater reflector at distances, respectively, 0.0, 1.8, 3.8, and 7.0 cm from the surface of the upper step of the intermediate-sized, 3-step core while curves [9], [8],
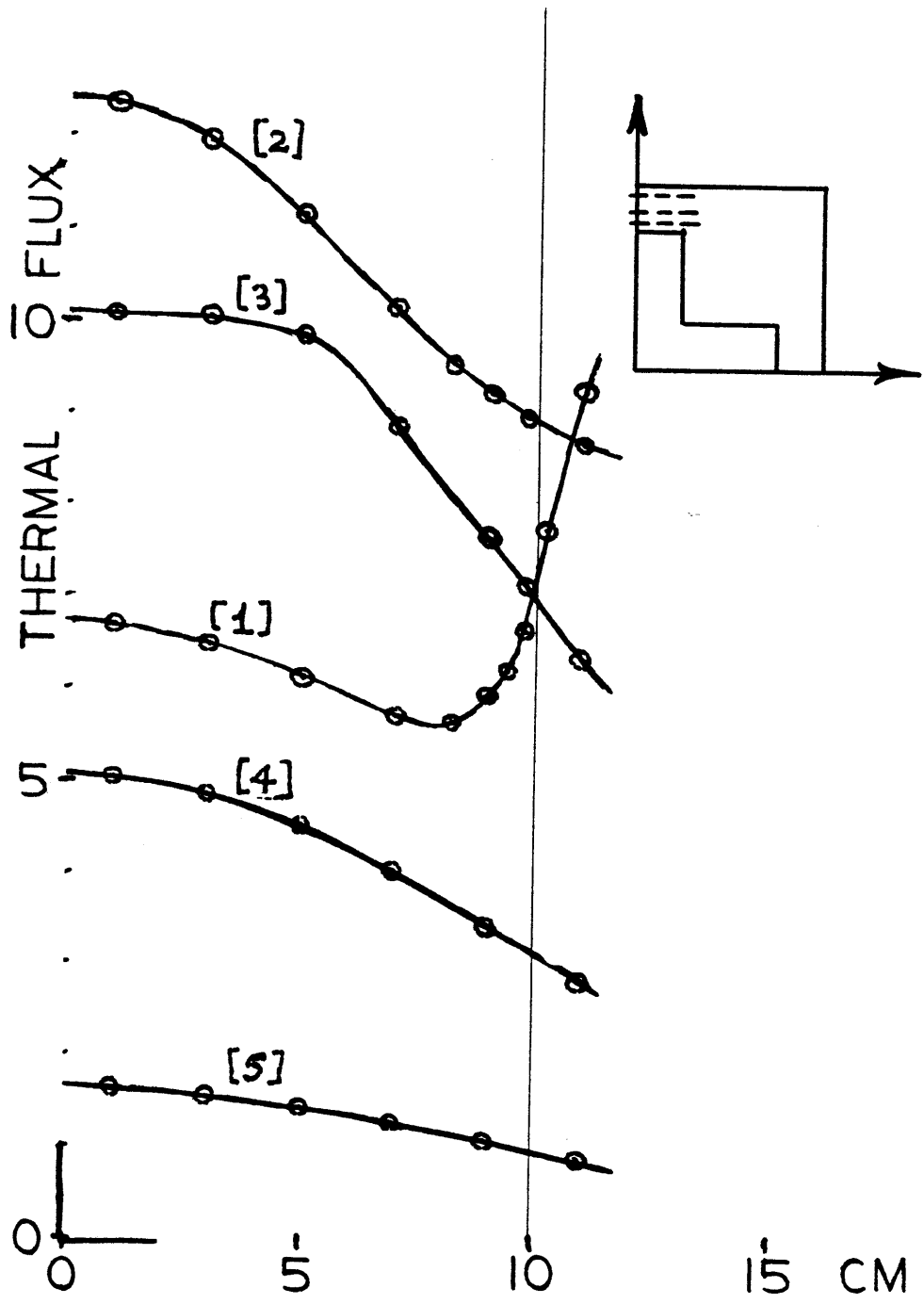
FIGURE 5.1 : FLUX SHAPES IN H_2O REFLECTOR
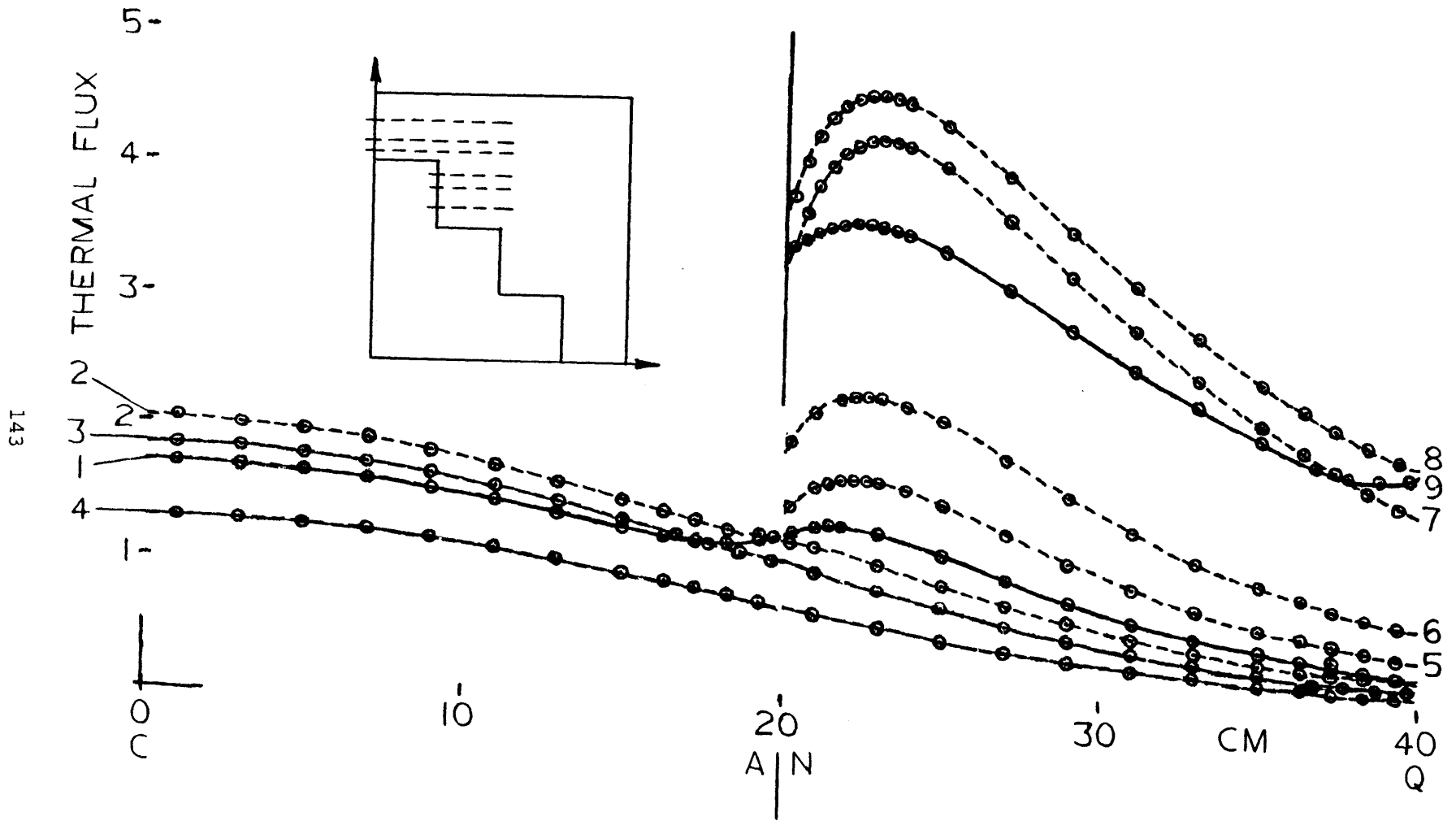
FIGURE 5.2

FLUX SHAPES IN H_2O REFLECTOR
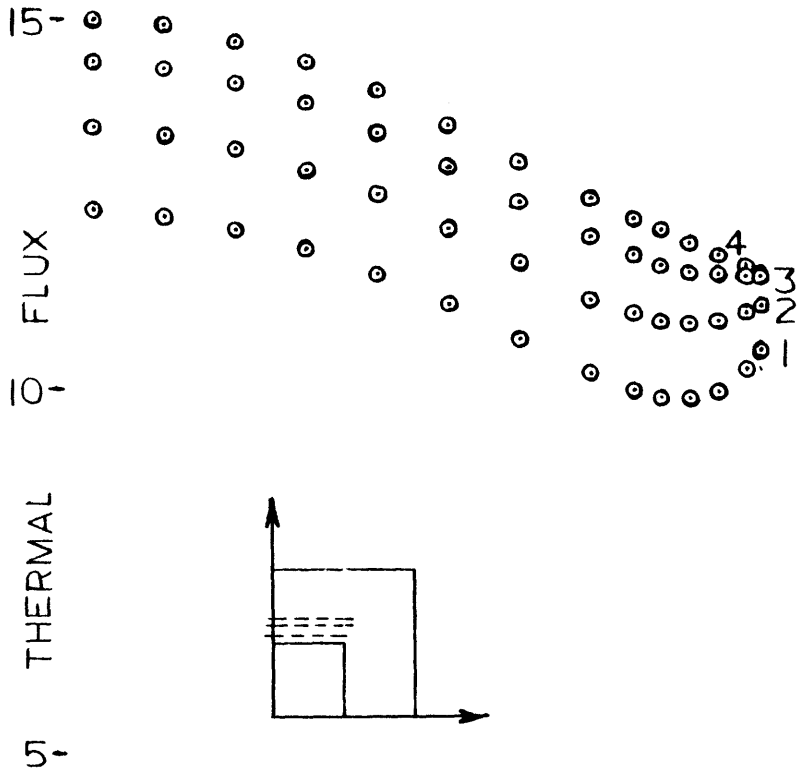
FIGURE 5.3A
FLUX SHAPES IN D$_2$O
REFLECTOR
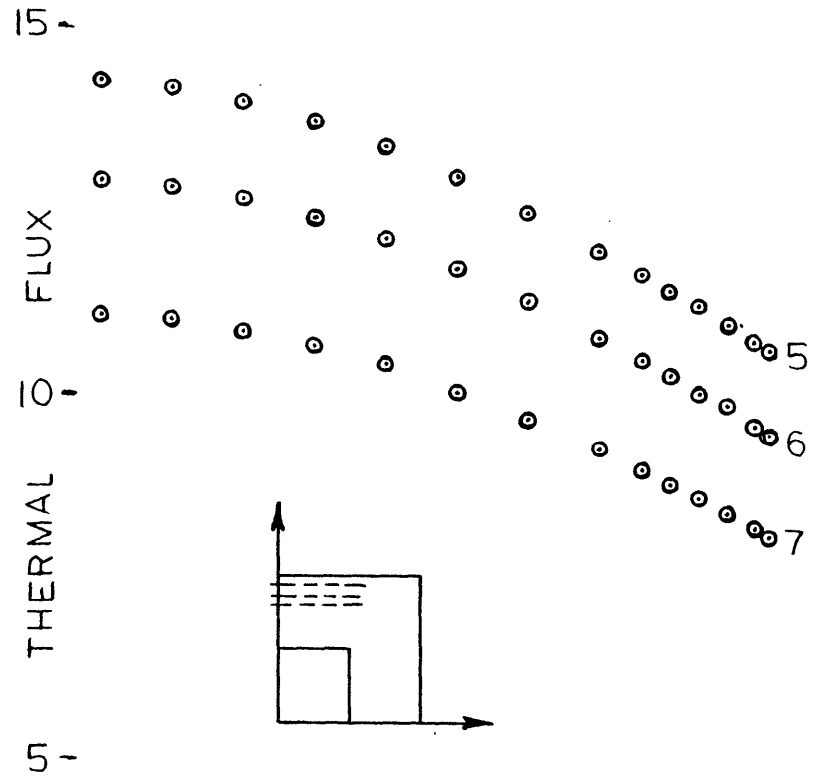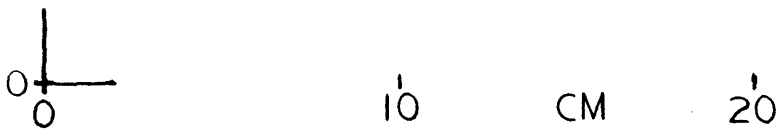
FIGURE 5.3B
FLUX SHAPES IN D$_2$O
REFLECTOR
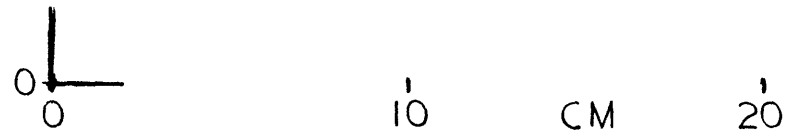
[7], [6] and [5] represent the thermal flux at distances,

respectively, 0.0, 1.8, 5.0, 13.0, 16.75 cm from the surface

of the middle step. Again, the shapes [1] and [2] are vastly

different from each other and so are [9] and [8]. Deeper inside

the reflector, the shapes are much more similar: [3] is similar

to [4] and [7] is similar to [6] and [5].

In Figure 5.3, the curves [1], [2], [3], [4], [5], [6] and

[7] are thermal flux-shapes in a heavy-water reflector at

distances, respectively, 0.0, 0.6, 2.2, 3.8, 7.0, 9.0 and 11.0 cm

from the surface of the small, square core. Of these shapes, [1],

[2] and [3] are one family and [4], [5], [6] and [7] are another.

It is evident from the above figures that a reflector zone

adjacent to the core is the transition region for flux shapes.

This zone, which we shall call the Reglector Buffer Zone (RBZ),

is roughly 2.0 cm-thick for the light-water-reflected models of

Figures 5.1 and 5.2 and 4.0 cm-thick for the heavy-water-reflected

model of Figure 5.3.

5.4 ANALYTICAL ACCOUNT FOR THE TRANS - CHANNEL LEAKAGE:

THE "SMITH" CORRECTION FACTOR.

In Chapter 3, Section 4 we derived an approximate flux-to-normal current boundary condition, Eq. (3.32), for the 90^0 wedge. The derivation was based on the assumption that the variation of the normal current, J_θ, along the boundary of the wedge over an interval about 4 reflector diffusion lengths wide is very slow. Inspection of Eq.(3.32) shows that the ratio Φ/J_θ is equal to the static impedance α plus a correction. The correction is $s(r)\equiv\alpha\cdot\exp(-r/L)$, where r is the distance of boundary point from the peak of the wedge. A few diffusion lengths away from the peak the correction $s(r)$ vanishes while at the peak the value $s(r=0)$ is equal to α, so that the flux-to-normal current ratio at the peak is equal to 2α.

The correction term in Eq. (3.32) provides a simple and accurate analytical account for the trans-channel leakage, when the assumption of slow variation of J_θ over 4L is realistic. This analytical account is an alternative to the numerical one, discussed in Section 5.2.

We shall call the correction factor $s(r)$ the "Smith" factor, after the author of Ref. [S-1].

146

The two-group extension of Eq. (3.32) is the pair of equations (3.32)' and (3.32)".

5.5 SPECIFICATIONS OF THE NUMERICAL TESTS.

In this section we give various specifications for the numerical tests which we performed on the method of implicit representation of reflectors. In the following sections we present and discuss the results of these tests.

The configurations and sizes of the various test reactor models used are given in Table 5.1. The same configurations and their relative sizes are shown in Figure 5.4.

A set of two-group, PWR data is given in Table 5.2. Table 5.3 contains two-group data for heavy water and graphite. Table 5.4 is a list of the compositions used in the tests.

The various finite-difference mesh-patterns employed in the computations are listed in Table 5.5.

The specifications of the two time-dependent problems tested are given in Table 5.6.

All computations were performed in the M.I.T. Information Processing Center. The computer codes CITATION[F-1] and GAKIN II [H-1] were employed for the steady-state and time-dependent calculations, respectively. The input of impedance boundary conditions to CITATION was effected without reprogramming (see Ap-

148

pendix B for details on the preparation of the input). The input

of impedance boundary conditions to GAKIN II required some minor

reprogramming (see Appendix C).

T A B L E 5.1

CONFIGURATIONS AND SIZES OF REACTOR

MODELS EMPLOYED IN NUMERICAL TESTS.

Name of Model	Number of Dimensions	Description of Core	Description of Reflector	Symmetry
1-d slab	1	Total core thickness=40 cm.	10 cm-thick slabs on either side of the core	Half
Square	2	Square, 40 cm × 40 cm	10 cm-thick slabs on each side of the core.	Octant
Cross	2	Total core consists of 5, square, 20 cm × 20 cm, fuel blocks arranged in the form of a cross.	Core embedded and centered in a square, 80 cm × 80 cm reflector. Outer sides of reflector are parallel to the sides of the square fuel blocks. Thus, minimum reflector thickness=10 cm.	Octant

Name of Model	Number of Dimensions	Description of Core	Description of Reflector	Symmetry
Three-steps	2	Total core consists of 24, square, 20 cm × 20 cm, fuel blocks arranged so that each quarter core has a three-step form.	Core embedded and centered in a square, 160 cm × 160 cm, reflector. Outer sides of reflector parallel to sides of fuel blocks. Thus, minimum refl. thickness=20 cm.	Octant
Three-Steps with Shroud	2	Same as 3 - steps model.	Core is surrounded by a 2 cm-thick, stainless steel shroud. Shrouded core is embedded and centered in a square, 160 cm × 160 cm, reflector. Outer sides of refl. parallel to sides of fuel blocks. Thus, min. refl. thickness=18 cm.	Octant

151

TABLE 5.1 (Continued)

Name of Model	Number of Dimensions	Description of Core	Description of Reflector	Symmetry
ZION	2	See Engineer's Thesis by L. Deppe, Nuclear Engineering Department, M.I.T., 1973.		Octant
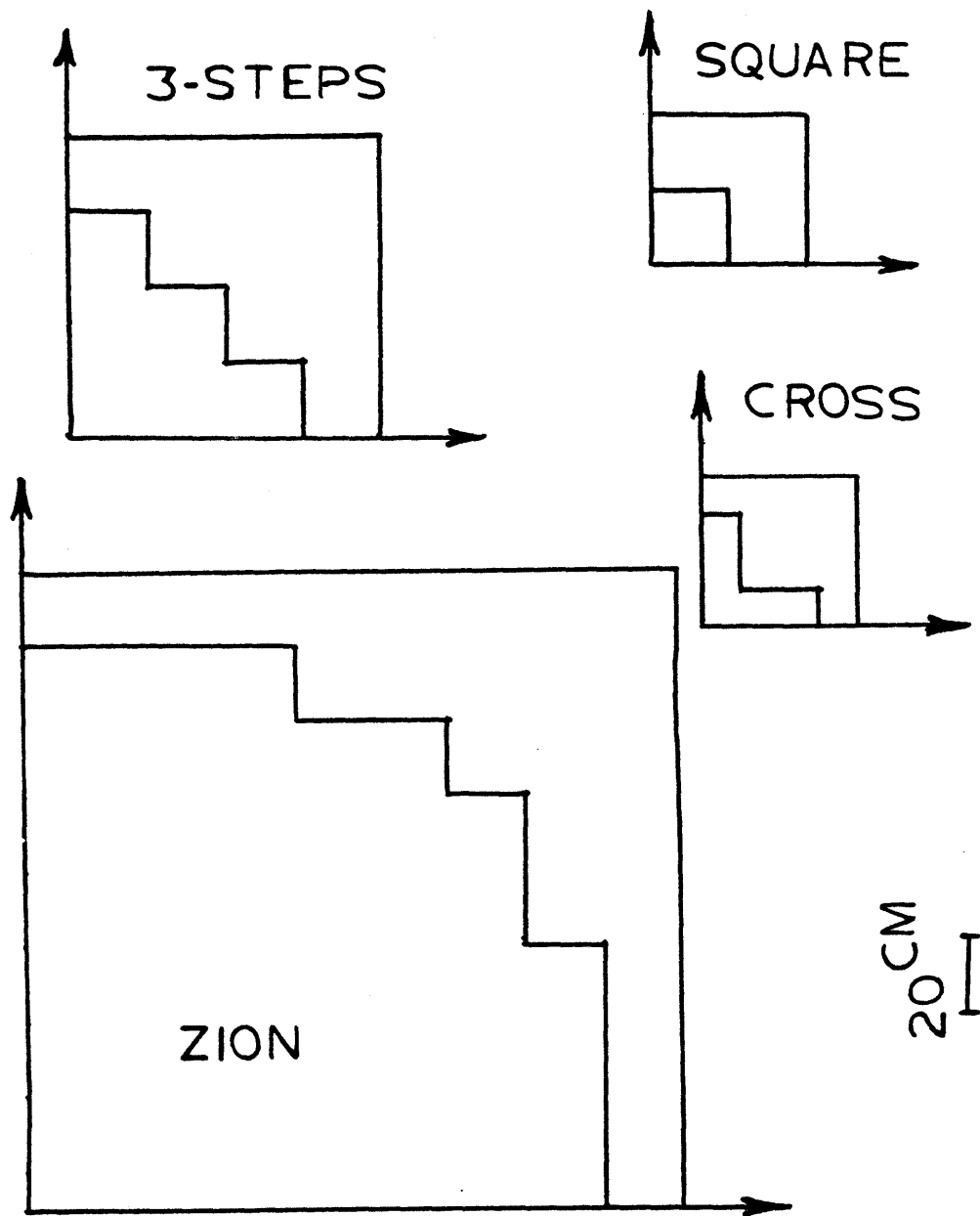
FIGURE 5.4
RELATIVE SIZE OF TEST-MODELS____

T A B L E 5.2

TWO - GROUP, PWR DATA[*]

Material Type	Σ_{tr}^1	Σ_{tr}^2	Σ_a^1	Σ_a^2	Σ_r^1	$\nu\Sigma_f^1$	$\nu\Sigma_f^2$
Fuel	.241010	.897882	.00827435	.068261	.018866	.00504978	.0884659
Reflector (Water)	.23742	1.3495	.000791834	.0286603	.0365214	—	—
Shroud	.37978	1.1017	.00446266	.0703	.00114323	—	—

Fission Spectrum: $x_1 = 1.0$, $x_2 = 0.0$

*Source: R.A. Shober, Nucl. Eng. Dept., M.I.T.

T A B L E 5.3

HEAVY WATER AND GRAPHITE

TWO - GROUP DATA

	HEAVY WATER [*]			GRAPHITE [**]		
g	D_g	Σ_g	$\Sigma_{1 \to 2}$	D_g	Σ_g	$\Sigma_{1 \to 2}$
1	1.294	0.01136	0.01136	0.968992	0.00498523	0.00498000
2	0.8551	0.0000953	——	0.789889	0.000296	——

[*] Source: W.J. Garland et al., Nucl. Sci. Eng. 55, 119 (1974).

[**] Source: T.Y.C. Wei, Doctoral Thesis, M.I.T., 1975.

T A B L E 5.4

COMPOSITIONS USED IN TESTS

#	Description
1	Typical PWR Composition. (Source: C.M. Kang, Doctoral Thesis, M.I.T.,1971).
2	Composition of Table 5.2
3	ZION Reactor Composition (Source: L.O.Deppe, Engineer's Thesis, M.I.T.,1973).
4	Fuel of Composition # 1. D_2O - Reflector of Table 5.3.
5	Fuel from Composition # 2. D_2O - Reflector of Table 5.3.
6	Fuel of Composition # 2. Graphite - Reflector of Table 5.3

TABLE 5.5

MESH PATTERNS

Pattern #	Description
1	Mesh Size $\equiv$ h = 1 cm everywhere.
2	h = 2 cm everywhere.
3	h = 0.2 cm within 4 cm-thick zones on either side of C-R interface. h = 2.0 cm everywhere else
4	h = 0.2 cm everywhere
5	h = 0.4 cm within 4 cm-thick zones on either side of C-R interface. h = 2.0 cm everywhere else.
6	h = 0.5 cm within a 4 cm-thick zone on the core side of C-R interface. h = 0.4 cm within a 4 cm-thick zone on the reflector side of C-R interface. h = 2.0 cm everywhere else.
7	The value of the spatially varying h can be infered from the abcisas of pairs of adjacent circles in Fig.5.16.
8	The value of the spatially varying h can be infered from the abcisas of pairs of adjacent x's or pairs of adjacent squares in Fig. 5.16.

157

T A B L E 5.6

SPECIFICATIONS OF TEST - TRANSIENTS

Reactor Configuration: 1-d Slab.

Compositions: # 5 and 6.

Group speeds: 5×10^6 and 2×10^5 cm/sec.

Delayed Neutron Data: U^{235}/thermal fission.

Initial Condition for Slow Transient: Steady State.

Initial Condition for Fast Transient: Steady State.

Driving Force of Slow Transient: Ramp reduction of thermal capture cross section in left half of the core. Ramp rate = 1%/sec.

Driving Force of Fast Transient: Ramp reduction of thermal capture cross section in left half of the core. Ramp rate = 500%/sec.

Spatial mesh size: h = 1.0 cm.

Initial Time-Step Used in Slow Transient Calculation - 1 msec.

Initial Time-Step Used in Fast Transient Calculation = 10 μsec.

5.6 TESTS ON SMALL - SIZED REACTOR MODELS.

In this section we present and discuss the results of numerical tests of the reflector-replacement method applied to small-sized reactor models, namely the "1-d Slab", the "Square" and the "Cross" (see specifications of reactor models in Table 5.1).

Table 5.7 contains a list of the various modes of implicit reflector representation tested on small-sized, light water-reflected reactor models in steady state, the corresponding eigenvalues and references to relevant figures. Many of the tests were performed with two different mesh-patterns, one coarse and one fine. In Table 5.7 the columns under the headings "Critical Eigenvalue" and "References to Figures" are each split into two half-columns. The left half-columns contain the results of the coarse-mesh calculations and the right half-columns contain the results of the fine-mesh calculations. The number of the mesh-pattern employed is explicitly indicated in parentheses at all row-half column intersections.

Table 5.8 is the counterpart of Table 5.7 for heavy water-reflected reactor models.

159

Table 5.9 contains results from tests on small-sized, light and heavy water-reflected reactor models in dynamic states.

T A B L E 5.7

TESTS ON SMALL-SIZED, LIGHT WATER-REFLECTED REACTOR

MODELS IN STEADY STATE

Model	Composit.	Type of Solution/ Type of Boundary Condition Applied	Critical Eigenvalue		References to Figures	
			Coarse Mesh, #	Fine Mesh, #	Coarse Mesh, #	Fine Mesh, #
1-d Slab	1 #	Full Core-Reflector Solution	0.9660755 (#2)	0.9671855 (#4)	Circles in Fig.5.5 (#2)	
		Impedances at C-R Interface	0.9672399 (#2)	0.9672012 (#4)	x's in Fig.5.5 (#2)	
Square	1 #	Full Core-Reflector Solution	0.8939846 (#2)	0.8966821 (#3)	Upper x's in Fig.5.6 (#2)	Lower x's in Figs 5.6 & 5.7 (#3)

Model Composition		Type of Solution/ Type of Boundary Condition Applied	Critical Eigenvalue		References to Figures	
			Coarse Mesh, #	Fine Mesh, #	Coarse Mesh, #	Fine Mesh, #
Square #1		Impedances at C-R Interface	0.8991820 (#2)	0.8994374 (#3)	Δ's in Fig.5.6 (#2)	Circles In Figs. 5.6&5.7 (#3)
Cross #1		Full Core-Reflector Solution	0.8971822 (#1)	0.8984979 (#5)	x's in Figs. 5.8, 5.9, 5.10, 5.11 (#1)	
		Impedances at C-R Interface	0.8784639 (#1)		Circles in Fig.5.8 & 5.9 (#1)	

T A B L E 5.7 (Continued)

Model	Type of Solution/ Type of Boundary Condition Applied	Critical Eigenvalue		References to Figures	
		Coarse Mesh, #	Fine Mesh, #	Coarse Mesh, #	Fine Mesh, #
Cross #1	Numerically-Corrected Impedances at C-R Interface	0.8784977 (#1)		∇'s in Figs. 5.8 and 5.9* (#1)	
	Smith-Corrected Impedances at C-R Interface	0.9020467 (#1)		Circles in Figs. 5.10 and 5.11 (#1)	

* Where the ∇'s are not shown, they coinside with the circles.
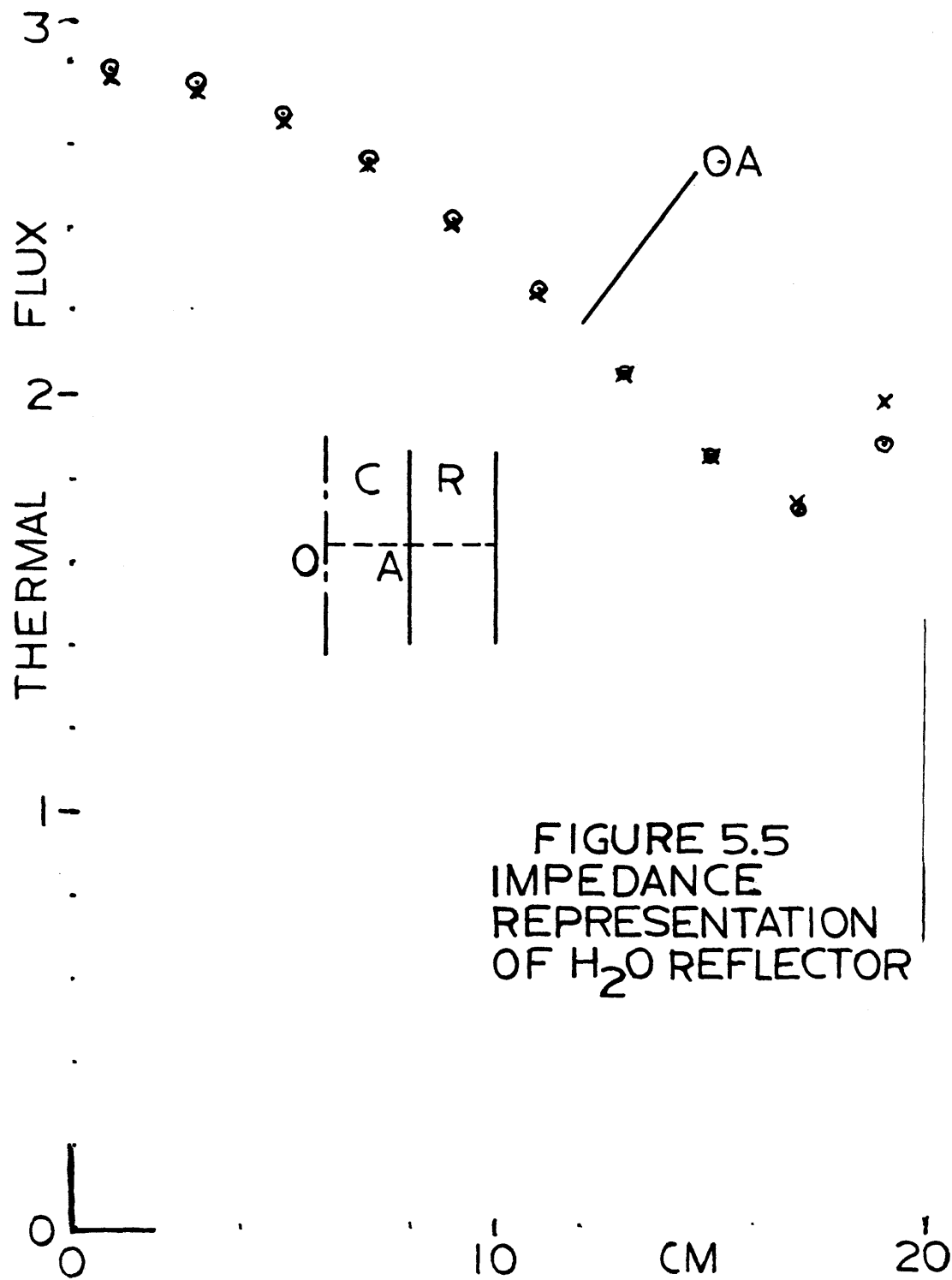
FIGURE 5.5
IMPEDANCE
REPRESENTATION
OF H_2O REFLECTOR

THERMAL FLUX

C | R

O | A

⊖A

3

2

1

0

0   10   CM   20
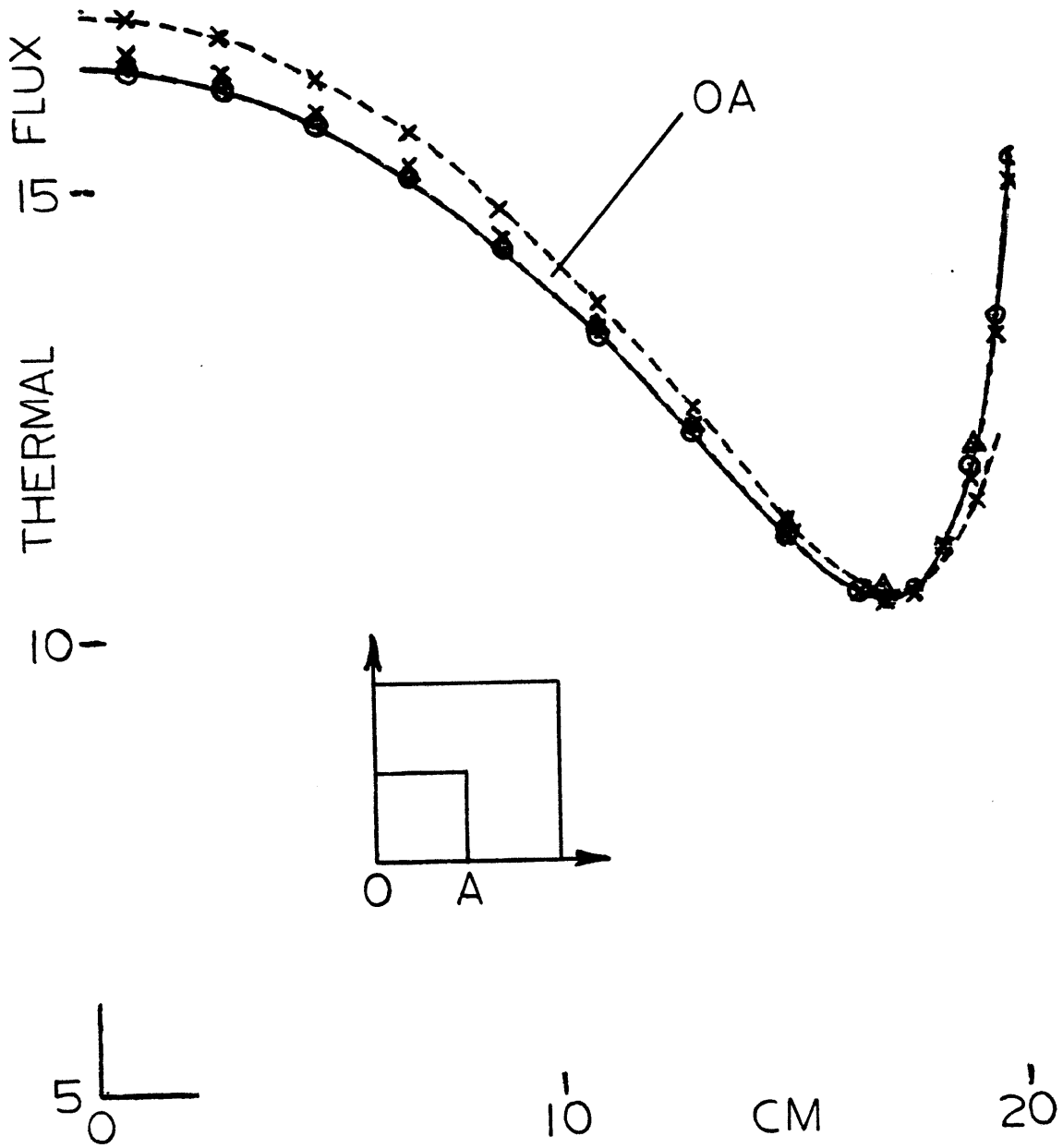
FIGURE 5.6
IMPEDANCE REPRESENTATION OF
H$_2$O REFLECTOR
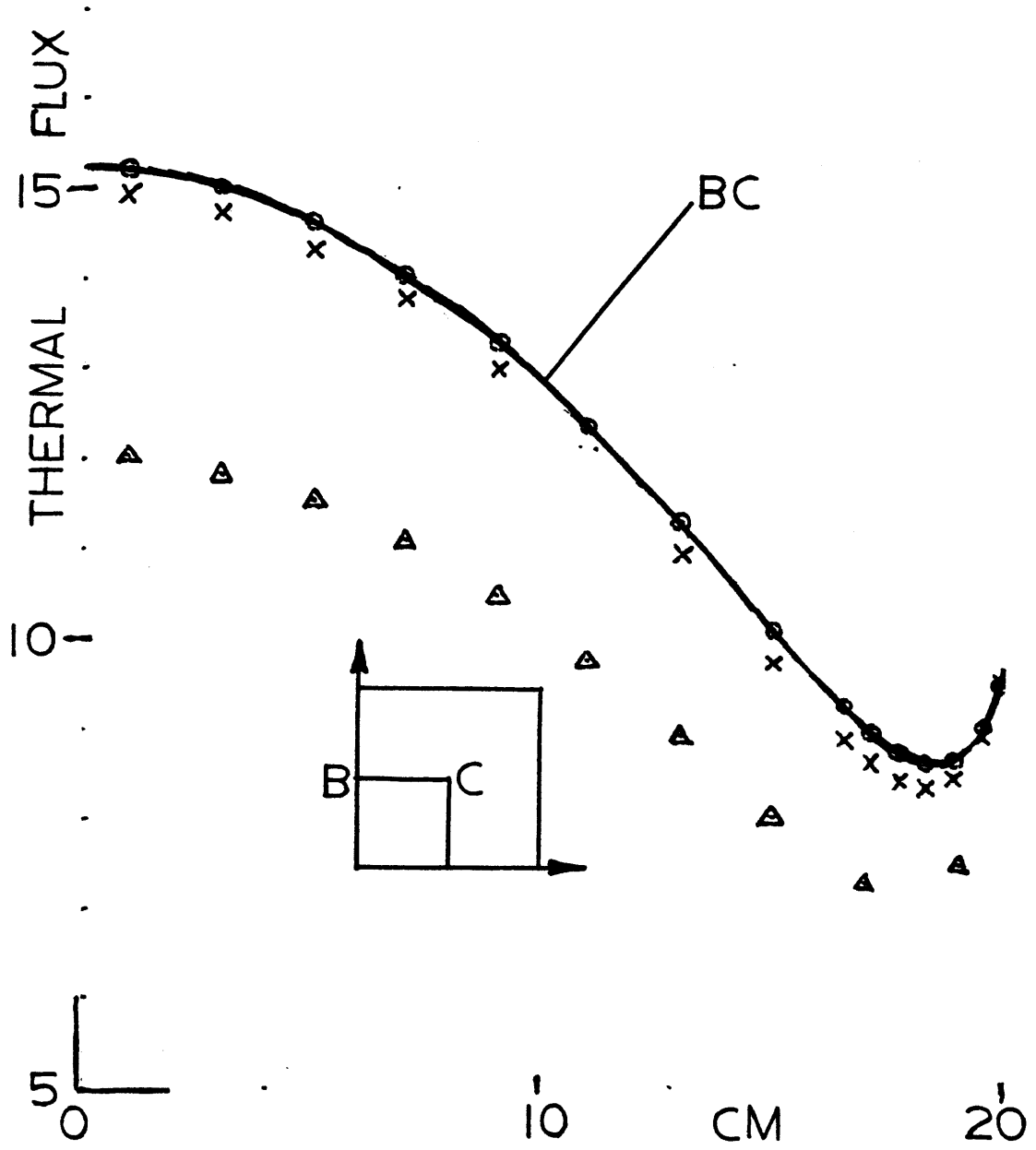
FIGURE 5.7
IMPEDANCE REPRESENTATION OF
H$_2$O REFLECTOR

166

FIGURE 5.8

IMPEDANCE REPRESENTATION OF
H_2O REFLECTOR

THERMAL FLUX

OA

15

10

5

0

10

20

30

CM

40

167

FIGURE 5.9
IMPEDANCE REPRE-
SENTATION OF H_2O
REFLECTOR
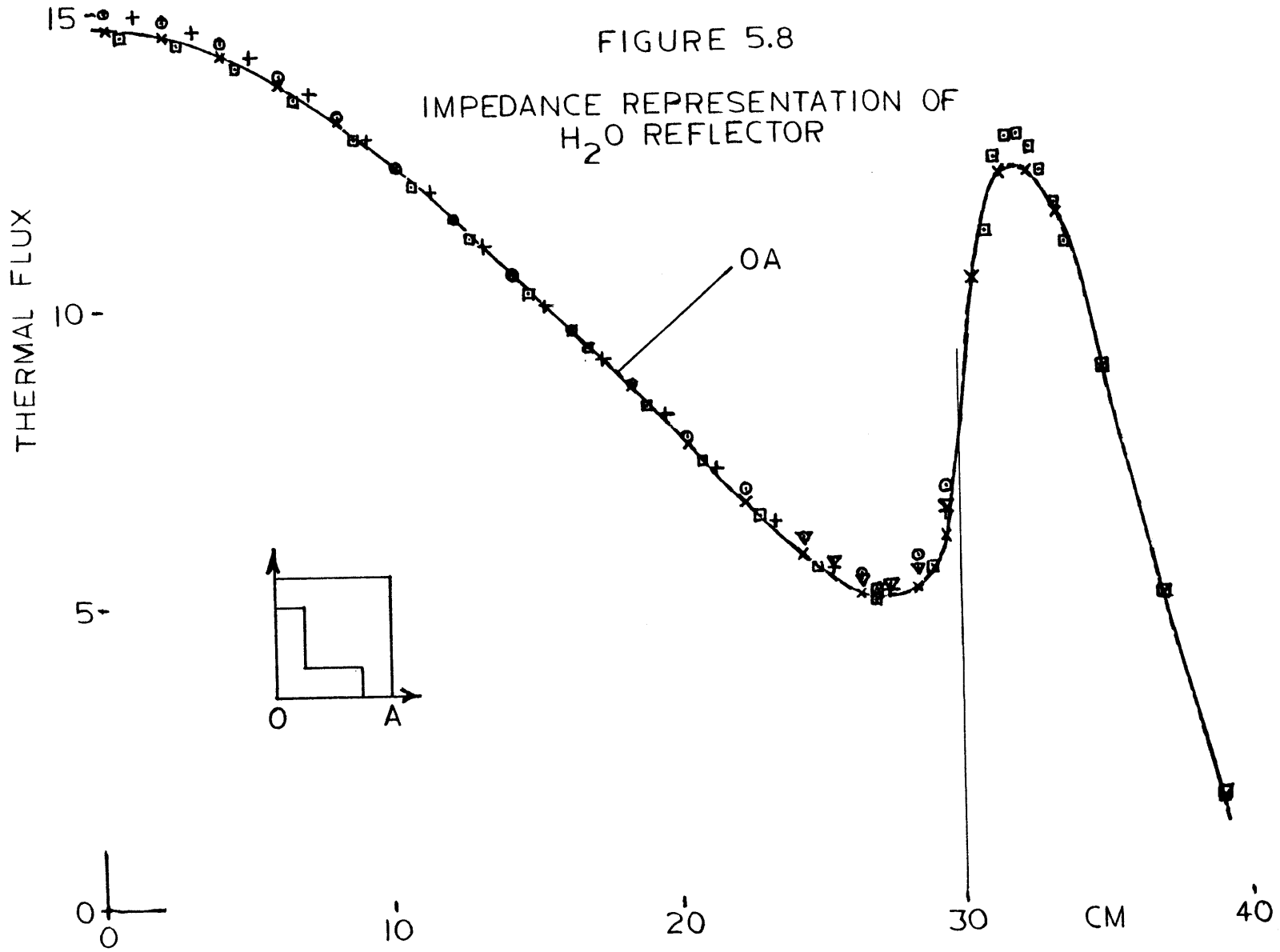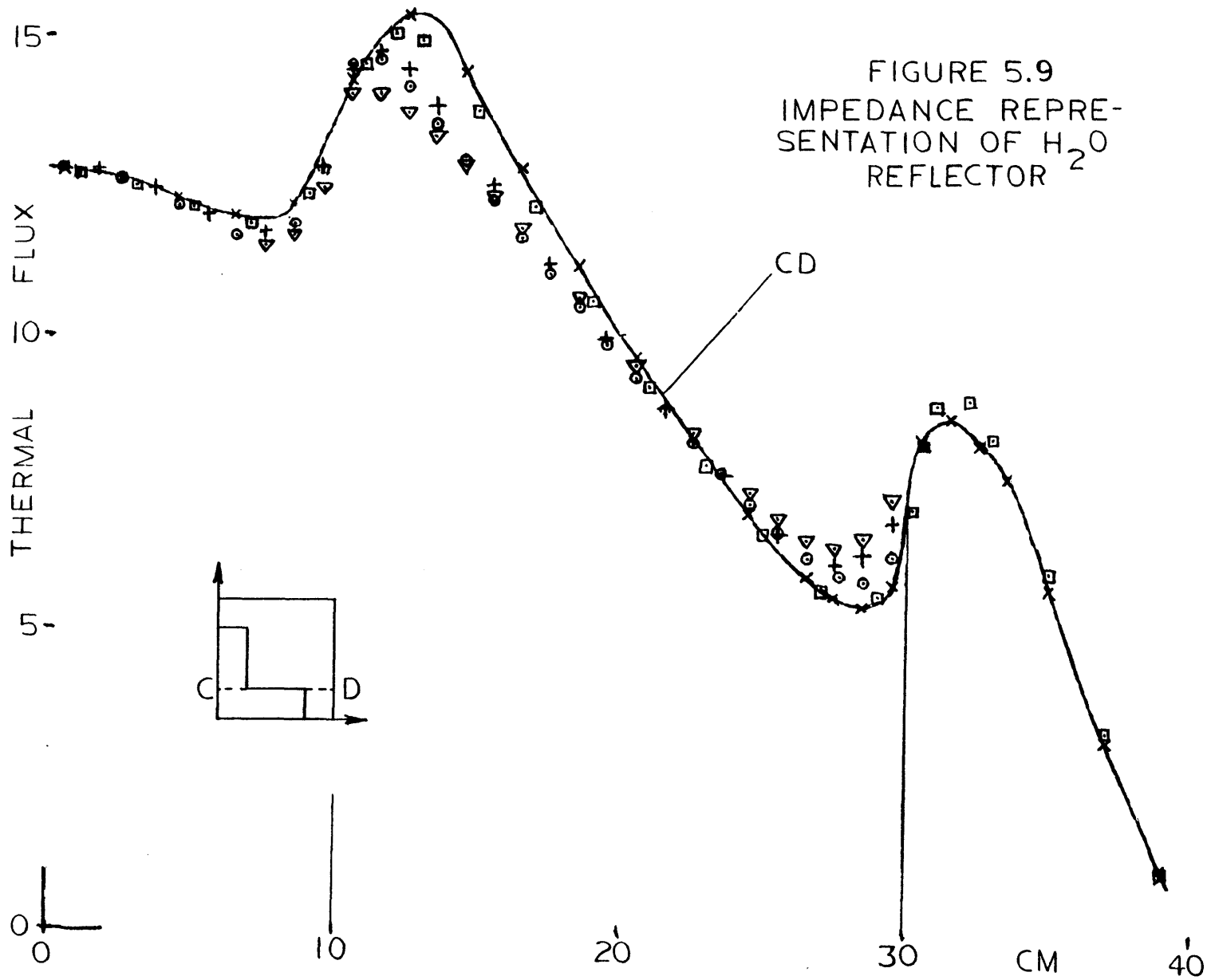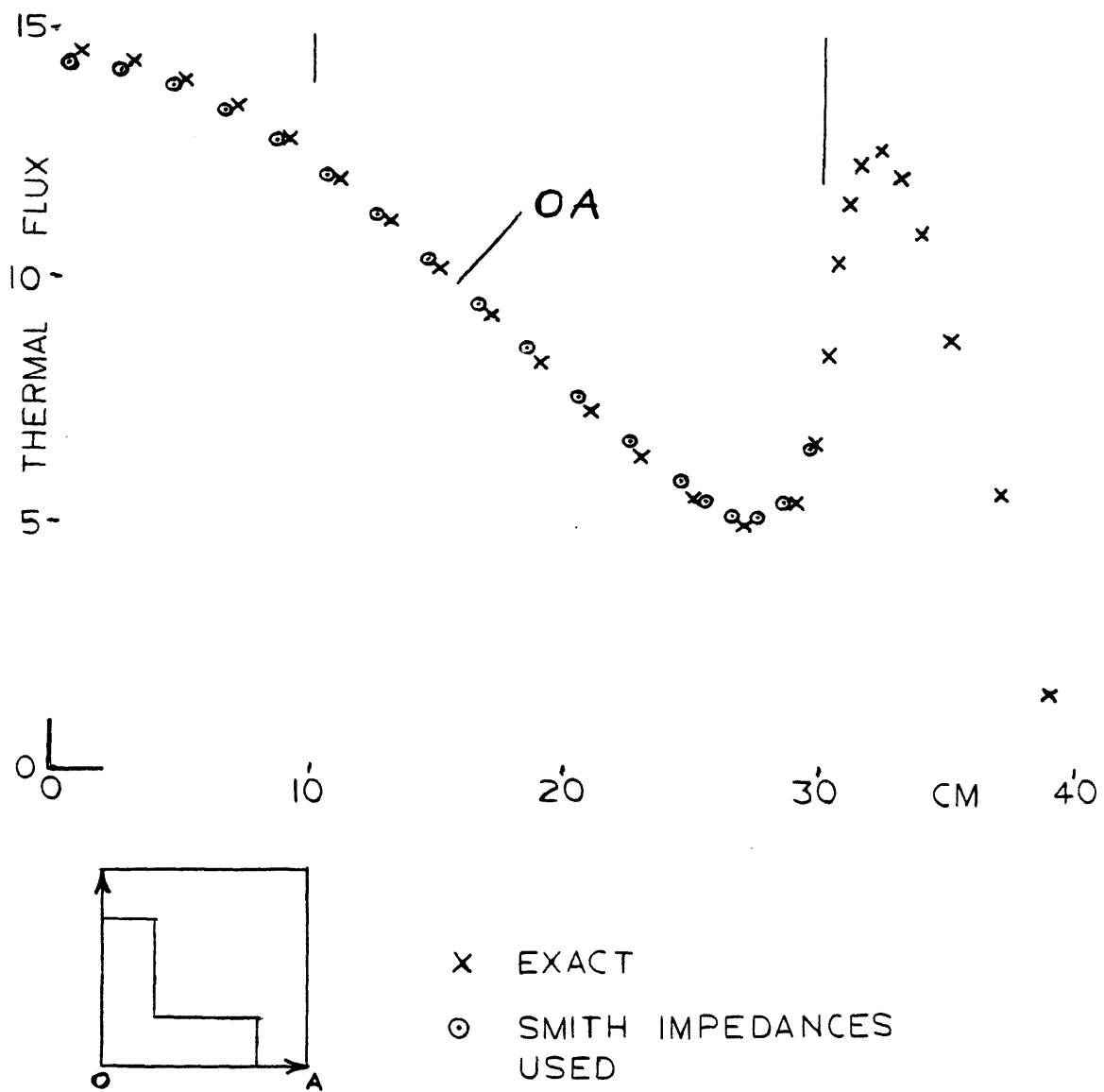
FIGURE 5.10

SMITH REPRESENTATION OF
H_2O REFLECTOR
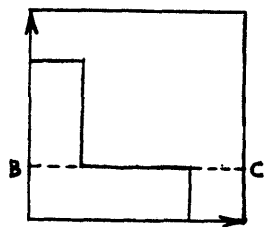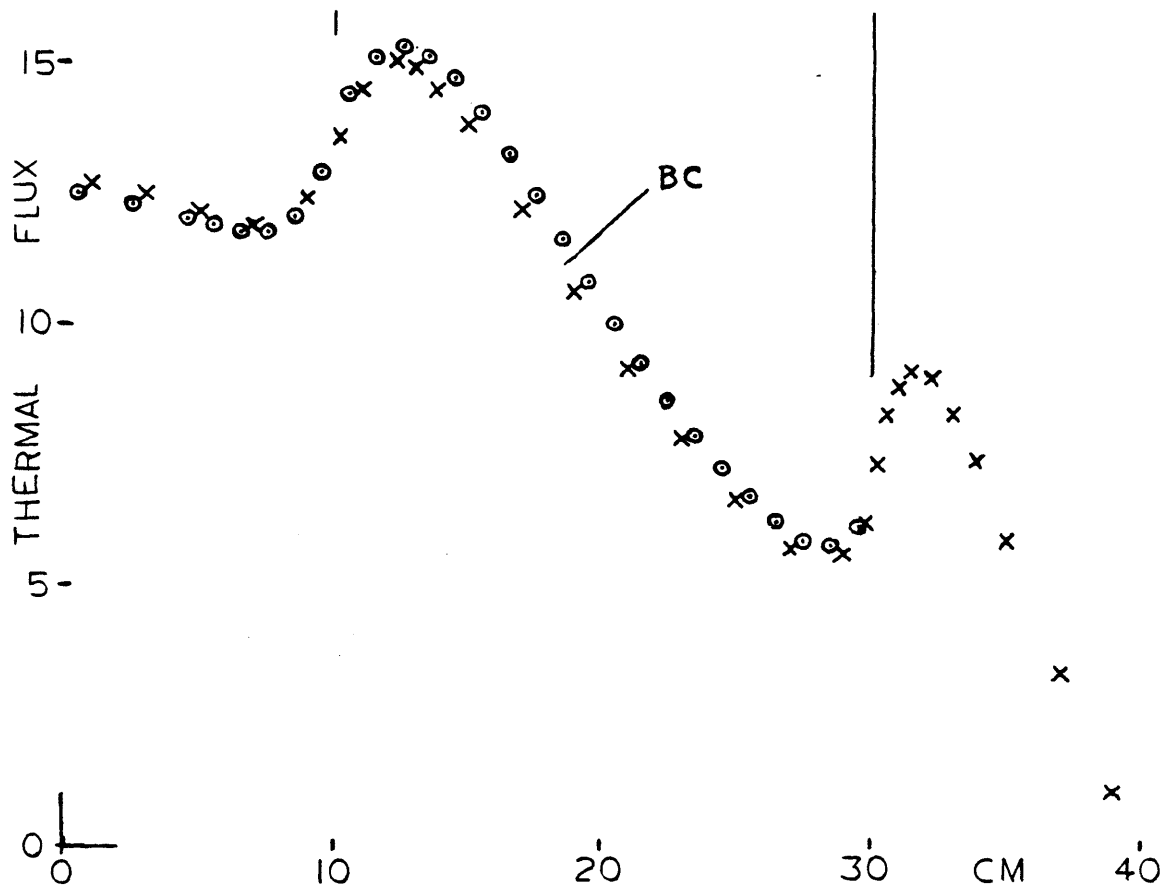
FIGURE 5.11
SMITH REPRESENTATION OF
H$_2$O REFLECTOR

X   EXACT

⊙   SMITH IMPEDANCES
    USED

T A B L E 5.8

TEST ON SMALL-SIZED, HEAVY WATER-REFLECTED REACTOR

MODELS IN STEADY STATE

Model Composition	Type of Solution/ Type of Boundary Condition Applied.	Critical Eigenvalue		References to Figures	
		Coarse Mesh, #	Fine Mesh, #	Coarse Mesh, #	Fine Mesh, #
Square #4 Reflector Thickness = 20 cm.	Full Core-Reflector Solution		0.9471047 (#5)		x's In Figs.5-17 & 5-19 (#5)
	Impedances at C-R Interface		0.9608409 (#5)		Circles in Fig.5.17 (#5)
	Impedances at Outer Surface of RBZ		0.9536103 (#5)		Circles in Fig. 5.18 (#5)

T A B L E 5.8 (Continued)

Model Composition	Type of Solution/ Type of Boundary Condition Applied.	Critical Eigenvalue		References to Figures	
		Coarse Mesh, #	Fine Mesh,#	Coarse Mesh, #	Fine Mesh, #
Square #4 Reflector Thickness=20cm	Numerically-Corrected* Impedances at Outer Surface of RBZ		0.9476528 (#5)		Circles in Fig. 5.19 (#5)

* The numerical correction consists in computation of the impedances with Σ_g's replaced by

$$\Sigma_g + D_g \cdot (\pi/80 \text{ cm})^2$$

THERMAL FLUX

15-

OA

BC

10-

5-
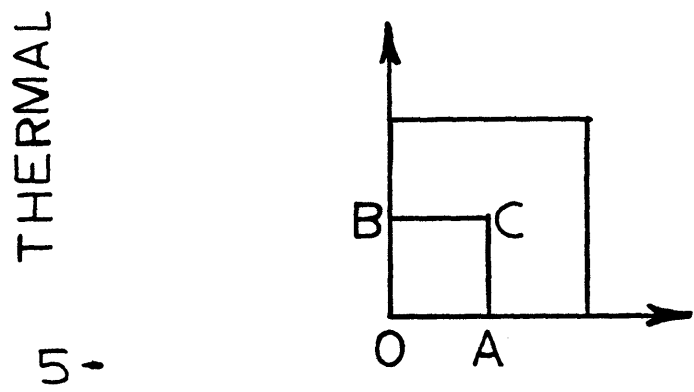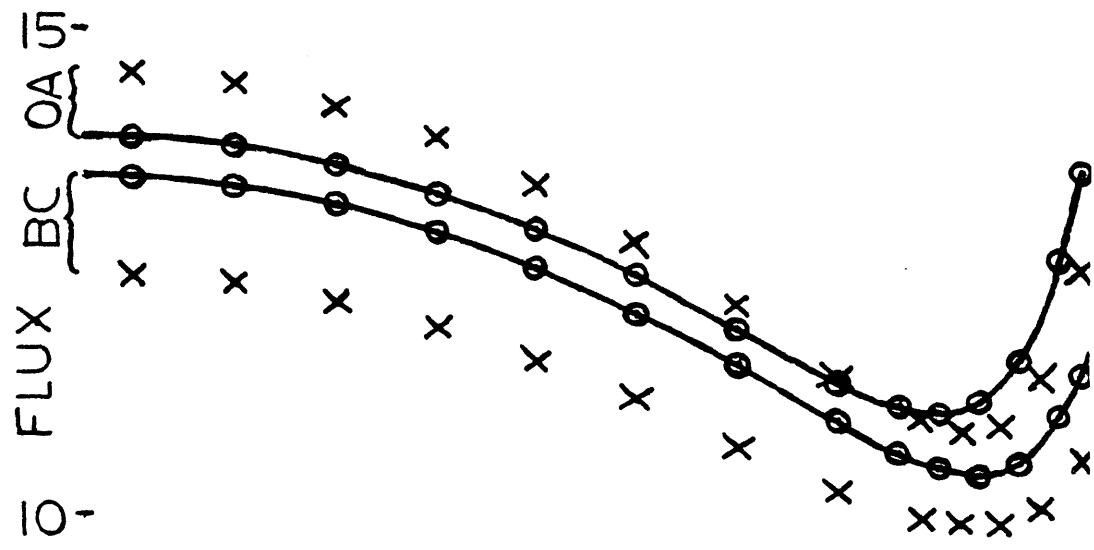
FIGURE 5.17

IMPEDANCE
REPRESENTATION
OF D$_2$O REFLECTOR

10   CM   20

THERMAL FLUX

5-

15-

OA

BC

10-

0-

B   C

O   A
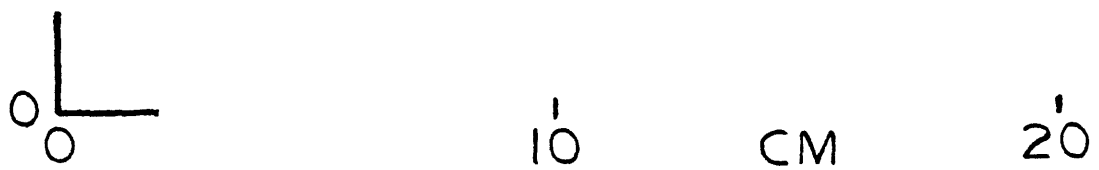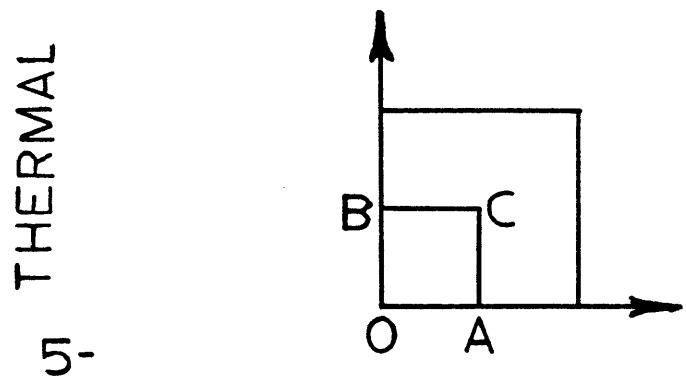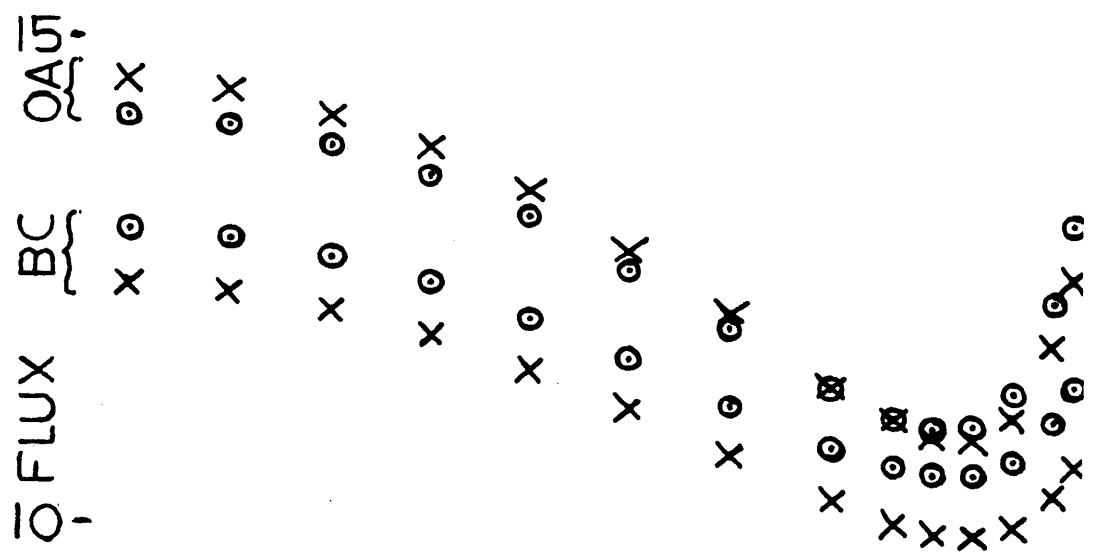
FIGURE 5.18
IMPEDANCE
REPRESENTATION
OF D$_2$O REGION
OUTSIDE RBZ

O
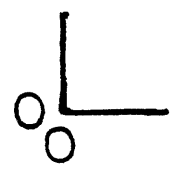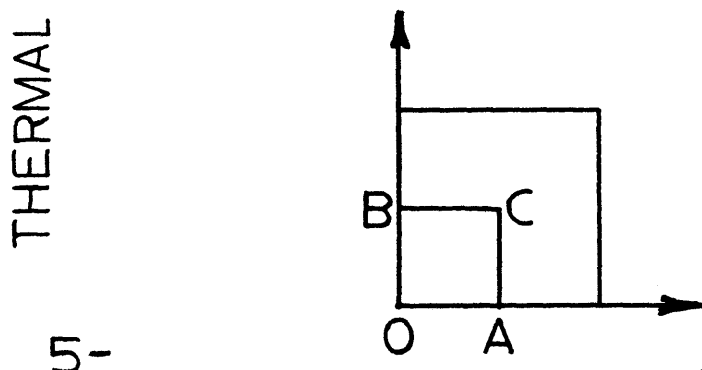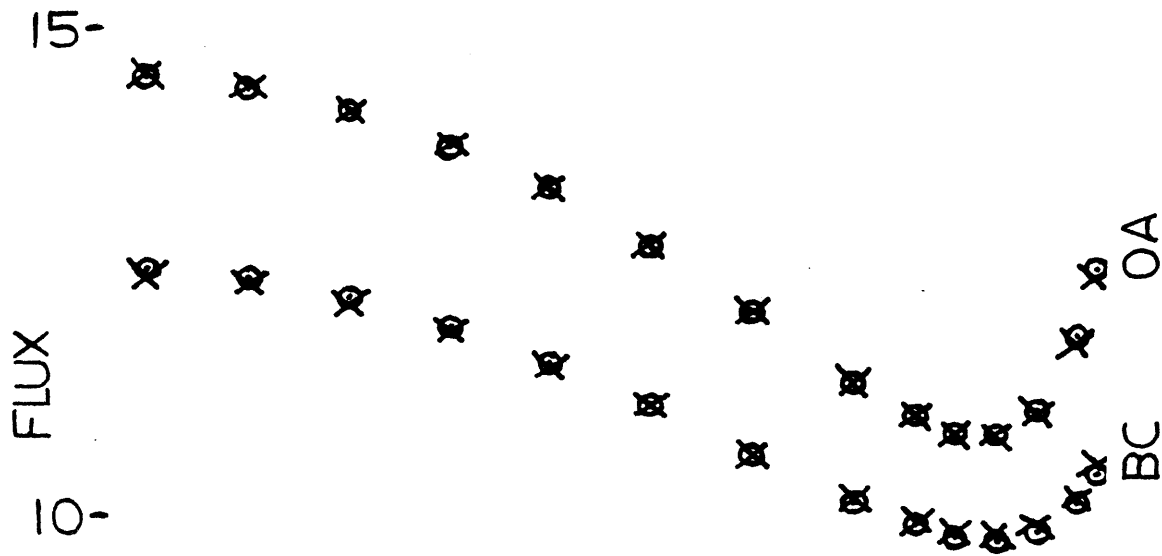
0   10   CM   20

FIGURE 5.19
REPRESENTATION
OF D_2O REGION
OUTSIDE RBZ
BY NUMERICALLY
CORRECTED
IMPEDANCES
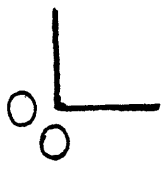
T A B L E 5.9

RESULTS OF THE IMPLICIT REPRESENTATION OF REFLECTORS

IN TEST - TRANSIENTS

"SLOW" TRANSIENT

t (sec)	% Error in Reactor Power					
	STATIC APPROX'N - NO RBZ		STATIC APPROX'N OUTSIDE RBZ		LINEAR APPROX'N - NO RBZ	
	H_2O	D_2O	H_2O	D_2O	H_2O	D_2O
0.0	0.0%	0.0%	0/0%	0.0%	Not tested	
0.1	0.0	-0.3	-0.1	-0.3		
0.5	1.4	-0.4	1.3	-0.2		
1.0	2.9	-0.1	2.7	-0.2		

T A B L E 5.9 (Continued)

RESULTS ON THE IMPLICIT REPRESENTATION OF REFLECTORS

IN TEST - TRANSIENTS

"FAST" TRANSIENT=

t (msec)	% Error in Reactor Power					
	STATIC APPROX'N - NO RBZ		STATIC APPROX'N OUTSIDE RBZ		LINEAR APPROX'N - NO RBZ	
	H_2O	D_2O	H_2O	D_2O	H_2O	D_2O
0.0	0.0%	0.0%	0.0%	0.0%	0.0%	Diverges
1.0	0.1	0.2	0.0	0.1	0.0	
5.0	1.6	7.7	0.7	5.4	0.0	
10.0	5.9	32.9	2.6	22.7	0.0	
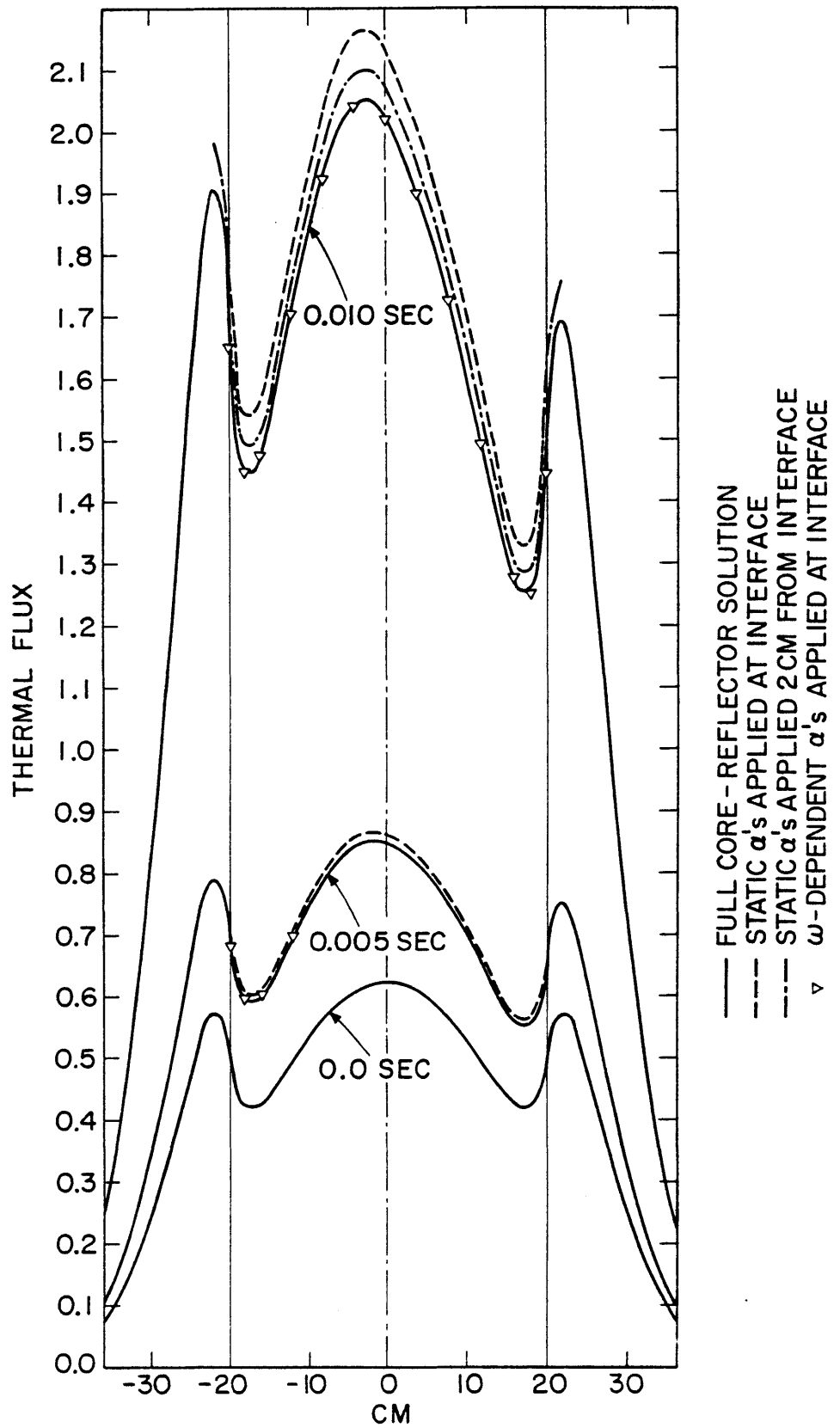
FIGURE 5.20 } PROMPT SUPERCRITICAL TRANSIENT: H₂O - REFLECTED SLAB
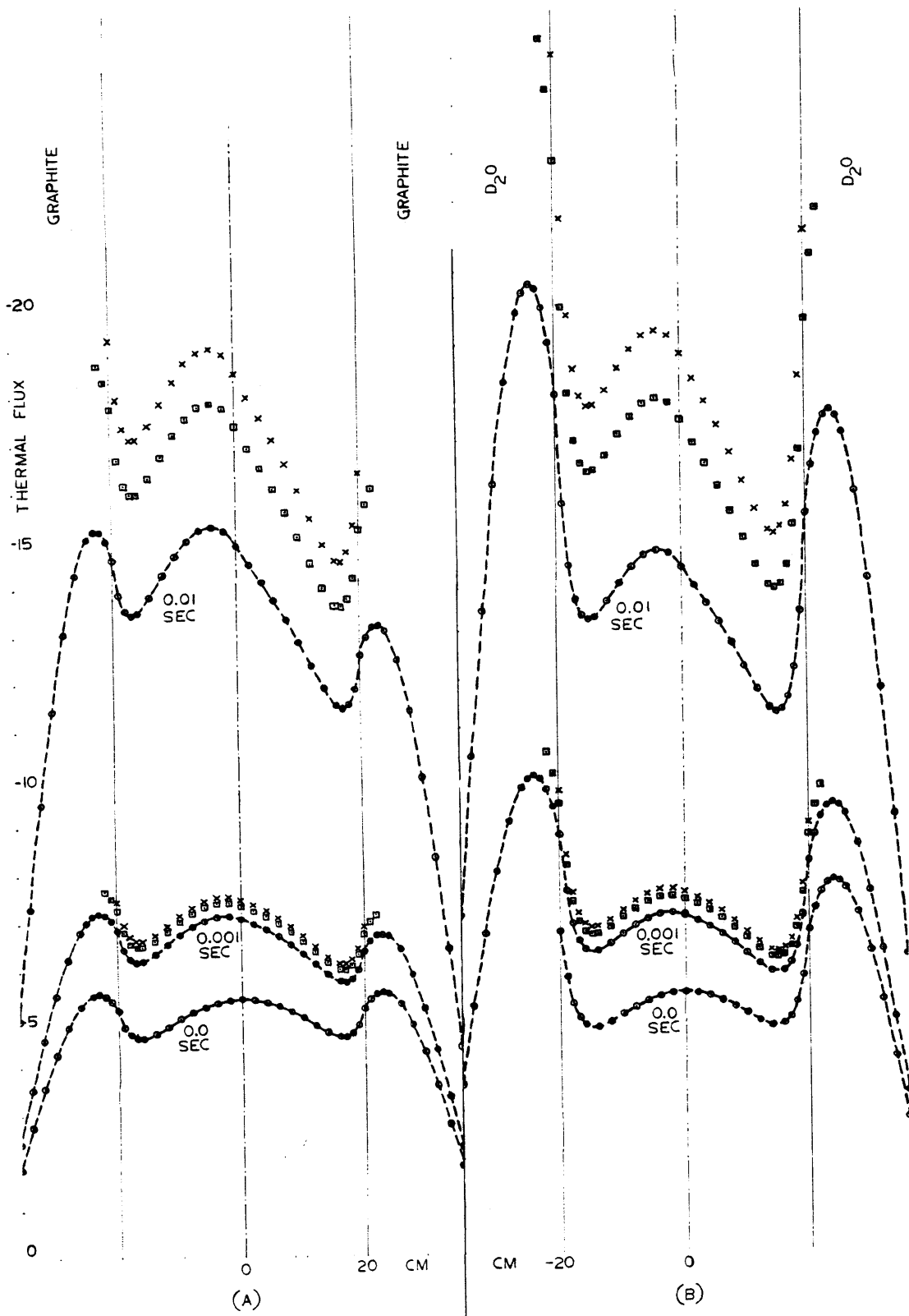
FIGURE 5.21
IMPEDANCE REPRESENTATION
OF (A)GRAPHITE (B)D$_2$O REFLECTOR
(FAST TRANSIENT)

Let us now discuss, briefly, the results of the tests performed on small-sized reactor models.

a) H_2O - reflected reactor models in steady state.

The tests on the "1-d Slab" model provide an opportunity for study of the mesh-size effect. In Figure 5.5 the circles and the x's represent the thermal flux in the core as found from a full core - reflector calculation and from a calculation with an implicit treatment of the reflector, respectively. The same , coarse mesh was used in both calculations. We see that the two sets of symbols do not exactly coincide with each other (although they should, because the algebraic impedance relation is exact in the case of the one-dimensional slab-geometry). The cause of the deviation is the reflector mesh-size: The circles were found from a finite-difference calculation with a coarse mesh both in the core and in the reflector. The x's were found from a finite-difference calculation with a coarse mesh in the core and an infinitely fine mesh in the reflector (the infinitely fine mesh being realized by the analytical impedance-relation). When a fine mesh is used in both calculations, the x's are found to coincide with the circles.

180

The tests on the "Square" reactor model provide another opportunity for study of the mesh-size effect this time in two dimensions. In Figure 5.6, the upper x's represent the thermal flux found from a coarse-mesh (mesh-pattern #2), full core-reflector calculation while the lower x's represent the same thermal flux found from a fine-mesh (mesh-pattern #3) calculation. The corresponding eigenvalues differ by 0.27%, as can be deduced from the data of Table 5.7. The difference in these results is due to the different mesh-sizes used. When the reflector is treated implicitly and the same two core-mesh-patterns are used as in the above full core-reflector calculations, the resulting eigenvalues differ from each other by only 0.03%. This very significant reduction in error in the critical eigenvalue gives a measure of the reflector-mesh-size effect in two dimensions. The "Cross" model results (Fig. 5.8 -5.11) provide some more information on the same effect. Figure 5.7 seems to show this same behavior even more strongly. (The triangles are the coarse mesh results). However the line BC is at an interface and CITATION computes flux values on mesh box centers. Thus the triangles in (5.7) do not represent fluxes on the boundary but rather at a centrimeter inside the core.

181

Regarding the accuracy of the reflector-replacement method itself, it is seen by comparison between the results of the "Square" (Fig. 5.7) and "Cross" models (Table 5.7 and Fig. 5.8-5.11), that the one-dimensional, slab-geometry impedances (which implement the insulated channel approximation) are especially poor in representing the reflector in the neighborhood of reentrant corners of the core surface. A great improvement in accuracy in such cases is obtained when the Smith correction factor is used (Fig. 5.10 and 5.11). This is obvious from the "Cross" model results: the percent error in the eigenvalue is 2.23 vs. 0.40 without and with the correction, respectively. For comparison, the percent error in the eigenvalue of the "Square" model, (which has no reentrant corners), with the reflector represented by just the one-dimensional, slab-geometry impedances is 0.27%.

In summary, the replacement of the H_2O- reflectors of the small-sized "Square" and "Cross" reactor models by boundary conditions has been effected with an accuracy of a few tenths of a percent for the eigenvalue and a few percent for the pointwise fluxes. With all fluxes normalized to the same total power, the maximum pointwise error is observed near the core surface, which is a relatively low-temperature region in the core.

182

b) A D_2O - reflected reactor model in steady state.

In each of the Figures 5.17 - 5.19 the x's and the circles
represent the thermal flux in the "Square" core as found from a
full core-reflector calculation and from a calculation with the
reflector treated implicitly, respectively. Specifically, when
one-dimensional, slab-geometry boundary conditions are used to
represent the entire heavy water-reflector, the thermal flux
depicted by circles in Figure 5.17 is found. When a 4 cm-thick
reflector buffer zone is treated explicitly and the one-
dimensional, slab-geometry boundary conditions are used to re-
present the rest of the heavy-water reflector, the flux depict-
ed by circles in Figure 5.18 is found. Finally, when a 4 cm-
thick RBZ is treated explicitly and the rest of the reflector is
represented by numerically-corrected, one-dimensional, slab-
geometry boundary conditions, where the numerical correction is
based on an assumed pure cosine-shape for the transverse
dependence of the flux, the result shown by the circles in Fig.
5.19 is found. We note how the error is successively reduced from
a significant value in Figure 5.17 to a near-zero value in
Figure 5.19.

From the Figures 5.6, 5.7 and 5.17 and from the Tables 5.7

183

and 5.8 we see that the representation of the entire reflector by one-dimensional, slab-geometry boundary conditions without numerical corrections is much more accurate when the reflector consists of light rather than of heavy-water.

c) The "1-d Slab" reactor model in dynamic state.

Two transients, one fast and one slow, both spatially asymmetric and driven by timewise-ramp reactivities have been considered with the "1-d Slab" model (see Table 5.6 for a detailed description of the transients). Three different reflector materials have been used with this model: light water, heavy water and graphite.

Regarding the slow transient in the light water-reflected slab, it is seen in Table 5.9 that the total power at the end of the transient is predicted with an error 2.9% and 2.7% respectively, when the static approximation is used with and without the explicit treatment of a reflector buffer zone.

The same table shows that the error in the total power at the end of the fast transient in the light water-reflected slab is 5.9% when the static-approximation impedances are applied at the core-reflector interface, 2.6% when the static-approximation im-

pedances are applied at the outer surface of a reflector buffer zone and 0% when the linear-approximation impedances are applied at the core-reflector interface. The pointwise thermal fluxes as found with the above three approximate representations of the reflector are shown in Figure 5.20. It is seen that the maximum pointwise error is practically the same as the corresponding error in total power and occurs at the locations of the extrema of the thermal flux. Of these locations, that of the maximum thermal flux is the hot spot in the slab while those of the minima are relatively low temperature locations. In summary, it is emphasized that, the explicit treatment of a reflector buffer zone reduces the error of the static approximation by about 50%, while the linear approximation, without the treatment of any RBZ, virtually elimanates hte error.

Regarding the slow transient in the heavy water-reflected slab, Table 5.9 shows that the total power at the end of the transient is predicted with an error 0.1% vs. 0.2%, when the static approximation is used with and without the explicit treatment of a RBZ, respectively.

For the fast transient in the heavy water-reflected slab, Table 5.9 lists an error in the prediction of the total power at the and of the transient equal to 32.9% when the static-approxi-

mation impedances are applied at the core-reflector interface and 22.7% when the static-approximation impedances are applied at the outer surface of a RBZ. The pointwise thermal fluxes corresponding to the above two approximate representations of the D_2O-reflector are shown in Figure 5.21(b).

The maximum pointwise error is again seen to be practically the same as the corresponding error in total power. As far as the linear approximation is concerned, it leads to numerical instabilities when applied to heavy-water reflected slabs. The inferior results of all three approximations (static with or without RBZ; linear) in the D_2O-case as compared to the results of the same approximations in the H_2O-case are due to the longer "memory-span" of heavy water. The quadratic-approximation relations should prove more effective in representing D_2O-reflectors in transient calculations.

With respect to "memory-span" graphite resembles heavy water, and the results of numerical tests with graphite resemble the above results for heavy water. The linear-approximation solution again diverges. Large errors are associated with the static approximation (see Figure 5.21(a)) although the explicit treatment of a RBZ cuts the error by about 30%.

5.7 TESTS ON INTERMEDIATE - SIZED REACTOR MODELS.

The results of numerical tests on the intermediate-sized reactor models "3-Steps" and "3-Steps with Shroud" are presented and discussed in this section.

The various boundary conditions tested and the corresponding eigenvalues and references to relevant figures are listed in Table 5.10. The structure of the table is the same as that of Tables 5.7 and 5.8. Figures 5.12-5.15 and 5.22 accompany Table 5.10. Fast fluxes are depicted in Figure 5.22while thermal ones are shown in the other figures. Table 5.11 gives the percent error in eigenvalue and pointwise thermal flux as computed from Table 5.10 and the above figures. Information on the cost and the number of iterations required for convergence of the above calculations is given in Table 5.12.

The effect of the reflector-mesh-size can be further illuminated from the results presented in this section. Let us consider the first row of Table 5.11. The same impedances are applied at the core-reflector interface in both the fine -and the coarse-mesh calculations. The small difference between the two results (0.64vs. 0.65%) is due to the different core-mesh-sizes. Consider now the

T A B L E   5.10

TESTS ON INTERMEDIATE-SIZED,LIGHT WATER-REFLECTED REACTOR

MODELS IN STEADY STATE

Model	Composition	Type of Solution/ Type of Boundary Condition Applied	Critical Eigenvalue		References to Figures	
			Coarse Mesh, #	Fine Mesh, #	Coarse Mesh, #	Fine Mesh, #
3 - Steps	# 2	Full Core-Reflector Solution		1.0007725 (#6)		Solid lines in Figs.5.12 5.13 & 5.22 (#6)
		Impedances at C-R Interface		0.9942630 (#6)		x's in Figs. 5.12 & 5.22 (#6)

T A B L E 5.10 (Continued)

Model	Composition	Type of Solution/ Type of Boundary Condition Applied	Critical Eigenvalue		References to Figures	
			Coarse Mesh,#	Fine Mesh,#	Coarse Mesh,#	Fine Mesh,#
3 - Steps	#2	Impedances at Outer Surface of RBZ		0.9970689 (#6)		Squares in Figs.5.12 & 5.22 (#6)
		Numerically - Corrected Impedances at Outer Surface of RBZ	0.9982689 (#2)		Dashed line in Fig.5.13 (#2)	

T A B L E 5.10 (Continued)

Model	Composit.	Type of Solution/ Type of Boundary Condition Applied	Critical Eigenvalue		References to Figures	
			Coarse Mesh, #	Fine Mesh, #	Coarse Mesh, #	Fine Mesh, #
3 - Steps	#2	Numerically - Corrected Impedances at C-R Interface	0.9954092 (#2)			
3-Steps & Shroud	#2	Full Core-Shroud- Reflector Solution		1.0008097 (#6)		Solid line in Fig. 5.14; x's in 5.15 (#6)

T A B L E 5.10 (Continued)

Model	Composition	Type of Solution/ Type of Boundary Condition Applied	Critical Eigenvalue		References to Figures	
			Coarse Mesh, #	Fine Mesh, #	Coarse Mesh, #	Fine Mesh, #
3-Steps with Shroud	# 2	Impedances at S-R Interface		0.9980435 (#6)		Dashed line in Fig.5.14 (#6)
		Impedances at C-S Interface		0.9947644 (#6)		Circles in Fig.5.15 (#6)
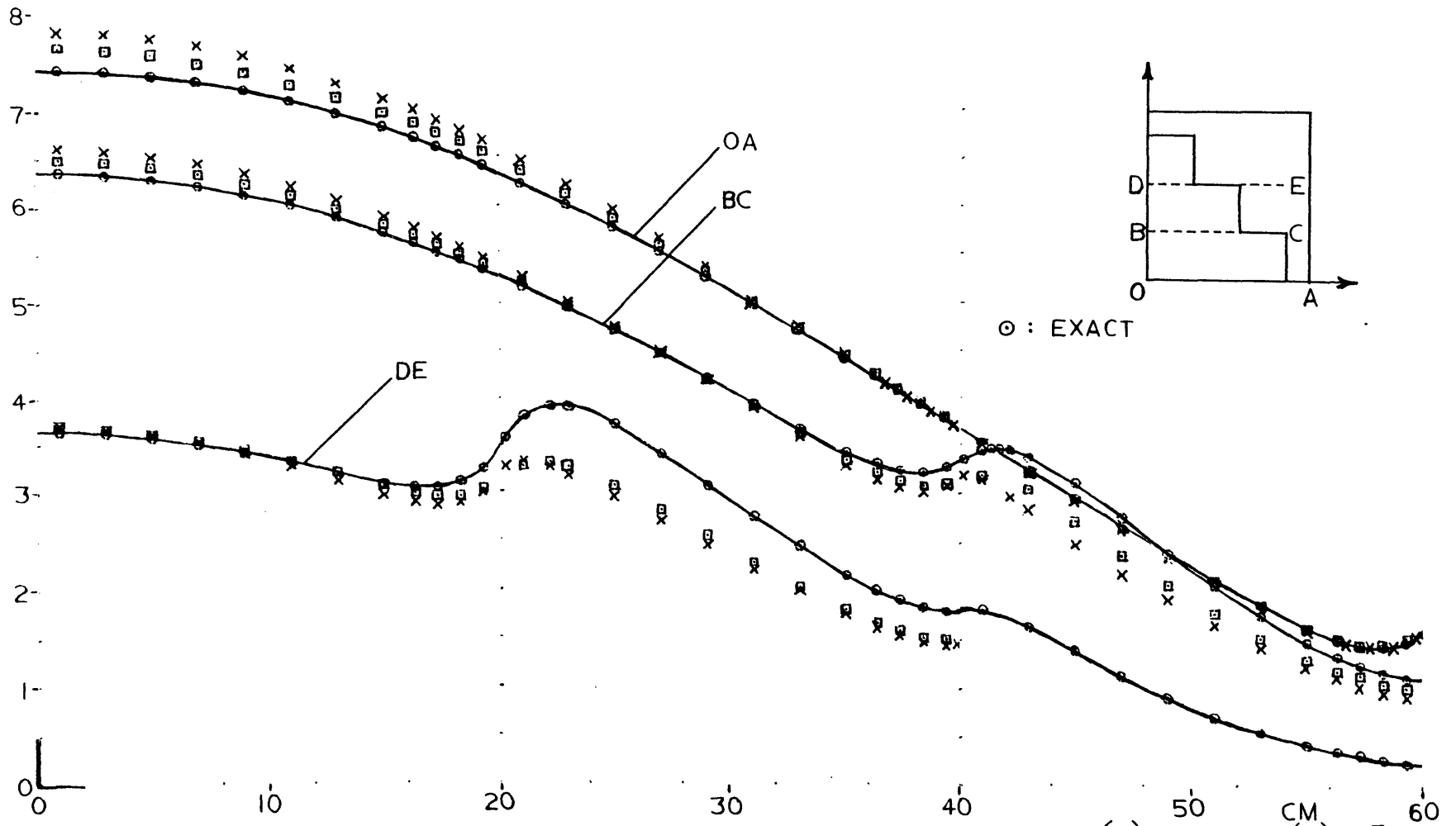
FIGURE 5.12 : IMPEDANCE REPRESENTATION OF LIGHT WATER REFLECTOR WITHOUT (×) AND WITH (⊡) THE PROVISION OF A RBZ

192

FIGURE 5.22 IMPEDANCE REPRESENTATION OF H_2O REFLECTOR WITHOUT (x) AND WITH (⊡) THE PROVISION OF A RBZ

⊙ : EXACT

193

FIGURE 5.13 } STATIC THERMAL FLUXES FOR A REACTOR WITHOUT SHROUD
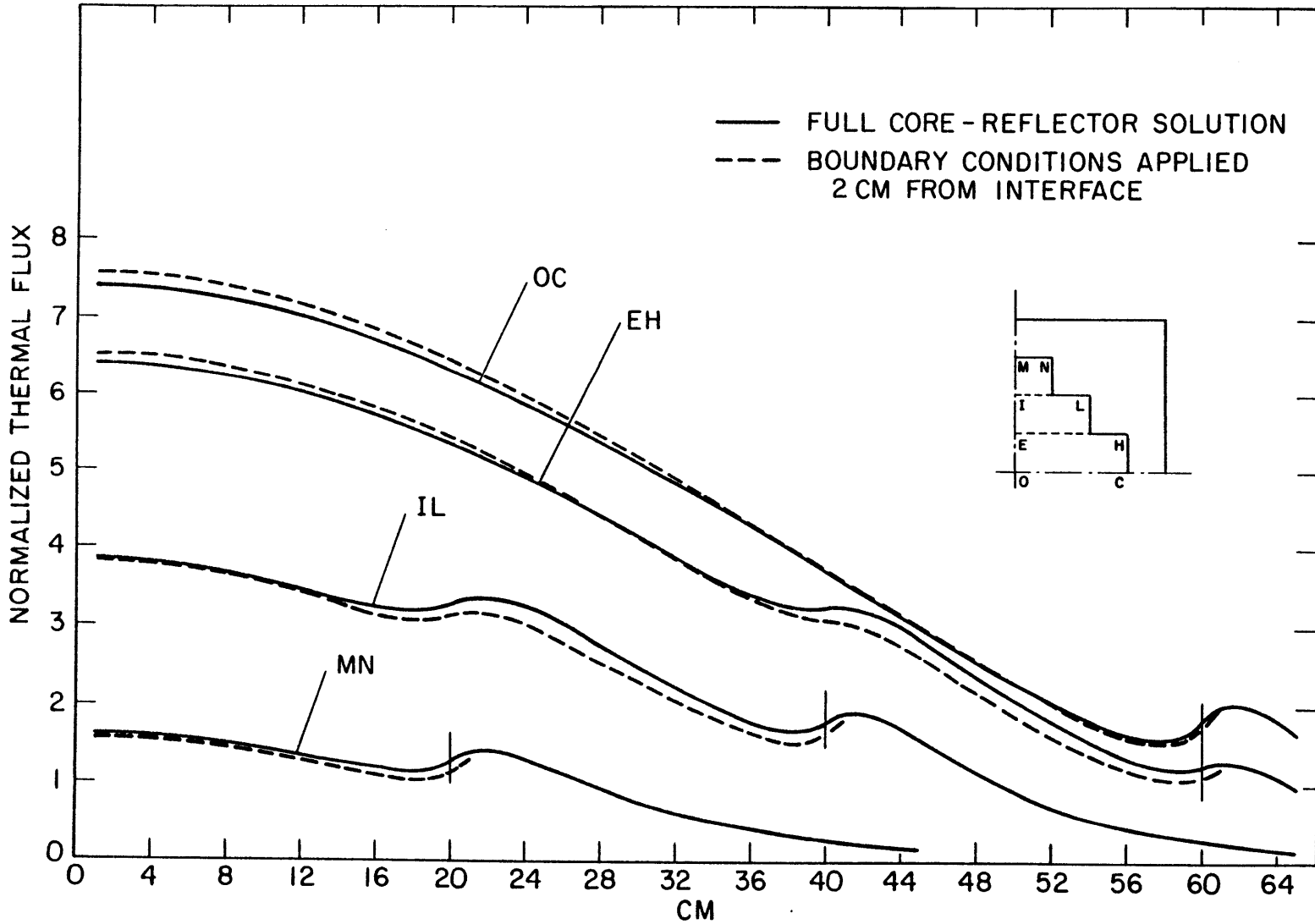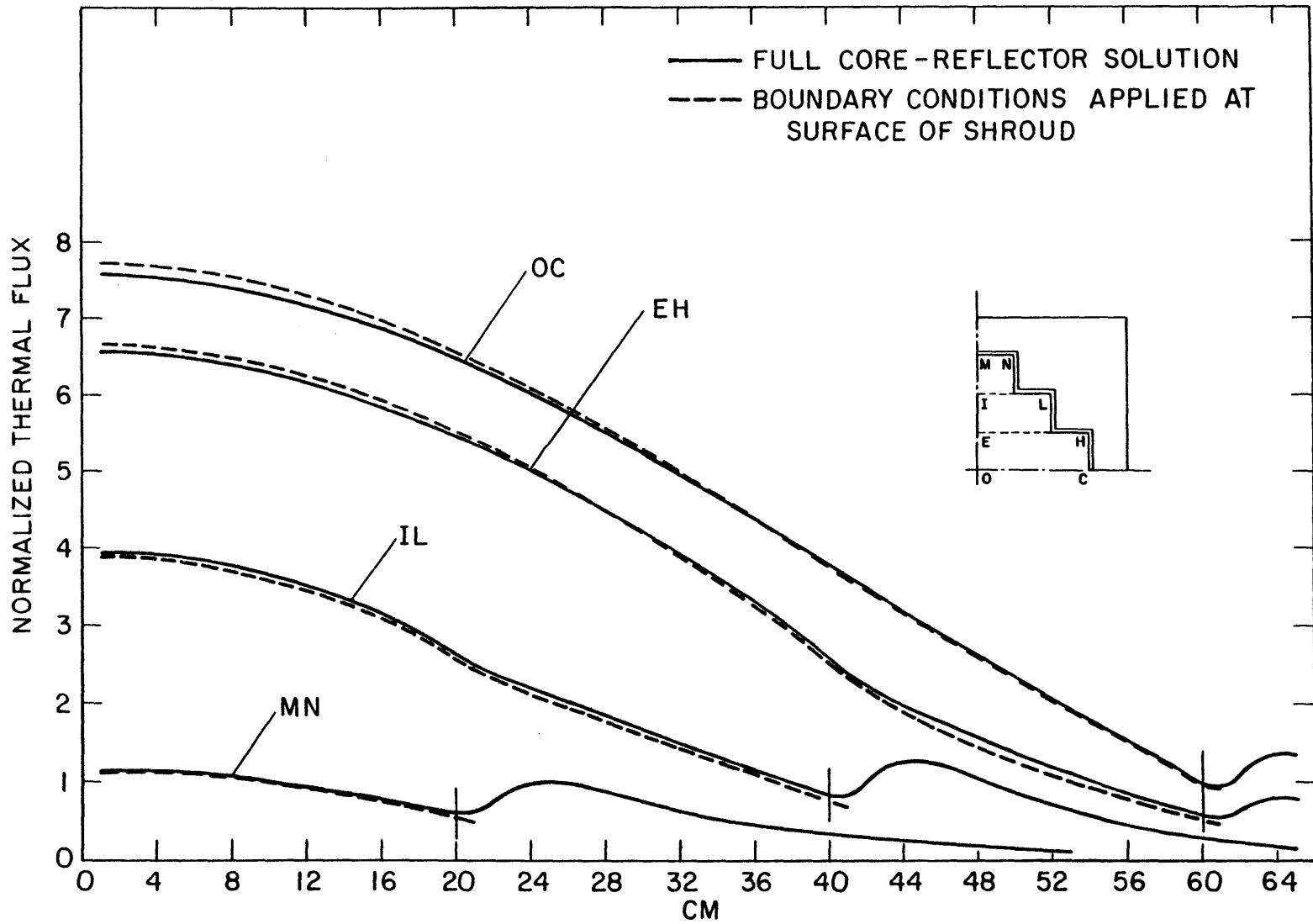
FIGURE } STATIC THERMAL FLUXES FOR A REACTOR WITH SHROUD
5.14 }
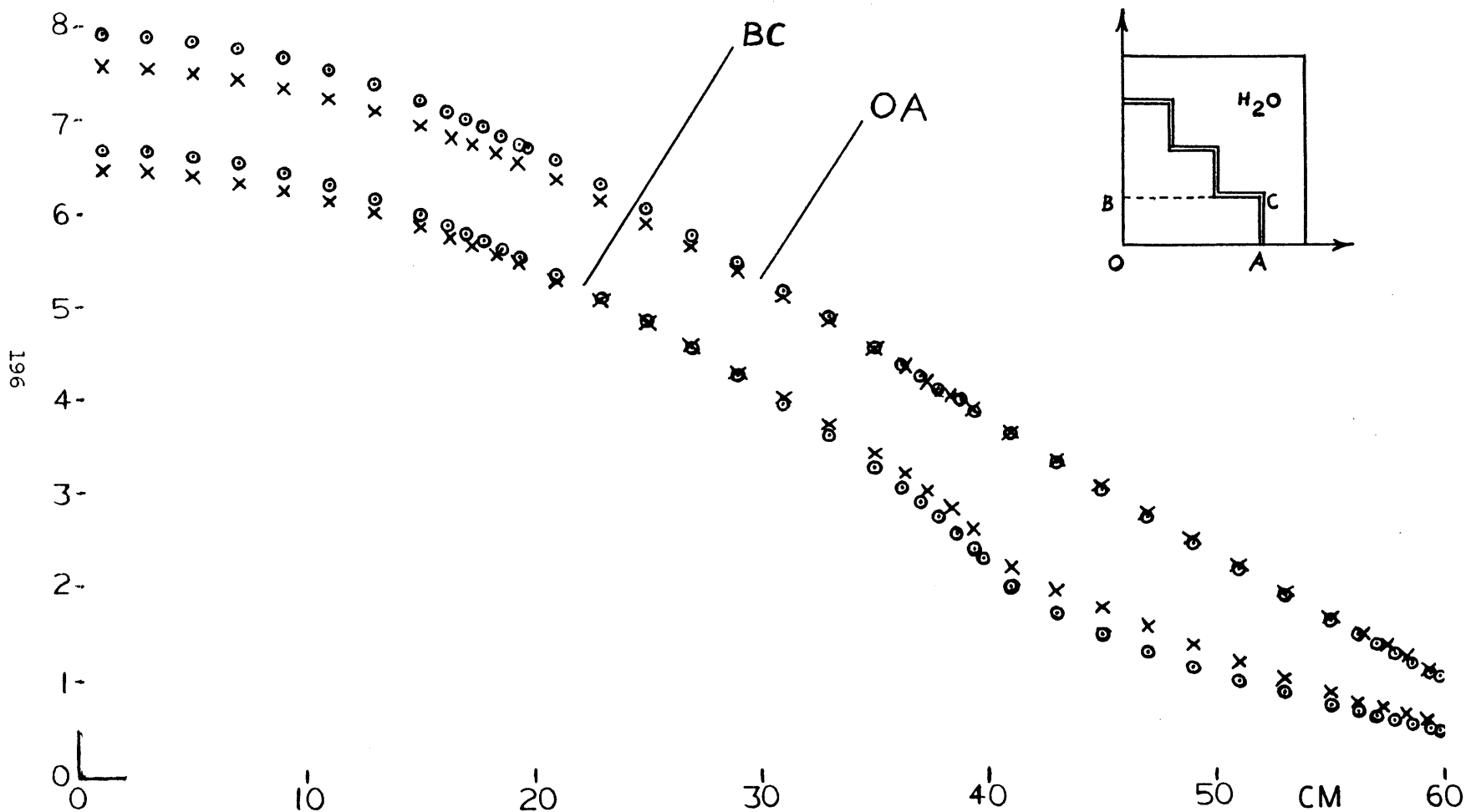
FIGURE 5.15 : IMPEDANCE REPRESENTATION OF H_2O REFLECTOR AND STEEL SHROUD

T A B L E 5.11

ERROR FROM THE IMPLICIT REPRESENTATION OF H_2O RE-

FLECTORS OF INTERMEDIATE - SIZED REACTORS

Model	Composit	Type of Boundary Condition Applied	% Error in Critical Eigenvalue		% Error in Thermal Flux at Center of Core		Maximum % Error in Thermal Flux[*]	
			Fine Mesh	Coarse Mesh	Fine Mesh	Coarse Mesh	Fine Mesh	Coarse Mesh
3 - Steps	# 2	Impedances at C-R Interf.	+0.64%	+0.65%	-5.23%	-5.36%	+14.80%	+16.00%
		Impedances at outer sur-face of RBZ	+0.37%	+0.40%	-3.16%	-3.58%	+9.13%	+11.62%

[*]The maximum % error in the thermal flux occurs (with all normalizations to the same total power) at the core surface, close to the peaks of the re-entrant corners.

Model	Composit	Type of Boundary Condition Applied	% Error in Critical Eigenvalue		% Error in Thermal Flux at Center of Core		Maximum % Error in Thermal Flux	
			Fine Mesh	Coarse Mesh	Fine Mesh	Coarse Mesh	Fine Mesh	Coarse Mesh
3 - S t e p s	# 2	Numerically-Corrected Impedances at C-R Interf.		+0.54%		-4.44%		+13.68%
		Numerically-Corrected Im-pedances at Outer Surface of RBZ		+0.25%		-2.31%		+ 8.13%
3-Steps with Shroud	# 2	Impedances at C-R Interf.	+0.32%	+0.28%	-2.50%	-2.02%	+5.32%	+ 3.03%

198

T A B L E 5.12

COST AND NUMBER OF ITERATIONS OF STEADY - STATE CALCU-

LATIONS IN INTERMEDIATE - SIZED REACTOR MODELS

Model	Composition	Type of Solution/ Type of Boundary Condition Applied	Computational Cost in Dollars		Number of Iterations Required for Convergence*	
			Coarse Mesh,#	Fine Mesh,#	Coarse Mesh,#	Fine Mesh,#
3 - Steps	#2	Full Core-Reflector Solution		36 (#6)		
		Impedances at C-R Interface	7.50 (#2)	19 (#6)	35 (#2)	52 (#6)
		Impedances at Outer Surface of RBZ	7.50 (#2)	20.50 (#6)	36 (#2)	49 (#6)

*The same convergence criteria were used in all computations.

T A B L E 5.12 (Continued)

Model	Composition	Type of Solution/ Type of Boundary Condition Applied	Computational cost in Dollars		Number of Iterations Required for Convergence	
			Coarse Mesh,#	Fine Mesh,#	Coarse Mesh,#	Fine Mesh,#
3-Steps	#2	Numerically-Corrected Impedances at Outer Surface of RBZ	8.50 (#2)		36 (#2)	
3-Steps with Shroud	#2	Full Core-Shroud- Reflector Solution		36 (#6)		58 (#6)
		Impedances at S-R Interface	7.50 (#2)	21 (#6)	38 (#2)	48 (#6)
		Impedances at C-S Interface		23 (#6)		52 (#6)

second row of the same table. The same impedances are applied at the outer surface of a reflector buffer zone in both the fine -and coarse-mesh calculations. The difference between these two results (0.37 vs. 0.40%) is increased over the difference between the results of the first row. Obviously, this increase is due to the different mesh-sizes used in the reflector buffer zone. This observation and those of Section 5.6 support the argument that for light water-reflected reactors numerical solutions are more sensitive to the reflector -than to the core-mesh-size.[*] It is reasonable to extrapolate this argument by saying that the reflector buffer zone is mesh-wise the most sensitive region in the reflector because all flux-shape transitions and strong curvatures of the thermal flux occur mostly within the reflector buffer zone.

However, the sensitivity of the reflector buffer zone to mesh-size is overwhelmed by the great improvement in accuracy effected by the freedom for flux-shape transitions provided by the explicit treatment of the zone (compare vertically any two entries of rows 1 and 2, Table 5.11).

---

[*] This sensitivity is obscured to a certain degree, depending on geometry and reactor size, by error cancellations.

Further examination of Table 5.11 shows that, as expected, impedance boundary conditions applied at the outer surface of the reflector buffer zone yield better accuracy when they are numerically-corrected for the transchannel leakage than when they are not (compare row 1 vs. 3 and row 2 vs. 4 in the table). However, as expected, corrected impedance boundary conditions applied at the core-reflector interface do not yield better accuracy than uncorrected impedance conditions applied at the surface of the buffer zone. This is because Condition (5.3) is not satisfied in this case.

Comparison between rows 2 and 5 in Table 5.11 shows that the transchannel leakage in the reflector is significantly reduced in the presence of the stainless steel shroud. The extent of the reduction is such that not only no additional RBZ outside the shroud is needed but also the shroud appears to accomodate flux-shape transitions better than a RBZ does for an unshrouded core.

One final piece of information from Table 5.11 concerns the effect of the shroud-mesh-size on the accuracy of the solution. Row 5 shows that the shrouded-core, coarse-mesh solution is more ac-curate than the corresponding fine-mesh solution. This peculiar feature is due to truncation-error cancellation.

The last three rows of Table 5.10 and Figures 5.14 and 5.15

show that computations with both the shroud and the reflector treated implicitly (by one-dimensional, slab-geometry boundary conditions) are less accurate than computations with only the reflector treated implicitly. For example, the error in the eigenvalue is 0.60% and 0.32%, respectively, for the same, fine mesh-pattern.

The above results, like those of the preceding section, involve errors of a few tenths of a percent in the critical eigenvalues and a few percent in the pointwise fluxes.[*] With all fluxes normalized to the same total power, the maximum pointwise percent error is again observed near the core surface.

The reduction in computational cost, due to the implicit treatment of a reflector, amounts to about 40% (for the same mesh-pattern), as can be deduced from Table 5.12. The same table shows that a comparable number of iterations is required for the convergence of a full core-reflector solution and the correspond-

---

[*]The error in the pointwise fast fluxes closely follows that in the pointwise thermal fluxes, as can be seen from Figures 5.22 and 5.12 which show the two-group fluxes corresponding to the same problem.

ing approximate solution with the reflector treated implicitly

(for the same mesh-pattern and convergence criteria).

5.8 TESTS ON A FULL-SCALE REACTOR MODEL.

In this section we present and discuss the results of numerical tests performed on a full-scale reactor model, that of the ZION reactor.

Two tests were performed on the ZION model: one with both the shroud and the reflector treated implicitly and one with only the reflector treated implicitly. In both tests, one-dimensional, slab-geometry impedances without numerical -or Smith- corrections were used. The critical eigenvalues found from these two approximate calculations are listed on the last two rows of Table 5.13. For comparison, the eigenvalue of the full core-reflector solution is given on the first row of the same table. The corresponding exact and approximate pointwise thermal fluxes are shown in Figure 5.16.

It is seen from the above table and figure that the implicit treatment of the reflector alone yields a solution which is practically free of error: the eigenvalue is predicted with an error less than 0.01% and the approximate, pointwise thermal fluxes as found from this calculation are practically indistinguishable from the exact ones (compare the x's with the circles in Figure 5.16).

205

When both the shroud and the reflector are treated implicitly, the eigenvalue is predicted with an error 0.04% while the thermal flux is predicted with an error of about 5% at the center of the core and about 10% near the core-reflector interface (compare squares and circles in Figure 5.16).

Finally, Table 5.14 indicates a reduction of about 40% in computational cost effected by means of the implicit treatment of the reflector. This result is in agreement with the corresponding result for intermediate-sized reactor models. It is seen from Table 5.14 that the number of iterations required for convergence is increased by about 25% when the reflector of the ZION model is treated implicitly (with the same convergence criteria). By contrast, no trend for any increase in the number of iterations was identified for intermediate-sized models.

T A B L E 5.13

TESTS ON A FULL - SCALE, LIGHT WATER - REFLECTED REACTOR MODEL IN

STEADY STATE

Model	Composit.	Type of Solution/ Type of Boundary Condition Applied	Critical Eigenvalue		Refs. to Figures	
			Coarse Mesh, #	Fine Mesh,#	Coarse Mesh,#	Fine Mesh,#
		Full Core-Shroud- Reflector Solution		1.2749023 (#7)		Circles in Fig. 5.16 (#7)
N O I Z	# 3	Impedances at S-R Interface		1.2748137 (#7)		x's in Fig. 5.16 (#7)
		Impedances at C-S Interface		1.2743673 (#7)		Squares in Fig. 5.16 (#7)
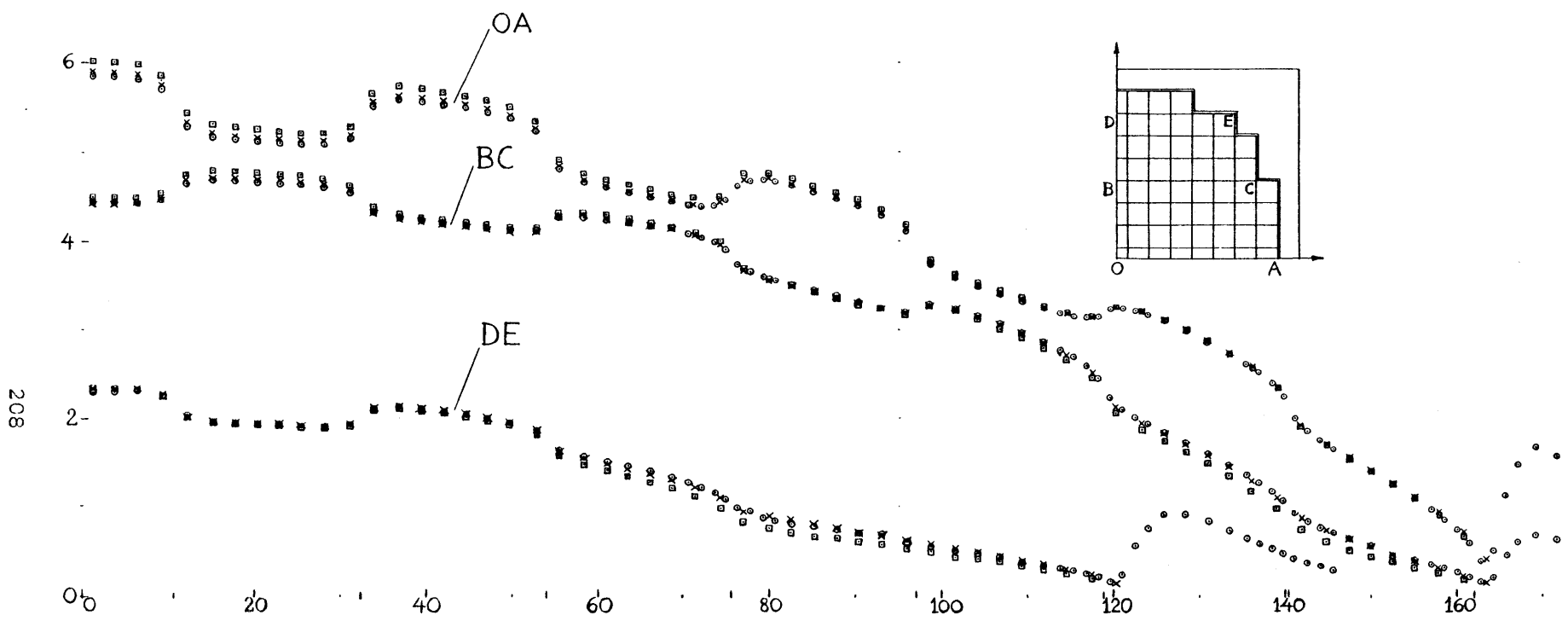
FIGURE 5.16 ZION REACTOR STATIC THERMAL FLUXES

IMPEDANCE REPRESENTATION OF
× REFLECTOR
□ REFLECTOR AND STEEL SHROUD

○ FULL CORE - SHROUD - REFLECTOR SOLUTION

T A B L E 5.14

COST AND NUMBER OF ITERATIONS OF STEADY - STATE CALCULATIONS IN A

FULL - SCALE REACTOR MODEL

Model	Composition	Type of Solution/ Type of Boundary Condition Applied	Computational Cost in Dollars		Number of Iterations Required for Convergence[*]	
			Coarse Mesh,#	Fine Mesh,#	Coarse Mesh,#	Fine Mesh,#
N O I Z N	#3	Full Core-Shroud- Reflector Solution		73 (#7)		100 (#7)
		Impedances at S-R Interface		45 (#7)		127 (#7)
		Impedances at C-S Interface		43 (#7)		127 (#7)

[*] The same convergence criteria were used in all computations.

5.9 SOME PRACTICAL CONSIDERATIONS CONCERNING THE ACCURACY OF THE IMPEDANCE - METHOD.

The numerical results reported in the previous three sections allowed us to estimate the effect of the light-water-reflector-mesh-size on the accuracy of a computation. We saw that this effect depends on the dimensionality, shape and size of the reactor model and can be significant. It is therefore an advantage of the impedence-method that it eliminates this source of error.

However, the impedance-method is approximate, and the acceptability of its predictions should be decided on the basis of some practical criterion. A reasonable criterion for acceptability of any approximate reactor-analysis method is that the error associated with the method not exceed the inherent uncertainty of the reactor model itself ——— which, in our case, is the group-diffusion theory model[H-2], [H-3], [H-4]. In this respect, most of the results presented in Sections 5.6 - 5.8 are satisfactory. Further refinement is needed for only the most inaccurate of the computations (i.e the space-and/or time-dependent D_2O and graphite cases and perhaps the two-zone reflector problem). To this end, improved boundary conditions should be derived, Kirchhoff's formula being the general, analytical tool for this purpose. A

reasonable refinement in accuracy should be aimed at; an accuracy much higher than the modeling accuracy is not worth the effort.

ACKNOWLEDGEMENTS

211

VI. CONCLUSION

6.1 CONCLUSIONS FROM THE PRESENT WORK.

The bulk of the present work and the conclusions thereof concern light water-reflected reactors. Heavy water-and graphite-reflected reactors have been considered in only a preliminary way.

I. Conclusions on the Replacement of Light Water - Reflectors.

I.1. Static, Two - Dimensional Problems.

(a) Within a light water reflector, straight channels perpendicular to the reflector interface are effectively better "insulated" neutronically from one another in the presence of a stainless steel shroud separating the core from the reflector than in the absence of it. As a consequence, the representation of only the reflector by one-dimensional, slab-geometry boundary conditions is more accurate when a shroud is present than when it is not.

(f) The representation of both light water-reflector and stainless steel shroud by one-dimensional, slab-geometry, composite (i.e. two-zone) boundary conditions is less accurate than that of part (e), above, but not dramatically so.

(g) The effect of a large core size on the accuracy of an implicit reflector representation is, as expected, favorable. With the ZION reactor, which is representative of large reactors of average computational severity, the implicit representation of the light water-reflector has given excellent results while less accurate - but by no means bad- results were obtained when both the water-reflector and the steel-shroud were treated implicitly.

(h) The accuracy of the implicit representation of the light water reflectors of large, unshrouded cores, containing (like the severe, IAEA two-dimensional benchmark problem [W-1]) some strongly absorbing blocks adjacent to the reflector, remains to be seen*. If needed -and it most probably will be- the Smith correction should prove a useful means for higher accuracy.

214

(b) With unshrouded cores, the explicit (i.e. as a distinct region) representation of a reflector buffer zone (about 2cm thick) adjacent to the core together with a representation of the rest of the reflector by one-dimensional, slab-geometry boundary conditions yields satisfactory accuracy. The reflector buffer zone allows for non-separable spatial flux shape transitions.

(c) Iterative transverse buckling corrections incorporated in the one-dimensional, slab-geometry boundary conditions improve the accuracy reported in (b), over that achieved when the iteratively corrected boundary conditions are applied at the outer surface of the reflector buffer zone.

(d) The Smith correction provides an alternative to the reflector buffer zone.

(e) With shrouded cores, the explicit representation of the shroud (about 2cm thick) together with the representation of the reflector by one-dimensional, slab-geometry boundary conditions yields satisfactory accuracy. In fact, the explicit representation (with a shrouded core) of the shroud only yields an identifiably better accuracy than the explicit representation (with the same core but unshrouded) of the reflector zone that replaces the shroud.

(j) A general feature of the application of the reflector-replacement method to large reactor models is the very accurate prediction of the critical eigenvalue - a not surprising result.

I.2. Time - Dependent, One - Dimensional Problems.

(a) Only thin (leaky) reactor models have been considered. The testing of the reflector -replacement method for these extreme problems has resulted in excellent agreement. Specifically, the "static approximation" has been found adequate for slow transients and the "linear approximation" extremely good for fast transients.

(b) When the static approximation is used for the implicit representation of the slab-reflector during a fast transient, a significant error results. This error, however, is greatly reduced when a reflector buffer zone adjacent to the core is explicitly treated, the rest of the reflector being represented by the static approximation relationships. Thus, the employment of the static approximation together with a reflector buffer zone is an alternative to -but not as accurate as- the linear approximation employed in the entire reflector.

I.3. Time - Dependent, Two-Dimensional Problems.

No problem in this class has been tested but we can extrapolate some of the above conclusions. For example, the static approximation should be adequate for the representation of two-dimensional reflectors during slow transients. If a reflector buffer zone is used for increased accuracy of the spatial approximation, then the accuracy of the temporal approximation will improve, too and the static approximation will be adequate for faster transients as well as slow ones.

II. A Few Conclusions on the Replacement of Heavy Water - or Graphite Reflectors.

II.1. Static, Two - Dimensional Problems.

Spatial flux shape transitions in a heavy water -or graphite-reflector develop over a wider buffer zone than in light water.

Outside the reflector buffer zone, the neutronic "insulation" of the channels perpendicular to the buffer zone surface is inferior to that observed with a light water reflector of comparable configuration and size. As a consequence, the representation

of the part of a heavy water -or graphite- reflector outside the

reflector buffer zone by one-dimensional, slab-geometry boundary

conditions is considerably less accurate than the corresponding

representation of a light water reflector of comparable configu-

ration and size. Thus the incorporation of a transverse buckling

correction to the one-dimensional, slab-geometry relations for

the representation of the outside-the-buffer-zone part of a

reflector is much more necessary for heavy water -or graphite-

reflectors than for light water-ones of comparable configuration

and size.

II.2 Time - Dependent, One-Dimensional Problems.

The static approximation is adequate for slow transients but

the linear approximation is inadequate for fast transients. In

fact the only (and not satisfactory) heavy water -or graphite-

reflector representation for fast transients has been obtained

by means of the static approximation applied outside a reflector

buffer zone.

In general, heavy water -and graphite- reflectors are more

difficult to represent by means of boundary conditions than light

water reflectors. This difference is due to the longer neutron

diffusion length (weaker absorption of neutrons) in heavy water
and graphite.

6.2 SUGGESTIONS FOR FURTHER WORK.

A. On the Representation of Reflectors by Boundary Conditions.

The two-group, diffusion theory reflector representation
introduced in the present thesis can be extended to account for:

   (i)   more energy groups,

   (ii)   fast reactor analysis,

   (iii) reflectors with properties changing with time and

   (iv)   reflectors which are better described by a higher-order
          angular approximation [T-1],[T-2].

In this thesis, the reflector representation procedure was
applied to reactors being analyzed by finite-difference equations.
The applicability of the procedure to higher-order nodal and
finite-element methods provides a logical sequel for investigation.

Moreover, with respect to application to finite-dif-
ference equations, there are further tests which will be necessary
to complete the investigation. These tests are listed below.

218

I. Tests with Light Water Reflectors.

I.1. Static, Two - Dimensional Problems.

(a) Replacement of One - Zone Reflectors.

Apply both the 90^0 and 270^0 Smith corrections to the "cross"

reactor model.

(b) Replacement of Two - Zone (Stainless Steel Shroud and Light

    Water) Reflectors.

    Approximate and test Kirchhoff's elbow formula together with

the one-zone equivalent for the light water surrounding the shroud.

I.2. Time - Dependent, Two - Dimensional Problems.

(a) Replacement of One - Zone Reflectors.

    Approximate (in both its space -and time- dependences) and

test the time dependent wedge relation.

(b) Replacement of Two - Zone Reflectors.

    Approximate (in both its space -and time- dependences) and

test the time-dependent Kirchhoff's elbow formula together with
the one-zone equivalent for the light water surrounding the shroud.

II. Tests with Heavy Water or Graphite Reflectors.

II.1. Static, Two - Dimensional Problems.

(a) Replacement of One-Zone Reflectors.

Approximate and test Kirchhoff's formula.

(b) Replacement of Two-Zone Reflectors.

II.2. Time - Dependent, One - Dimensional Problems.

Derive (by keeping τ^2 term in the Taylor series expansion
(4.49)) and test "quadratic approximation" for fast transients.

II.3 Time - Dependent, Two - Dimensional Problems.

Approximate and test the time-dependent Kirchhoff's formulas.

REFERENCES

[B-1]. Born, M. and Wolf, E.: "Principles of Optics", Fifth Ed., Pergamon Press, 1975.

[C-1]. Carslaw , H.S. and Jaeger, J.C.: "Conduction of Heat in Solids", Second Ed., Oxford University Press, 1959.

[C-2]. Clark, M., Jr. and Hansen, K.F.: "Numerical Methods of Reactor Analysis", Academic Press, 1964.

[C-3]. Collin, R.E.: "Field Theory of Guided Waves", McGraw-Hill Book Company, 1960.

[D-1]. Delp, D.L. et al., "FLARE, A Three-Dimensional Boiling Water Reactor Simulator", GEAP-4598, General Electric Company, July 1964.

[F-1]. Fowler, T.B. et al.: "Nuclear Reactor Core Analysis Code: CITATION", ORNL - TM - 2496, Rev. 2, Oak Ridge National Laboratory, July 1971.

[G-1]. Galanin, A.D.: "Application of the Method of Effective Boundary Conditions for Calculating the Critical Dimensions of Reactors", International Conference on the Peaceful Uses of Atomic Energy, Geneva, Paper P/664, $\underline{5}$, 451 (1955).

[G-1]. Gradshteyn, I.S. and Ryzhik, I.M.: "Table of Integrals, Series and Products", 4th Ed., Academic Press, New York, 1965.

[H-1]. Hansen, K.F. and Mason, J.H.:"GAKIN II: A One-Dimensional Multigroup Diffusion Theory Reactor Kinetics Code", AEC Research and Development Report COO-2262-3, MITNE-151.

[H-2]. Henry, A.F.: "Nuclear - Reactor Analysis", The M.I.T. Press, 1975.

[H-3]. Henry, A.F.: "Approximations That Make Space-Dependent Kinetics Computations More Efficient", Paper 1, NEACRP/ CSNI Specialists' Meeting on New Developments on Three-Dimensional Kinetics, Garching (Germany), January 1975.

[H-4]. Henry, A.F.: "Refinements in Accuracy of Coarse-Mesh Finite-Difference Solution of the Group-Diffusion Equations", Proceedings of a Seminar on Numerical Reactor Calculations, IAEA, Vienna, Jan. 1972.

[H-5]. Hildebrand, F.B.: "Advanced Calculus for Applications", Prentice-Hall, Inc., 1962.

[K-1]. Kalambokas, P.C. and Henry, A.F.: The Replacement of Reflectors by Albedo-Type Boundary Conditions",

Proceedings of Conf. on Computational Methods in Nucl.
Eng., Charleston, S.C., April 1975.

[L-1]. Lebedev, N.N.: "Sur une formule d' inversion", Comptes
Rendus (Doklady) de l' Académie des Sciences de l'URSS
52, 655 (1964) (in French).

[L-2]. Lebedev, N.N.: "On the Integral Expansion of Arbitrary
Functions in Terms of Cylindrical Functions of Imaginary
Order and Argument", Applied Math. and Mech. 13, 465
(1949) (in Russian).

[L-3]. Lukic, Y.: "Flux-Current Matrix Relation at the Core -
Reflector Interface of a Slab Reactor", Special Problems
Project Supervised by Prof. A.F. Henry, M.I.T., Aug. 1972.

[M-1]. Magnus, W., Oberhettinger, F. and Soni, R.P.: "Formulas
and Theorems for the Special Functions of Mathematical
Physics", 3rd ed., Springer-Verlag, New York, 1966.

[O-1]. Oberhettinger, F. and Higgins, T.P.: "Tables of Lebedev,
Mehler and Generalized Mehler Transforms", Boeing
Scientific Research Laboratories, Seattle, Wash., 1961.

[P-1]. Papoulis, A.: "Systems and Transforms with Applications

in Optics", McGraw-Hill Book Company, 1968.

[P-2]. Papoulis, A.: "The Fourier Integral and Its Applications", McGraw-Hill Book Company, 1962.

[R-1]. Robinson, C.P. and Eckard, J.D.: "A Higher Order Difference Method for Diffusion Theory", Trans. Amer. Nuc. Soc. 15, 297 (1972).

[S-1]. Smith, J.H.: "Analysis for Diffusion Theory Flux Peaking at a Sharp Corner", Nucl. Sci. and Eng. 15, 468 (1963).

[S-2]. Sommerfeld, A.: "Optik", Vorlesungen über theoretische Physik, Band IV, 1950 (in German).

[T-1]. Terney, W.B.: "Albedo-Adjusted Fast-Neutron Diffusion Coefficients in Reactor Reflectors", Nucl. Sci. and Eng. 57, 239, (1975).

[T-2]. Terney, W.B.: "Albedo-Adjusted Reflector Fast Diffusion Coefficients", Trans. Amer. Nuc. Soc. 18, 319 (1974).

[T-3]. Titchmarsh, E.C.: "Introduction to the Theory of Fourier Integrals", 2nd Ed., Oxford University Press, 1948.

[W-1]. Wagner, M.R.: "Current Trends in Multidimensional Static Reactor Calculations", Proc.Conf.Comput.Meht. in Nucl. Eng., Charleston, S.C., April 1975.

APPENDIX A.

EVALUATION OF THE IMPEDANCE - KERNEL $G_{\theta_0}\left(\xi, \frac{r}{L}\right)$.

The kernel is defined by:

$$G_{\theta_0}\left(\xi, \frac{r}{L}\right) \equiv \int_0^\infty K_{ip}(\xi) \cdot K_{ip}\left(\frac{r}{L}\right) \cdot \frac{\sinh(\pi p)}{\tanh(\theta_0 p)} \cdot dp$$

(3.17)

In (3.17) we introduce a new variable, ν:

$$\nu \equiv ip$$

(A.1)

whence:

$$p = -i\nu$$

(A.2)

Since:

$$\sinh(\theta \cdot p) = \sinh(-i \cdot \theta \cdot \nu) = -i \cdot \sin(\theta \cdot \nu)$$

and

$$\cosh(\theta \cdot p) = \cosh(-i \cdot \theta \cdot \nu) = \cos(\theta \cdot \nu),$$

Eq. (3.17) becomes:

$$G_{\theta_o} = -i \cdot \int_0^{i\infty} K_\nu(\xi) \cdot K_\nu\left(\frac{r}{L}\right) \cdot \frac{\sin(\pi\nu)}{\tan(\theta_o \nu)} \cdot d\nu$$

(A.3)

The integration indicated in (A.3) is to be carried out along the positive imaginary axis on the complex ν-plane.

Since the integrand in (A.3) is an even function of the pure imaginary variable ν, it follows that:

$$G_{\theta_o} = -\frac{i}{2} \cdot \int_{-i\infty}^{+i\infty} K_\nu(\xi) \cdot K_\nu\left(\frac{r}{L}\right) \cdot \frac{\sin(\pi\nu)}{\tan(\theta_o \nu)} \cdot d\nu$$

(A.4)

226

The integration indicated in (A.4) is to be carried out along the whole imaginary axis on the complex ν-plane.

I. Let us consider first the case:

$$\xi < \frac{r}{L} \qquad \text{(A.5)}$$

For a reason that will become apparent in the sequel, we employ the identity:

$$K_\nu(\xi) \equiv \frac{\pi}{2} \cdot \frac{I_{-\nu}(\xi) - I_\nu(\xi)}{\sin(\pi\nu)} \qquad \text{(A.6)}$$

where $I_{\pm\nu}$ is the modified Bessel function of the first kind and of order $\pm\nu$,

to effect the splitting:

$$G_{\theta_o} = G^{minus} - G^{plus} \qquad \text{(A.7)}$$

where:

$$G^{minus} \equiv -\frac{\pi i}{4} \cdot \int_{-i\infty}^{+i\infty} I_{-\nu}(\xi) \cdot K_\nu\left(\frac{r}{L}\right) \cdot \frac{1}{\tan(\theta_o \nu)} \cdot d\nu$$

$$\text{(A.8)}$$

and

$$G^{plus} \equiv -\frac{\pi i}{4} \cdot \int_{-i\infty}^{+i\infty} I_\nu(\xi) \cdot K_\nu\left(\frac{r}{L}\right) \cdot \frac{1}{\tan(\theta_o \nu)} \cdot d\nu$$

(A.9)

In (A.8) we can substitute:

$$K_\nu\left(\frac{r}{L}\right) = K_{-\nu}\left(\frac{r}{L}\right)$$

(A.10)

because K_ν is even with respect to ν.

If, further, we introduce in (A.8) a new variable, μ, defined by:

(A.11)

$$\mu \equiv -\nu$$

Eq. (A.8) becomes:

$$G^{minus} = +\frac{\pi i}{4} \cdot \int_{-i\infty}^{+i\infty} I_\mu(\xi) \cdot K_\mu\left(\frac{r}{L}\right) \cdot \frac{1}{\tan(\theta_o \mu)} \cdot d\mu$$

(A.12)

228

By comparing (A.12) to (A.9) we find:

$$G^{minus} = -G^{plus} \qquad \text{(A.13)}$$

We substitute (A.13) into (A.7) and obtain:

$$G_{\theta_0} = -2 \cdot G^{plus} \qquad \text{(A.14)}$$

or, if we take into account the definition of G^{plus}, we get:

$$G_{\theta_0} = \frac{\pi i}{2} \cdot \int_{-i\infty}^{+i\infty} I_\nu(\xi) \cdot K_\nu\left(\frac{r}{L}\right) \cdot \frac{1}{\tan(\theta_0 \nu)} \cdot d\nu$$

$$\text{(A.15)}$$

Next we evaluate G_{θ_0} by replacing the integration path indicated in (A.15) by a suitably chosen __closed__ contour and then applying Cauchy's theorem.

Consider, on the right half of the complex ν-plane, a semi-circumference Γ with its center at the origin and of radius R.

The semi-circumference Γ intersects the imaginary ν-axis at two points, A and B, with ordinates -R and +R. The segment AB of the imaginary ν-axis is, therefore, a diameter of Γ.

Let us form a closed contour, C, consisting of:

- the semi-circumference Γ and of

- the diameter AB, with a small indentation of radius ρ at the origin, so that the so-formed closed contour C does not enclose the origin.

We define the contour integral:

$$G_c \equiv \frac{\pi i}{2} \cdot \oint_C I_\nu(\xi) \cdot K_\nu\left(\frac{r}{L}\right) \cdot \frac{1}{\tan(\theta_0 \nu)} \cdot d\nu$$

(A.16)

where the direction of the integration along the contour C is clockwise.

The difference:

$$G_c - G_{\theta_0}$$

becomes identical to the integral along the indentation, if:

230

- $\rho \to 0$,

- $R \to \infty$ and

- the value of the (common) integrand of G_c and G_{θ_0} on the semi-circumference Γ tends to zero as $R \to \infty$.

Obviously, if Γ passes through a pole of the integrand of G_c, the value of the integrand on Γ blows up.

The integrand of G_c has an infinite number of poles, located on the real ν-axis. The exact locations of the poles are defined by the equation:

$$\tan\left(\theta_0 \nu\right) = 0$$

or

$$\nu = \frac{n\pi}{\theta_0} \; ; \; n = 0, 1, 2, \cdots \qquad \text{(A.17)}$$

Consider a sequence of concentric semi-circumferences on the right half of the ν-plane, with the origin as their common center and of radii:

$$R_n = \frac{n\pi}{\theta_0} + \frac{\pi/4}{\theta_0} \qquad \text{(A.18)}$$

231

None of these semi-circumferences passes through a pole.

Furthermore, as $R_n \to \infty$, the value of the integrand of G_c,

$$I_\nu\left(\xi\right) \cdot K_\nu\left(\frac{r}{L}\right) \cdot \frac{1}{\tan\left(\theta_0 \nu\right)} \quad ,$$

on the semi-circumferences tends to zero. (On the contrary, the value of the integrand of G_{θ_0} (Eq. A.4),

$$K_\nu\left(\xi\right) \cdot K_\nu\left(\frac{r}{L}\right) \cdot \frac{1}{\tan\left(\theta_0 \nu\right)} \quad ,$$

on the semi-circumference does not tend to zero. Thus, the splitting (A.6)-(A.7) is a twist of convenience in the course of the evaluation of the impedance kernel G_{θ_0}).

Hence,

$$\lim_{n \to \infty} G_{c_n} = \lim_{R \to \infty} G_c = G_{\theta_0} + \begin{bmatrix} \text{Integral} \\ \text{Along} \\ \text{Indentation} \end{bmatrix} \quad ,$$

where:

$$G_{C_n} = \frac{\pi i}{2} \cdot \oint_{C_n} I_\nu(\xi) \cdot K_\nu\left(\frac{r}{L}\right) \cdot \frac{1}{\tan(\theta_o \nu)} \cdot d\nu$$

<div align="right">(A.19)</div>

and each of the closed contours C_n consists of the semi-circumference of radius R_n and the corresponding diameter on the imaginary ν-axis, indented at the origin, so that the latter is not enclosed by C_n. The direction of the integration along each one of the C_n's is <u>clockwise</u>.

According to Cauchy's theorem[P-2], the value of a counterclockwise contour integral is equal to $+2\pi i$ times the sum of the residues at those poles of the integrand, which are enclosed by the contour. The value of a clockwise contour integral is equal to $-2\pi i$ times the sum of the same residues.

Thus,

$$\lim_{n \to \infty} G_{C_n} = -2\pi i \cdot \sum_{n=1}^{\infty} Res\left(\frac{n\pi}{\theta_o}\right) \qquad \text{(A.20)}$$

<div align="center">233</div>

(The pole corresponding to n = 0 is excluded from the sum in (A.20), because this pole is not enclosed by the contour C).

The residues at the poles of the integrand of G_c on the right half of the complex ν-plane are:

$$Res\left(\frac{n\pi}{\theta_0}\right) =$$

$$= \frac{\pi i}{2} \cdot \left(\nu - \frac{n\pi}{\theta_0}\right) \cdot I_\nu\left(\xi\right) \cdot K_\nu\left(\frac{r}{L}\right) \cdot \frac{1}{\tan(\theta_0\nu)}\bigg|_{\nu = \frac{n\pi}{\theta_0}}$$

or

$$Res\left(\frac{n\pi}{\theta_0}\right) = \frac{\pi i}{2\theta_0} \cdot I_{\frac{n\pi}{\theta_0}}\left(\xi\right) \cdot K_{\frac{n\pi}{\theta_0}}\left(\frac{r}{L}\right)$$

$$(A.21)$$

We substitute (A.21) into (A.20) and get:

$$\lim_{n \to \infty} G_{c_n} = \frac{\pi^2}{\theta_0} \cdot \sum_{n=1}^{\infty} I_{\frac{n\pi}{\theta_0}}\left(\xi\right) \cdot K_{\frac{n\pi}{\theta_0}}\left(\frac{r}{L}\right)$$

$$(A.22)$$

234

But:

$$\lim_{n \to \infty} G_{c_n} = G_{\theta_0} + \begin{bmatrix} \text{Integral} \\ \text{along} \\ \text{Indentation} \end{bmatrix} \qquad (A.23)$$

By virtue of a theorem given in Ref. [H-4], we evaluate:

$$\begin{bmatrix} \text{Integral} \\ \text{Along} \\ \text{Indentation} \end{bmatrix} = \pi i \cdot \text{Res}(0) \qquad (A.24)$$

From Eq. (A.21) we get:

$$\text{Res}(0) = \frac{\pi i}{2\theta_0} \cdot I_0(\xi) \cdot K_0\left(\frac{r}{L}\right) \qquad (A.25)$$

and thus

$$\begin{bmatrix} \text{Integral} \\ \text{Along} \\ \text{Indentation} \end{bmatrix} = -\frac{\pi^2}{2\theta_0} \cdot I_0(\xi) \cdot K_0\left(\frac{r}{L}\right) \qquad (A.26)$$

235

Substitution of (A.26) and (A.22) into (A.23) yields:

$$\frac{\pi^2}{\theta_0} \cdot \sum_{n=1}^{\infty} I_{\frac{n\pi}{\theta_0}}(\xi) \cdot K_{\frac{n\pi}{\theta_0}}\left(\frac{r}{L}\right) =$$

$$= G_{\theta_0} - \frac{\pi^2}{2\theta_0} \cdot I_0(\xi) \cdot K_0\left(\frac{r}{L}\right) \qquad (A.27)$$

Special Cases:

a) $\theta_0 = \frac{\pi}{2}$.

From (A.27) we have:

$$G_{\frac{\pi}{2}} = \pi \cdot I_0(\xi) \cdot K_0\left(\frac{r}{L}\right) + 2\pi \cdot \sum_{n=1}^{\infty} I_{2n}(\xi) \cdot K_{2n}\left(\frac{r}{L}\right)$$

$$(A.28)$$

On the right hand side of (A.28), we add and subtract the quantity:

$$\pi \cdot \sum_{n=1}^{\infty} I_{2n-1}(\xi) \cdot K_{2n-1}\left(\frac{r}{L}\right)$$

236

and rearrange to get:

$$G_{\frac{\pi}{2}} = \frac{\pi}{2} \cdot \left[I_0(\xi) \cdot K_0\left(\frac{r}{L}\right) + 2 \cdot \sum_{n=1}^{\infty} I_n(\xi) \cdot K_n\left(\frac{r}{L}\right) \right] +$$

$$+ \frac{\pi}{2} \cdot \left[I_0(\xi) \cdot K_0\left(\frac{r}{L}\right) + 2 \cdot \sum_{n=1}^{\infty} (-1)^n \cdot I_n(\xi) \cdot K_n\left(\frac{r}{L}\right) \right]$$

(A.29)

Given the inequality (A.5), there are simple, closed expressions for both bracketed quantities in (A.29):

$$\text{First Bracketed Quantity} = K_0\left(\left| \xi - \frac{r}{L} \right|\right)$$

(A.30)

$$\text{Second Bracketed Quantity} = K_0\left(\xi + \frac{r}{L}\right)$$

(A.31)

237

We substitute (A.30) and (A.31) into (A.29) and get:

$$G_{\frac{\pi}{2}} = \frac{\pi}{2} \cdot \left\{ K_0\left(\left|\xi - \frac{r}{L}\right|\right) + K_0\left(\xi + \frac{r}{L}\right) \right\} \qquad \text{(A.32)}$$

Expression (A.32) can also be found directly from mathematical tables (see, for example, Ref.[G-1]).

b) $\quad \theta_0 = \frac{\pi}{4}$.

From (A.27) we have:

$$G_{\frac{\pi}{4}} = 2\pi \cdot I_0(\xi) \cdot K_0\left(\frac{r}{L}\right) + 4\pi \cdot \sum_{n=1}^{\infty} I_{4n}(\xi) \cdot K_{4n}\left(\frac{r}{L}\right)$$

$$\text{(A.33)}$$

If we subtract (A.28) from (A.33), we get:

$$G_{\frac{\pi}{4}} - G_{\frac{\pi}{2}} = \pi \cdot I_0(\xi) \cdot K_0\left(\frac{r}{L}\right) +$$

$$+ 2\pi \cdot \sum_{n=1}^{\infty} I_{4n}(\xi) \cdot K_{4n}\left(\frac{r}{L}\right) -$$

(Eq. Cont.)

238

$$-2\pi \cdot \sum_{n=1}^{\infty} I_{4n-2}(\xi) \cdot K_{4n-2}\left(\frac{r}{L}\right)$$

(A.34)

or:

$$G_{\frac{\pi}{4}} - G_{\frac{\pi}{2}} = \pi \cdot I_0(\xi) \cdot K_0\left(\frac{r}{L}\right) +$$

$$+ 2\pi \cdot \sum_{n=1}^{\infty} \cos\left(\frac{n\pi}{2}\right) \cdot I_n(\xi) \cdot K_n\left(\frac{r}{L}\right)$$

(A.35)

or, given (A.5),

$$G_{\frac{\pi}{4}} - G_{\frac{\pi}{2}} = \pi \cdot K_0\left(\sqrt{\xi^2 + \left(\frac{r}{L}\right)^2}\right)$$

(A.36)

We eliminate $G_{\frac{\pi}{2}}$ between (A.36) and (A.32) and get:

$$G_{\frac{\pi}{4}} = \frac{\pi}{2} \cdot \left\{ K_0\left(|\xi - \frac{r}{L}|\right) + K_0\left(\xi + \frac{r}{L}\right) + \right.$$

$$\left. + 2 \cdot K_0\left(\sqrt{\xi^2 + \left(\frac{r}{L}\right)^2}\right) \right\}$$

(A.37)

Expression (A.37) can also be found directly from mathematical tables.

II. Let us now consider the case:

$$\xi > \frac{r}{L} \tag{A.38}$$

Given (A.38), all the above development is valid, provided the roles of ξ and $\frac{r}{L}$ are interchanged.

APPENDICES B AND C:

Library copies only

APPENDIX B.

IMPLEMENTATION OF TWO - GROUP, IMPEDANCE BOUNDARY CONDITIONS

WITH THE COMPUTER - CODE "CITATION".

Notation.

<u>Superscript g</u>: refers to energy-group g (g = 1 or 2).

<u>Subscript i,j</u>: refers to the centerpoint of the two-dimensional
mesh-element (i,j).

<u>Subscript s</u>:   refers to the midpoint of one side of a mesh-
element.

B.1 FAST-NEUTRON FLOW INTO A REGION REPRESENTED BY IMPEDANCES.

Consider a mesh-element adjacent to a boundary, along which
an impedance-condition is to be applied. See Figures B.1 and B.2.

241
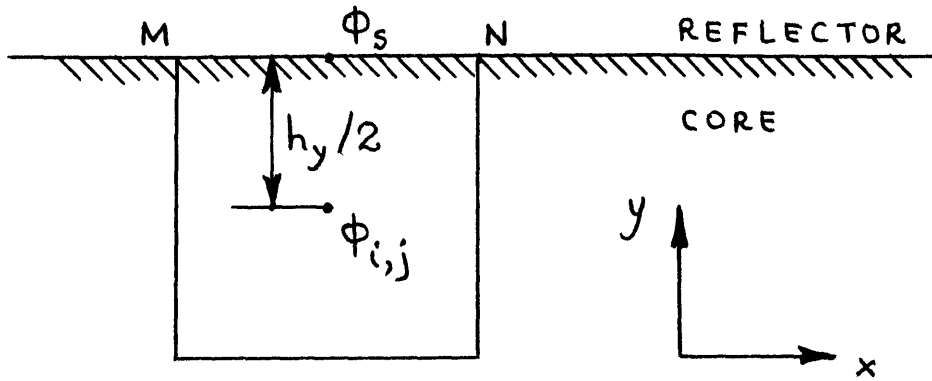
Figure B.1

Mesh - Element Adjacent to a x-Direction Boundary.
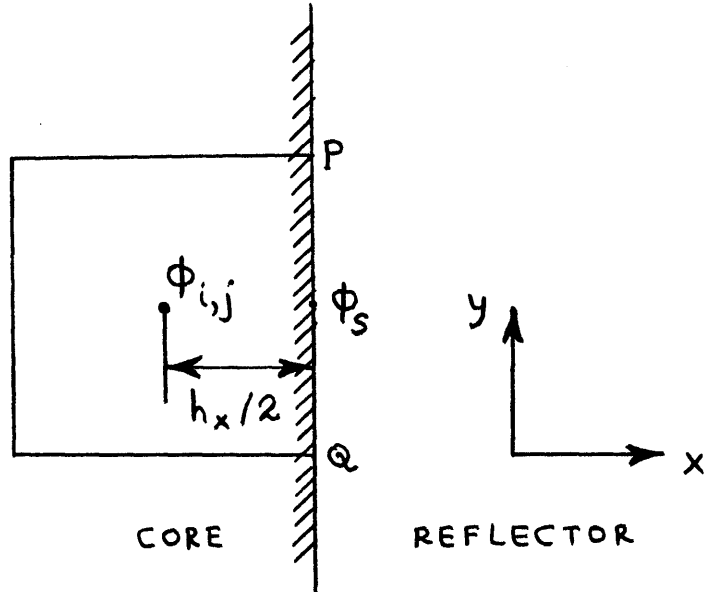
Figure B.2

Mesh - Element Adjacent to a y-Direction Boundary.

242

The impedance boundary-condition for fast neutrons is:

$$\frac{J_s^1}{\Phi_s^1} = \beta_{11} \qquad \text{(B.1)}$$

a) Let us concentrate on Figure B.1 first.

We have:

$$J_s^1 = -D_{i,j}^1 \cdot \frac{\partial \Phi^1}{\partial y}\bigg|_s \approx D_{i,j}^1 \cdot \left[\Phi_{i,j}^1 - \Phi_s^1\right] \cdot \frac{1}{h_y/2}$$

$$\text{(B.2)}$$

We substitute J_s^1 from (B.2) into (B.1) and get:

$$D_{i,j}^1 \cdot \frac{\Phi_{i,j}^1 - \Phi_s^1}{\Phi_s^1 \cdot h_y/2} \approx \beta_{11} \qquad \text{(B.3)}$$

We rearrange (B.3) in the form:

$$\Phi_s^1 \approx \frac{1/\beta_{11}}{\dfrac{1}{\beta_{11}} + \dfrac{h_y/2}{D_{i,j}^1}} \cdot \Phi_{i,j}^1 \qquad \text{(B.4)}$$

The leakage of fast neutrons through the face MN is:

$$\mathbb{L}^1_{MN} \approx h_x \cdot J_s^1 = h_x \cdot \beta_{11} \cdot \Phi_s^1 \approx$$

$$\approx \frac{h_x}{\dfrac{1}{\beta_{11}} + \dfrac{h_y/2}{D^1_{i,j}}} \cdot \Phi^1_{i,j} \qquad \text{(B.5)}$$

(In the development of (B.5), use was made of Eqs. (B.1) and (B.4).

b) We now consider Figure B.2.

    We find:

$$\mathbb{L}^1_{PQ} \approx \frac{h_y}{\dfrac{1}{\beta_{11}} + \dfrac{h_x/2}{D^1_{i,j}}} \cdot \Phi^1_{i,j} \qquad \text{(B.6)}$$

    The proof of (B.6) is similar to the proof of (B.5).

B.2 THERMAL-NEUTRON FLOW FROM A REGION REPRESENTED BY IMPEDANCES.

    The impedance boundary condition for thermal neutrons may be written in the form:

244

$$\frac{J_s^2}{\phi_s^2} = \beta_{21} \cdot \frac{\phi_s^1}{\phi_s^2} + \beta_{22} \qquad \text{(B.7)}$$

a) Refering to Figure B.1, we have:

$$J_s^2 = - D_{i,j}^2 \cdot \frac{\partial \phi^2}{\partial y}\bigg|_s \approx D_{i,j}^2 \cdot \left[\phi_{i,j}^2 - \phi_s^2 \right] \cdot \frac{1}{h_y / 2}$$

$$\text{(B.8)}$$

We substitute J_s^2 from (B.8) into (B.7). The result is:

$$D_{i,j}^2 \cdot \frac{\phi_{i,j}^2 - \phi_s^2}{\phi_s^2 \cdot h_y / 2} \approx \beta_{21} \cdot \frac{\phi_s^1}{\phi_s^2} + \beta_{22}$$

$$\text{(B.9)}$$

We solve (B.9) for ϕ_s^2:

$$\phi_s^2 \approx$$

$$\approx \frac{1}{1 + \frac{h_y/2}{D_{i,j}^2} \cdot \beta_{22}} \cdot \left\{ \phi_{i,j}^2 - \frac{h_y/2}{D_{i,j}^2} \cdot \beta_{21} \cdot \phi_s^1 \right\}$$

(B.10)

The leakage of thermal neutrons through the face MN is given by:

$$\mathbb{L}_{MN}^2 \approx h_x \cdot J_s^2 = h_x \cdot \beta_{21} \cdot \phi_s^1 + h_x \cdot \beta_{22} \cdot \phi_s^2 \approx$$

$$\approx h_x \cdot \beta_{21} \cdot \phi_s^1 + \frac{h_x \cdot \beta_{22}}{1 + \frac{h_y/2}{D_{i,j}^2} \cdot \beta_{22}} \cdot \left\{ \phi_{i,j}^2 - \frac{h_y/2}{D_{i,j}^2} \cdot \beta_{21} \cdot \phi_s^1 \right\}$$

(B.11)

(In the development of (B.11), use was made of Eqs. (B.7) and (B.10)). (B.11) can be rearranged as follows:

$$\mathbb{L}_{MN}^2 \approx \phi_s^1 \cdot \left\{ h_x \cdot \beta_{21} \cdot \frac{1/\beta_{22}}{\frac{1}{\beta_{22}} + \frac{h_y/2}{D_{i,j}^2}} \right\} +$$

246

$$+ \phi_{i,j}^{2} \cdot \frac{h_x}{\dfrac{1}{\beta_{22}} + \dfrac{h_y/2}{D_{i,j}^{2}}} \tag{B.12}$$

By substituting Φ_s^1 in terms of $\Phi_{i,j}^1$ from Eq. (B.4) into (B.12) we obtain:

$$L_{MN}^{2} \approx$$

$$\approx \frac{h_x \cdot \beta_{21}}{\beta_{11} \cdot \beta_{22}} \cdot \frac{1}{\dfrac{1}{\beta_{11}} + \dfrac{h_y/2}{D_{i,j}^{1}}} \cdot \frac{1}{\dfrac{1}{\beta_{22}} + \dfrac{h_y/2}{D_{i,j}^{2}}} \cdot \phi_{i,j}^{1} +$$

$$+ \frac{h_x}{\dfrac{1}{\beta_{22}} + \dfrac{h_y/2}{D_{i,j}^{2}}} \cdot \phi_{i,j}^{2} \tag{B.13}$$

247

b) Refering to Figure B.2, we have:

$$L^2_{PQ} \approx \frac{h_y \cdot \beta_{21}}{\beta_{11} \cdot \beta_{22}} \cdot \frac{1}{\frac{1}{\beta_{11}} + \frac{h_x/2}{D^1_{i,j}}} \cdot \frac{1}{\frac{1}{\beta_{22}} + \frac{h_x/2}{D^2_{i,j}}} \cdot \phi^1_{i,j} +$$

$$+ \frac{h_y}{\frac{1}{\beta_{22}} + \frac{h_x/2}{D^2_{i,j}}} \cdot \phi^2_{i,j} \qquad\qquad \text{(B.14)}$$

B.3 HOW TO INPUT IMPEDANCE BOUNDARY CONDITIONS TO "CITATION".

a) The balance of fast neutrons in the element of Figure B.1
is expressed by the equation:

Leakage through the three interior faces (i.e. left, bottom
and right) + Leakage through face MN +

$$+ \Sigma_1 \cdot \phi^1_{i,j} \cdot h_x \cdot h_y = 0 \qquad\qquad \text{(B.15)}$$

The leakage through face MN is quantified by Eq. (B.5).
We substitute (B.5) into (B.15) and get:

Leakage through the three interior faces $+ \dfrac{h_x}{\frac{1}{\beta_{11}} + \frac{h_y/2}{D^1_{i,j}}} \cdot \phi^1_{i,j} +$

$$+ \Sigma_1 \cdot \phi^1_{i,j} \cdot h_x \cdot h_y = 0$$

$$\text{(B.16)}$$

If an extrapolated (instead of an impedance) boundary condition were specified for the face MN, the corresponding balance equation would be (B.16) with the following modification: β_{11} would be replaced by the fast-group extrapolation parameter $(\equiv D^1_{i,j}$ / extrapolation length)[F-1].

Therefore, and in view of the fact that CITATION accepts group-dependent extrapolation lengths as inputs, the quantity β_{11} can be input as if it were an extrapolation parameter for the fast group.

The thermal-neutron balance in the element of Figure B.1 is expressed by the equation:

Leakage through the three interior faces + Leakage through MN +

$$+ \Sigma_2 \cdot \phi^2_{i,j} \cdot h_x \cdot h_y = \Sigma_{1 \to 2} \cdot \phi^1_{i,j} \cdot h_x \cdot h_y \qquad \text{(B.17)}$$

The leakage through MN is given by (3.13). We substitute (B.13) into (B.17), regroup and get:

249

Leakage through interior faces +

$$+ \frac{h_x}{\frac{1}{\beta_{22}} + \frac{h_y/2}{D^2_{i,j}}} \cdot \phi^2_{i,j} + \Sigma_2 \cdot \phi^2_{i,j} \cdot h_x \cdot h_y =$$

$$= \Sigma^*_{1\rightarrow2} \cdot \phi^1_{i,j} \cdot h_x \cdot h_y \qquad (B.18)$$

where:

$$\Sigma^*_{1\rightarrow2} \equiv \Sigma_{1\rightarrow2} - \qquad (B.19)$$

$$- \frac{1}{h_y} \cdot \frac{\beta_{21}}{\beta_{11} \cdot \beta_{22}} \cdot \frac{1}{\frac{1}{\beta_{11}} + \frac{h_y/2}{D^1_{i,j}}} \cdot \frac{1}{\frac{1}{\beta_{22}} + \frac{h_y/2}{D^2_{i,j}}}$$

Thus, the quantity β_{22} can be input as if it were an

extrapolation parameter for the thermal group ($\equiv D^2_{i,j}$ /

extrapolation length), while the quantity β_{21} can be incorporated

to a modified scattering cross section for the mesh element under

consideration. This modified cross section value is given by

Eq. (B.19).

b) Consider now the mesh-element of Figure B.3.

The impedance conditions for the face PQ can be input to the code according to rules obtained from the material of Section B.3 -this section- , part a) -above- , if the roles of h_x and h_y are interchanged.

c) Consider next the element of Figure B.3.
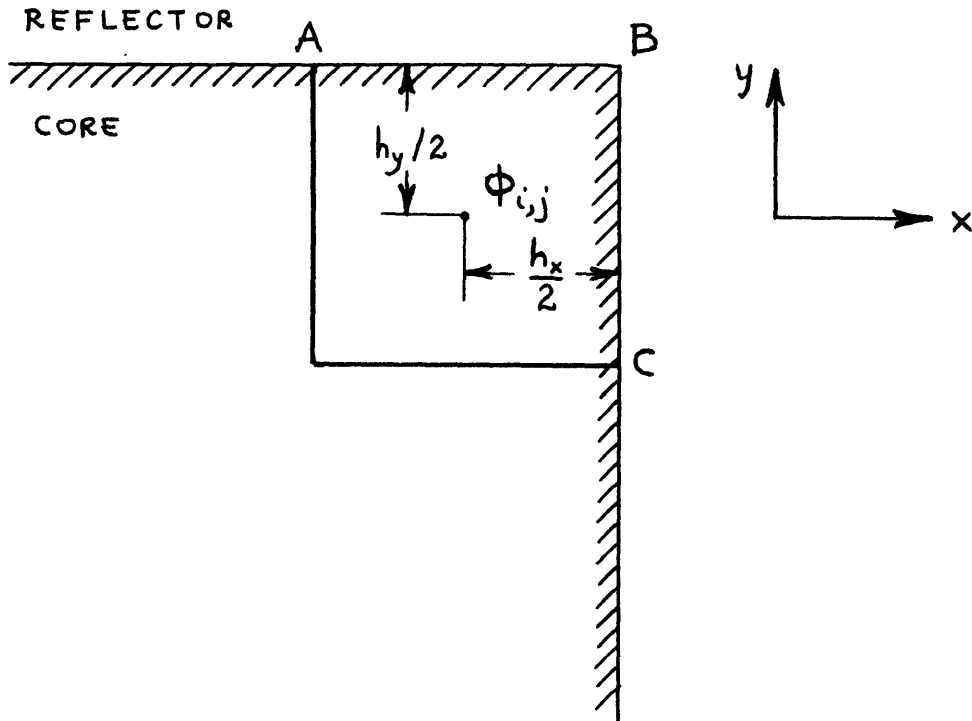
Figure B.3

Corner Element

251

The thermal neutron balance in the element of Figure B.3

is expressed by the equation:

Leakage through left and bottom faces +

+ Leakage through AB +

+ Leakage through BC +

$$+ \Sigma_2 \cdot \phi_{i,j}^2 \cdot h_x \cdot h_y = \Sigma_{S_{1 \to 2}} \cdot \phi_{i,j}^1 \cdot h_x \cdot h_y \qquad \text{(B.20)}$$

The leakage through AB is given by Eq. (B.13). The leakage

through BC is given by Eq. (B.13) with the roles of h_x and h_y

interchanged. We substitute these leakage expressions into

(B.20), regroup and get:

Leakage through left and bottom faces +

$$+ \frac{h_x}{\dfrac{1}{\beta_{22}|_{AB}} + \dfrac{h_y/2}{D_{i,j}^2}} \cdot \phi_{i,j}^2 + \frac{h_y}{\dfrac{1}{\beta_{22}|_{BC}} + \dfrac{h_x/2}{D_{i,j}^2}} \cdot \phi_{i,j}^2 =$$

$$= \Sigma_{1 \to 2}^{**} \cdot \phi_{i,j}^1 \cdot h_x \cdot h_y \qquad \text{(B.21)}$$

252

where:

$$\Sigma^{**}_{1\to 2} \equiv \Sigma_{1\to 2} \quad - \tag{B.22}$$

$$-\frac{1}{h_y}\cdot\frac{\beta_{21}\big|_{AB}}{\beta_{11}\big|_{AB}\cdot\beta_{22}\big|_{AB}}\cdot\frac{1}{\dfrac{1}{\beta_{11}\big|_{AB}}+\dfrac{h_y/2}{D^1_{i,j}}}\cdot\frac{1}{\dfrac{1}{\beta_{22}\big|_{AB}}+\dfrac{h_y/2}{D^2_{i,j}}}$$

$$-\frac{1}{h_x}\cdot\frac{\beta_{21}\big|_{BC}}{\beta_{11}\big|_{BC}\cdot\beta_{22}\big|_{BC}}\cdot\frac{1}{\dfrac{1}{\beta_{11}\big|_{BC}}+\dfrac{h_x/2}{D^1_{i,j}}}\cdot\frac{1}{\dfrac{1}{\beta_{22}\big|_{BC}}+\dfrac{h_x/2}{D^2_{i,j}}}$$

We conclude that, for the element of Figure B.3,
$\beta_{11}\big|_{AB}$, $\beta_{22}\big|_{AB}$, $\beta_{11}\big|_{BC}$, and $\beta_{22}\big|_{BC}$ can be input to CITATION
as if they were extrapolation parameters while $\beta_{21}\big|_{AB}$ and $\beta_{21}\big|_{BC}$
can be incorporated to $\Sigma^{**}_{1\to 2}$.

ACKNOWLEDGEMENT

The incorporation of β_{21} to a modified scattering cross
section was suggested by Dr. J.W. Stewart.

253

A P P E N D I X   C.

MODIFICATIONS IN THE CODE "GAKIN II" FOR ALLOWING INPUT OF IM-

PEDANCE BOUNDARY CONTIONS.

The modifications specified in this Appendix are for two

energy-groups only. In the modified code, the reflected-boundary-

condition option has been replaced by the impedance-boundary-

condition option. Thus, BCL=1 or BCR=1 means impedance-boundary-

condition for the left or right boundary, respectively.

Notation of Reflector Parameters.

SG: Macroscopic Cross Section for Removal of Neutrons from Group

      G.

S12:   Macroscopic Cross Section for Scattering of Neutrons from

      Group 1 to Group 2.

DG: Diffusion Coefficient for Group G.

RETH: Reflector Thickness.

BGG': G-th Row- and G'-th Column-Element of Inverse-Impedance

      Matrix.

C.1   IMPLEMENTATION OF THE LINEAR - APPROXIMATION BOUNDARY

    CONDITIONS.

FORTRAN Statements for the Computation of the Linear - Ap-

proximation Inverse - Impedances, $\beta(\omega)$.

Notation

OMEGL: Instantaneous frequency at Left Interface.

OMEGR: "   "   " Right   "

OMEGA: Denotes Either OMEGL or OMEGR.

BGG'L: Linear-Approximation Inverse-Impedance for the Left

    Reflector.

BGG'R: Linear-Approximation Inverse-Impedance for the Right

BGGA: Reflector.

    Denotes Either BGGL or BGGR.

The following set of six FORTRAN Statements contains the

computation of BGGA.

```
SG=SOG+(OMEGA*VINV(G))

IF(OMEGA.LT.O.O)SG=SOG

BG=DSQRT(SG/DG)

YG=BG*RETH

HTG=(DEXP(YG)-DEXP(-YG))/(DEXP(YG)+DEXP(-YG))

BGGA=BG*DG/HTG
```

For convenience, in the sequel we shall refer to the above set as [CALCULATE BGGA].

Next, the following set of twelve FORTRAN Statements contains the instructions for the computation of B21A.

```
S1=SO1+(OMEGA*VINV(1))

S2=SO2+(OMEGA*VINV(2))

IF(OMEGA.LT.O.O)S1=SO1

IF(OMEGA.LT.O.O)S2=SO2

B1=DSQRT(S1/D1)

B2=DSQRT(S2/D2)

SI=S12/(S2-(D2*(B1**2)))

Y1=B1*RETH

Y2=B2*RETH

HT1=(DEXP(Y1)-DEXP(-Y1))/(DEXP(Y1)+DEXP(-Y1))

HT2=(DEXP(Y2)-DEXP(-Y2))/(DEXP(Y2)+DEXP(-Y2))
```

B21A=SI*D2*((B1/HT1)-(B2/HT2))

We shall refer to this latter set as [CALCULATE B21A].

Modifications* in Subroutine CALC.

- -

115 CONTINUE

   CALL RHS(G,PSI,...,IPR,WZ)

120 IF(SORCE)130,140,130

130 CALL SOURCE(...)

140 CALL LHS(G,...,PB,WZ)

   CALL MATINV(...)

- -

   END

_____

* The modified or new FORTRAN statements are underlined.

257

Modifications in Subroutine ITER.

```
        DD(1)=1.0D0

        DU(1)=0.0

        GO TO 130

120     DD(1)=DD(1)+SIGX(1,G,G)

        IF(G.EQ.1)DD(1)=DD(1)+TWB11

        IF(G.EQ.2)DD(1)=DD(1)+TWB22

130     Z=SIGX(1,G,G)

        PL=2
```

```
        IF(BCR.EQ.1) GO TO 180

        DD(PT)=1.0D0

        DL(PT)=0.0

        GO TO 190

180     IF(G.EQ.1)DD(PT)=DD(PT)+TWB11

        IF(G.EQ.2)DD(PT)=DD(PT)+TWB22

190     CONTINUE

        PL=1

        IF(BCL.EQ.0)PL=2
```

END

The quantities TWB11 and TWB22 which appear in the above
modifications are defined as twice B11 and twice B22, respective-
ly; the latter quantities are computed by means of the FORTRAN
set [CALCULATE BGGA] with OMEGA set equal to zero.

Modifications in Subroutine LHS

SUBROUTINE LHS(G,...,IPR,PB,WZ)

— —

DIMENSION WZ(PT)

OMEGL=WZ(1)

[CALCULATE B11L, B22L]

OMEGR=WZ(PT)

[CALCULATE B11R,B22R]

PL=2

IF(G.EQ.1)TWBGGL=2.0D0*B11L

IF(G.EQ.1)TWBGGR=2.0D0*B11R

IF(G.EQ.2)TWBGGL=2.0D0*B22L

IF(G.EQ.2)TWBGGR=2.0D0*B22R

```
       DO 1 R=1,REG
```

- -

```
       GO TO 5
65     DD(1)=VINV(G)+(CM(1,G)+CP(1,G)-
      1TI1(1)+TWAGGL)*FF2(1)
       DU(1)=-CP(1,G)*FF2(2)
```

- -

```
       GO TO 605
33     DD(PT)=VINV(G)+(CP(PT,G)+CM(PT,G)-
      1TI1(REG)+TWAGGR)*FF2(PT)
       DL(PT)=-CM(PT,G)*FF2(PT-1)
605    CONTINUE
```

- -

```
       END
```

Modifications in Subroutine PROD

- -

260

```
        GPU=G-1
  260   X=X+SIGX(R,G,GP)*PSI(P,GP)

        IF(P.EQ.1.AND.GRP.EQ.2)X=X-(TWB21*PST(1,1))

        IF(P.EQ.PT.AND.GRP.EQ.2)X=X-(TWB21*PSI(PT,1))

  270   PROD=X

        RETURN

        END
```

The quantity TWB21 which appears in the above FORTRAN

Statements is defined as twice B21; the latter quantity is comput-

ed by means of the FORTRAN set [CALCULATE B21A] with OMEGA set

to zero.

Modifications in Subroutine RHS


```
        SUBROUTINE RHS(G,PSI,...,IPR,WZ)
```

```
        DIMENSION WZ(PT)
```

```
      IF(G.EQ.1)GO TO 1000

      OMEGL=WZ(1)

      [CALCULATE B21L]

      OMEGR=WZ(PT)

      [CALCULATE B21R]

1000  CONTINUE

      X3=NX(G)

      PL=1
```

- -

```
16 DO 17 GP=GL,GU

   GD=GP-GRP

   T3=T3+SD(G,GD)*PSI(P,GP)

17 CONTINUE

18 CONTINUE

   IF(P.E.Q.1.AND.G.EQ.2)T1=T1-(2.0*B21L*PSI(1,1))

   IF(P.EQ.PT.AND.G.EQ.2)T1=T1-(2.0*B21R*PSI(PT,1))

   T1=T1*FF2(P)

   T2=T2*FF1(P)
```

- -

```
      END
```

C.2 IMPLEMENTATION OF THE STATIC - APPROXIMATION BOUNDARY

CONDITIONS.

Modifications in the Subroutines CALC, ITER and PROD: The same

as in Section C.1.

Modifications in the Subroutines LHS and RHS: Set OMEGL=OMEGR=0.0;

otherwise the modifications are the same as in Section C.1.

263